

UNCLASSIFIED

AD NUMBER

AD454492

LIMITATION CHANGES

TO:

Approved for public release; distribution is unlimited. Document partially illegible.

FROM:

Distribution authorized to U.S. Gov't. agencies and their contractors;
Administrative/Operational Use; SEP 1964. Other requests shall be referred to Office of Naval Research, Washington, DC 20360. Document partially illegible.

AUTHORITY

onr ltr, 28 jul 1977

THIS PAGE IS UNCLASSIFIED

THIS REPORT HAS BEEN DELIMITED
AND CLEARED FOR PUBLIC RELEASE
UNDER DOD DIRECTIVE 5200.20 AND
NO RESTRICTIONS ARE IMPOSED UPON
ITS USE AND DISCLOSURE,

DISTRIBUTION STATEMENT A

APPROVED FOR PUBLIC RELEASE;
DISTRIBUTION UNLIMITED,

UNCLASSIFIED

AD 4 5 4 4 9 2

DEFENSE DOCUMENTATION CENTER

FOR

SCIENTIFIC AND TECHNICAL INFORMATION

CAMERON STATION ALEXANDRIA, VIRGINIA



UNCLASSIFIED

NOTICE: When government or other drawings, specifications or other data are used for any purpose other than in connection with a definitely related government procurement operation, the U. S. Government thereby incurs no responsibility, nor any obligation whatsoever; and the fact that the Government may have formulated, furnished, or in any way supplied the said drawings, specifications, or other data is not to be regarded by implication or otherwise as in any manner licensing the holder or any other person or corporation, or conveying any rights or permission to manufacture, use or sell any patented invention that may in any way be related thereto.

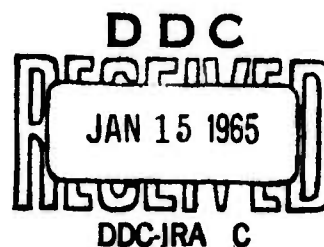
SU-SEL-64-106

ORIGINAL CONTAINS COLOR PLATES: ALL OTHER
REPRODUCTIONS WILL BE IN BLACK AND WHITE
ORIGINAL MAY BE SEEN IN DDC HEADQUARTERS

The Synthesis Of Oblique Ionograms By Digital Computer

by
T.A. Croft

September 1964



Technical Report No. 89

Prepared under
Office of Naval Research Contract
Nonr-225 (64), NR 088 019, and
Advanced Research Projects Agency ARPA Order 196-64

RADIOSCIENCE LABORATORY
STANFORD ELECTRONICS LABORATORIES
STANFORD UNIVERSITY • STANFORD, CALIFORNIA



CATALOGED BY DDC

AS AD No. _____

454492

454492

DDC AVAILABILITY NOTICE

Qualified requesters may obtain
copies of this report from DDC.
Foreign announcement and dissemination of this report by DDC is
not authorized.

ORIGINAL CONTAINS COLOR PLATES: ALL DDC,
REPRODUCTIONS WILL BE IN BLACK AND WHITE
ORIGINAL MAY BE SEEN IN DDC HEADQUARTERS

SEL-64-106

THE SYNTHESIS OF OBLIQUE IONOGRAMS
BY DIGITAL COMPUTER

by

T. A. Croft

September 1964

Reproduction in whole or in part
is permitted for any purpose of
the United States Government.

Technical Report No. 89

prepared under

Office of Naval Research Contract Nonr 225(64), NR 088-019

and

Advanced Research Projects Agency ARPA Order 196-64

Radioscience Laboratory
Stanford Electronics Laboratories
Stanford University Stanford, California

ABSTRACT

Oblique ionograms--records of sweep-frequency ionospheric sounders with transmitter-receiver separation of hundreds or thousands of kilometers--differ from vertical-incidence ionograms in that they cannot be inverted to give ionospheric electron density without making unrealistically drastic assumptions concerning the nature of the ionosphere. Oblique ionograms, however, can be calculated from a known ionosphere. This report describes a method for performing the calculation using a digital computer.

The technique takes full account of earth and ionosphere curvatures and allows arbitrary choice of electron density with height and longitudinal distance but not with lateral distance. The geomagnetic field is neglected in the interest of economy, but it could be included. Examples of synthetic oblique ionograms for a Chapman ionosphere are presented, both with and without an E layer, over path lengths from 0 to 8000 km. Results included show the effects of layer height, thickness, tilts, and a variety of non-Chapman electron-density distributions. The synthetic ionograms include the raypath takeoff angles and also the absolute group time delay; these are particularly useful since they are not available on experimental ionograms.

CONTENTS

	<u>Page</u>
I. INTRODUCTION	1
II. RAYTRACING AND THE RAYSET INFORMATION-STORAGE TECHNIQUE	3
III. METHOD OF OBLIQUE-IONOGRAM SYNTHESIS	7
IV. VERTICAL-INCIDENCE IONOGRAMS	9
V. SYNTHETIC IONOGRAMS	10
A. A Chapman layer and various ranges	12
B. Weak and strong E layers at various ranges	24
C. Changes in layer height	37
D. Changes in scale height	41
E. Horizontal gradients within a Chapman layer	45
F. Two parabolic layers at various ranges	54
G. An unusual example	66
VI. EXAMPLES SHOWING DETAILS OF SYNTHESIS	73
A. Details of the nose of IID 111 two-hop echo	73
B. Details of the E-layer effect in IID 012	74
C. Origin of a one-hop trace in a 5000-km ionogram	80
VII. SELECTED EXPERIMENTAL IONOGRAMS SHOWING AGREEMENT WITH THEORY	82
VIII. SUMMARY	87
REFERENCES	88

ILLUSTRATIONS

<u>Figure</u>		<u>Page</u>
1	The nature of "raysets"	4
2	Electron-density distribution for Chapman layer, IID 011 . .	14
3	Ionogram for IID 011; separation distance, 0 km	15
4	Ionogram for IID 011; separation distance, 1000 km	16
5	Ionogram for IID 011; separation distance, 2000 km	17
6	Ionogram for IID 011; separation distance, 3000 km	18
7	Ionogram for IID 011; separation distance, 4000 km	19
8	Ionogram for IID 011; separation distance, 5000 km	20
9	Ionogram for IID 011; separation distance, 6000 km	21
10	Ionogram for IID 011; separation distance, 7000 km	22
11	Ionogram for IID 011; separation distance, 8000 km	23
12	Electron-density distributions for IIDs 011, 012, and 089	25
13	Ionogram for IID 012; separation distance, 0 km	26
14	Ionogram for IID 012; separation distance, 1000 km	27
15	Ionogram for IID 012; separation distance, 2000 km	28
16	Ionogram for IID 012; separation distance, 3000 km	29
17	Ionogram for IID 012; separation distance, 4000 km	30
18	Ionogram for IID 012; separation distance, 5000 km	31
19	Ionogram for IID 012; separation distance, 6000 km	32
20	Ionogram for IID 012; separation distance, 7000 km	33
21	Ionogram for IID 012; separation distance, 8000 km	34
22	Ionogram for IID 089; separation distance, 0 km	35
23	Ionogram for IID 089; separation distance, 3000 km	36
24	Electron-density distributions for IIDs 011, 053, and 054	38
25	Ionogram for IID 053; separation distance, 3000 km; low Chapman layer	39
26	Ionogram for IID 054; separation distance, 3000 km; high Chapman layer	40
27	Electron-density distributions for IIDs 011, 055, and 056. .	42
28	Ionogram for IID 055; separation distance, 3000 km; small scale height	43
29	Ionogram for IID 056; separation distance, 3000 km; large scale height	44

ILLUSTRATIONS (Cont'd)

<u>Figure</u>		<u>Page</u>
30	Electron densities at path endpoints for IIDs 093 and 094	47
31	Ionogram for IID 093; separation distance, 2000 km	48
32	Ionogram for IID 093; separation distance, 4000 km	49
33	Ionogram for IID 093; separation distance, 6000 km	50
34	Ionogram for IID 094; separation distance, 2000 km	51
35	Ionogram for IID 094; separation distance, 4000 km	52
36	Ionogram for IID 094; separation distance, 6000 km	53
37	Electron densities in two parabolic layers--IIDs 111 and 124	55
38	Ionogram for IID 111; separation distance, 0 km	56
39	Ionogram for IID 111; separation distance, 1375 km	57
40	Ionogram for IID 111; separation distance, 1833 km	58
41	Ionogram for IID 111; separation distance, 2750 km	59
42	Ionogram for IID 111; separation distance, 5500 km	60
43	Ionogram for IID 124; separation distance, 0 km	61
44	Ionogram for IID 124; separation distance, 1375 km	62
45	Ionogram for IID 124; separation distance, 1833 km	63
46	Ionogram for IID 124; separation distance, 2750 km	64
47	Ionogram for IID 124; separation distance, 5500 km	65
48	Electron-density distributions for IID 133	67
49	Ionogram for IID 133; separation distance, 0 km	68
50	Ionogram for IID 133; separation distance, 1375 km	69
51	Ionogram for IID 133; separation distance, 1833 km	70
52	Ionogram for IID 133; separation distance, 2750 km	71
53	Ionogram for IID 133; separation distance, 5500 km	72
54	Graph illustrating synthesis of IID 111 ionogram	73
55	Printed raysets at 16.5 Mc for IID 012	75
56	Computed ionogram points taken from data of Fig. 55	77
57	Graph of raypath range vs takeoff angle for IID 012	78
58	Partially synthesized ionogram showing points plotted directly from the computer output	79
59	Long-range, one-hop propagation in a Chapman layer for IID 011	81

ILLUSTRATIONS (Cont'd)

<u>Figure</u>		<u>Page</u>
60	Experimental ionograms similar to those of IID 011	84
61	Experimental ionograms similar to those of IID 012	85
62	Experimental ionograms similar to those of IID 133	86

I. INTRODUCTION

Many research organizations throughout the world are presently collecting data in the form of oblique ionograms. Such data are directly useful in determining the communication channels that are open along the particular path spanned by the oblique sounders. These data also show great promise for use in the study of upper-atmospheric electron-density distribution, which may lead to a better understanding of the behavior of the ionosphere. The primary difficulty at the moment is that there is no practical way to determine the electron-density distribution from an oblique ionogram unless one is willing to make gross simplifying assumptions.

The purpose of this paper is to introduce a technique that may prove to be of significant value as a part of the current effort to gain a better understanding of oblique ionograms. If one begins with a known a priori electron-density distribution, it is economically feasible to use digital-computer raytracing techniques for the synthetic generation of the corresponding oblique ionograms. The basic idea, then, is that one can generate a library of synthetic ionograms whose structure and detail can be analyzed and understood completely. Later one could refer to this library and compare the synthetic ionograms with actual experimental ionograms with a hope that the comparison will aid in drawing useful conclusions concerning the nature of electron-density distribution which actually existed along the path.

The synthetic records also provide information not available on their real counterparts. During the manufacture of the synthetic ionograms, it is particularly easy to determine the takeoff angles of the raypaths that lead to various details of the structure of the oblique ionograms. This information is not usually available and it should be useful to those who design antennas used in gathering oblique ionograms. The takeoff angles should also prove helpful in the interpretation of actual ionograms because they show which portions of the total echo structure are rendered invisible because of low antenna gain at the particular vertical angles in question.

The synthetic records show the actual time delay between transmitter and receiver. This information is helpful because experimental records have arbitrary time base-lines as a result of an inherent inability to determine the total accumulated time delay accurately. In addition, the synthetic records could show the signal strength of each component of each trace, but these data were not included on the records given here.

II. RAYTRACING AND THE RAYSET INFORMATION-STORAGE TECHNIQUE

A large amount of the work that must be done to make synthetic ionograms consists of the tracing of radio waves in the upper atmosphere by a digital computer. A number of organizations currently have raytracing programs in operation. The particular program used for the generation of data in this paper was described in a previous report by the author [Ref. 1]. It should be emphasized that any digital raytracing program could be used in exactly the same way as described here, provided that it accurately calculates the range and group time delay of each ray. The raytracing program used here consisted basically of the successive solutions of Snell's Law as a ray was followed through a horizontally stratified ionosphere wherein each stratum was about 1 km thick. Because the geomagnetic field was neglected, the ionograms generated in this study will be found to lack an extraordinary trace.

One of the major factors that must be considered in synthesizing oblique ionograms is the cost of raytracing. Unfortunately, this cost is a difficult factor to evaluate because it can vary by an order of magnitude, depending on the particular situation at hand. Nevertheless, the following rough estimates are offered: for each hop of each ray in an ionosphere consisting of 300 strata, each 1 km thick, the cost is \$0.01. If horizontal gradients of electron density (tilts) are present in the ionosphere, then the cost goes up, to approximately \$0.10. Although no data are available, it is this author's understanding that the inclusion of the magnetic field drives the cost up by another factor of perhaps 10, so that the cost could be as much as \$1.00 per hop per ray. The importance of cost control can be appreciated when one considers that this laboratory alone traces approximately 10^5 rays per year.

The building block of this method is the "rayset"--the name given to the set of numbers that characterizes the raypath information acquired through raytracing. Each such set of numbers describes one hop of one ray and is stored on one punched card. For example, if a ray executes three hops, the computer will make three punched cards containing all the key information that characterizes each hop. This system is illustrated by Fig. 1.

FIRST RAYSET									
IID	Freq.	B=1	β	ψ_1	T_{q1}	$T_{\phi 1}$	R_1	H_1	$I_1=0$
SECOND RAYSET									
IID	Freq.	B=2	β	ψ_2	T_{q2}	$T_{\phi 2}$	R_2	H_2	$I_2=0$
ETC.									

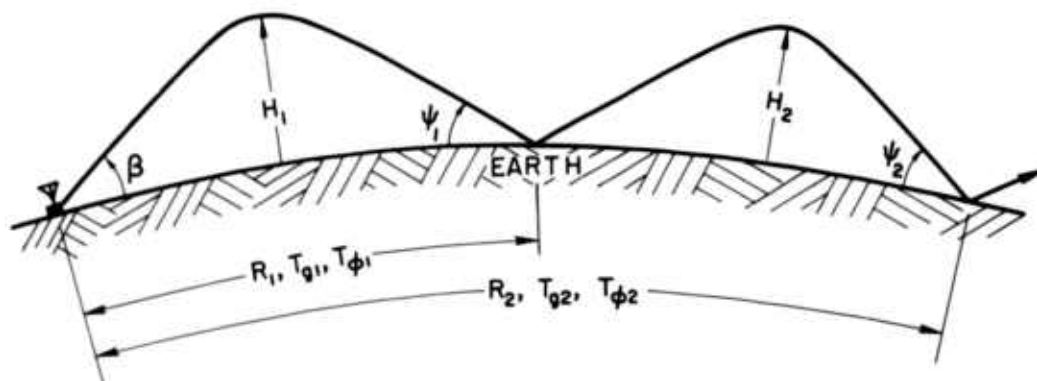


FIG. 1. THE NATURE OF "RAYSETS."

Consider the process that goes on inside a digital computer during raytracing. Each ray is calculated individually. The computer is instructed to go to a designated starting point and consider a ray, originating in that point, propagating at a given initial takeoff angle above the surface of the earth. The computer then follows that ray in circular coordinates and, using appropriate equations, it calculates the curved path of the ray as it traverses a medium of varying index of refraction. Many things can happen to the ray. It can be refracted by the ionosphere and execute normal hops as it does in the first two hops of Fig. 1. It can go so far that it exceeds a specified maximum range and the computer will be instructed to shut off. Similarly, the ray might exceed a specified maximum height. With horizontal gradients present, the ray may take off and climb high into the ionosphere only to come down on top of a densely ionized, localized area; then it may refract back upward. In such a case it is said that the ray executed a "perigee." This frequently happens when raytracing is conducted in an ionosphere with a E layer whose critical frequency increases with increasing range.

It may happen that the ray trapped between the E and F layers will eventually escape. However the valley in the N-h profile between the E and F layers may fill up with electrons as the range increases further, and the ray may find that it cannot continue to propagate because the index of refraction is imaginary in all forward directions. In such a case the ray is terminated by the computer, although physically the energy must reflect back out of such a "closed trap."

As the computer follows the progress of each ray, it momentarily stops every time a ray encounters the earth, a perigee, or its termination. At that time the computer stores on magnetic tape the set of numbers, called a rayset, that will later be punched into a card.

Consider the first hop; when the computer finds that the ray strikes the earth, as it does in the center of Fig. 1, it stores the numbers shown in the top row. The IID (Ionosphere Identification) is a three-digit number that identifies the particular electron-density distribution; the frequency is the number of kilocycles; the parameter B (bounce) will be given as 1 because this is the first time the ray has hit the earth; the parameter β is the takeoff angle; and ψ_1 is the landing angle as shown. The three parameters T_{g1} , $T_{\phi 1}$, and R_1 are the group time delay, phase time delay, and the ground range from the transmitter to the point of impact. The height H_1 is the height of the apogee of the ray as shown. The parameter I_1 (indicator) is a number that is coded 0 through 6 and tells just what the ray did. Notice that $I = 0$ when the ray hits the earth, $I = 1$ if the ray exceeds maximum height, and $I = 2$ or 3 if the ray exceeds maximum range. Similarly, $I = 4$ or 5 if the ray executes perigees and $I = 6$ if the ray encounters a closed trap.

When the computer detects that the ray has encountered the ground for a second time, as shown at the right of Fig. 1, it stores the second rayset shown across the center of the figure. Here the information is similar to that in the first rayset except that $B = 2$ because this is the second encounter with the ground.

As a matter of interest, it might be noted that the definitions of the various parameters as shown in Fig. 1 apply only when $I = 0$. When I is nonzero, the ranges, times, angles, and heights are defined

differently, in such a way as to maximize the ability of the user to reconstruct the ray trajectory. As an example of this, consider that the third hop of a ray exceeds maximum range, going upward as it appears to do on Fig. 1; the indicator would be $I = 2$. In this case, the time and the range would be measured to the point of termination, the height would be the height of termination, and the angle ψ would be the angle of the ray relative to the horizontal. If the ray had exceeded maximum range coming down, these same definitions would have applied except that the indicator would be $I = 3$.

III. METHOD OF OBLIQUE-IONOGRAM SYNTHESIS

In order to make an artificial oblique ionogram similar to one that might be obtained between two stations 3000 km apart, a common first reaction is an inclination to compute rays of several frequencies that propagate a distance very close to 3000 km. This technique would yield the desired answers and, in fact, the author has developed a specialized program that will search for and calculate only those rays that go to specified ranges. However, it turns out to be necessary to calculate an entire family of rays during the search process when looking for the takeoff angle that will lead a ray to the desired range. Consequently, it is a very inefficient process if one uses information only from rays that propagate the desired distance.

The method that has been used to produce the ionograms given here is probably near to being the most economical approach. In essence the raysets are used as data for a digital program that first separates the rayset cards so that it may consider at any one time only those cards that have the same hop number, B . Considering one such group of cards and one frequency at a time, the program interpolates in a three-dimensional space whose axes are ground range R , group time delay T_g , and takeoff angle β . The program considers as a group all those raysets that have the same B and frequency F and, within these groups, it considers the raysets in order of increasing β . In this order, it examines successive values of R until it finds two values that are the end points of an interval containing the desired range. It then assumes that between the two raysets all relations are linear and it performs an interpolation to find the values of T_g and β at the desired range.

In the majority of circumstances, this procedure produces answers that are quite reasonable, since for small increments of takeoff angle the relationships really are nearly linear between successive raypaths. On occasion, however, this assumption breaks down and it is necessary for human intervention at this point--examination of the printed raysets and comparison with the computed answers--to see that the assumption is truly reasonable. One can tell from trends exhibited by the numbers

whether or not linearity is a valid approximation. In cases where it appears that nonlinear relationships actually must hold, it is necessary to interpolate according to some logical nonlinear scheme, or else to perform more raytracing.

This process is usually carried out at frequency intervals of approximately 4 Mc. The answers are then plotted on a graph of group time delay vs frequency and this plot is the synthetic ionogram. After such a preliminary plot is made, the one-hop data points can be connected with a line, and the two- and three-hop data can be treated similarly. The computer tells whether each point is an upper or lower ray, as determined from the algebraic sign of $dR/d\beta$. From these lines and the blank spaces between them, the exact frequencies and takeoff angles that still need to be raytraced can be deduced with fairly good accuracy.

Since this method involves interpolation, the synthetic ionograms show the data points that were actually calculated. Thus, the reader can judge for himself which of the results presented here are based on mathematics and which are based on judgment.

In general, if the electron-density distribution is a smooth curve when plotted as a function of height and range, then the ionogram will also consist of smooth curves. In this situation, a synthetic ionogram can be produced with a minimum of raytracing because it is possible to interpolate over greater ranges when parameters are smoothly varying functions. Thus the amount of digital calculation can be kept to a minimum. It is a feature of the method of simulation that, once a synthetic ionogram is made for a given ionosphere and a given range, it is considerably less expensive to make other ionograms for different ranges for the same ionosphere. This advantage results because the raytracing, once done, can be used again in the inexpensive "oblique-ionogram program" at new, different ranges. The only cost of producing such extra ionograms is the cost of the few special rays that must be computed, together with the cost of personnel time.

IV. VERTICAL-INCIDENCE IONOGRAMS

A vertical-incidence ionogram is essentially an oblique ionogram at zero range. The synthesis of these records is extremely easy since it is necessary only to integrate group time delay vertically. A special computer program was written to carry out this procedure, utilizing the same ionosphere description cards that were made for the raytracing program; six of the resulting records are included.

V. SYNTHETIC IONOGRAMS

In this section 39 synthetic oblique ionograms and six vertical ionograms are presented that were generated by the method described. Since this is the first effort along these lines, an attempt has been made to select examples of electron-density distribution that illustrate the most commonly encountered gross characteristics of the ionosphere.

Nine ionograms are made with the Chapman ionosphere and various ranges between transmitter and receiver. Then an E layer is added to the Chapman layer and the ionograms are recalculated. The effect of the density of the E layer is investigated briefly. Another group of ionograms shows what happens when Chapman-layer height and thickness are changed. Positive and negative horizontal gradients of electron density are studied in a group of six ionograms. Then, two different parabolic layers are investigated at each of five ranges. Finally, a rather unusual, layered ionosphere is used to generate some fairly intricate ionograms.

When a Chapman layer is mentioned in the following descriptions, this notation is implied:

- N = electron density (in electrons/cc)
- N_0 = maximum electron density in the layer
- h_m = height of maximum electron density N_0 (in km)
- h_s = scale height of Chapman layer (in km)
- $z = (\text{height} - h_m) / (h_s)$.

With this notation, a Chapman layer means an electron density N such that

$$N = N_0 \exp(1 - z - e^{-z}) .$$

Before the data are presented, one further item deserves mention. Because this work neglects the magnetic field, the actual magnitude of the frequencies at which calculations are made is not really the variable of interest. The more significant variable is the ratio of the radio frequency to the plasma frequency of the medium. This conclusion will be seen to follow if one considers that the index of refraction used in

computations of ray paths is simply n , where

$$n^2 = 1 - (f_p^2/f^2),$$

in which f_p is the local plasma frequency and f is the operating frequency. Therefore, if following results indicate that a certain time delay exists along a certain path at some specific frequency, then the time delay presented would also be correct for half that frequency, provided the ionospheric electron density were reduced throughout the entire range of heights by the factor $(1/2)^2$. Any other factor will also work.

As a consequence of this reasoning, it might be convenient to plot both the oblique-incidence ionograms and their associated electron-density profiles on graphs such that the electron-density and frequency scales are logarithmic. Then it would not be necessary to commit oneself to a specific frequency scale on the ionograms but, rather, one could label the horizontal axis in terms of the parameter f/f_c , where f_c is the critical frequency.

Most experimental ionograms, however, are presently being made by the equipment manufactured by Granger Associates, wherein the frequency scale is a sequence of four different linear scales. In an effort to maximize the similarity of these synthetic ionograms to the actual experimental data that are available, they are presented on a "Granger Scale," which makes it necessary to assign specific frequencies to the horizontal axis. Each such plot will be accompanied by a corresponding ionogram that has a logarithmic frequency scale, since some oblique sounders present their data in this manner. Also, this approach will permit the reader to apply the sliding-frequency-scale principle if he so desires.

Small solid triangles along the ionogram frequency axes indicate the vertical-incidence critical frequency of the particular ionosphere. In most cases this value is near 9 Mc, because most of the synthetic ionospheres have arbitrarily been assigned to a maximum electron density of $10^6/\text{cc}$. Also, the small open triangles in the body of the ionogram indicate frequencies at which raytracing was done without finding any propagation modes at the particular range.

The format of the vertical-incidence ionograms was chosen to maximize its similarity to the standard format with which this author is familiar. Also, the vertical-ionogram records show the "true-height profile," which is simply the input data describing the vertical distribution of electron density. This profile is interesting in that it shows the answer which one should get from a reduction of the vertical-incidence record.

A. A CHAPMAN LAYER AND VARIOUS RANGES

Figure 2 shows the electron-density distribution in the Chapman layer whose IID (Ionosphere Identification) is 011. This ionosphere has $h_m = 300$ km, $h_s = 100$ km, and $N_0 = 10^6$. These parameters were chosen because they produce a density that is typical of the actual distribution encountered in practice. Later, the effect of variations in these parameters will be illustrated. Notice that $f_c = 9$ Mc, approximately, but that this value need not be regarded as a fixed quantity because of our ability to apply a sliding-scale concept to the plasma and operating frequencies, as previously mentioned.

Figures 3 through 11 show ionograms that were synthetically generated with the assumption that the separation distances between the transmitter and receiver were 0, 1000, 2000, 3000, 4000, 5000, 6000, 7000, and 8000 km, in that sequence. Notice that under this scheme, Fig. 3 is simply a vertical-incidence ionogram; Fig. 4 is an oblique ionogram in which the stations are separated by 1000 km, and so forth. Each trace is labeled to indicate the number of hops of the rays that generated it. The upper- and lower-ray portions of each echo are easily identified and thus are not labeled. Each point that has been calculated is identified by a dot along the curve on the "Granger" plot. Near most of the dots are small numbers, which indicate the takeoff angles of the particular rays involved.

For these and for most of the ionograms in this report, calculation was cut off at three hops; therefore, the absence of four-hop returns is not significant. Because this particular ionosphere does not have any horizontal electron-density gradients, it would be possible to generate a fourth-hop return on the 8000-km plot by simply doubling the

numbers associated with the two-hop return on the 4000-km plot. However, such a process can be carried on without end and consequently the arbitrary decision was taken to stop at three (or later four) hops.

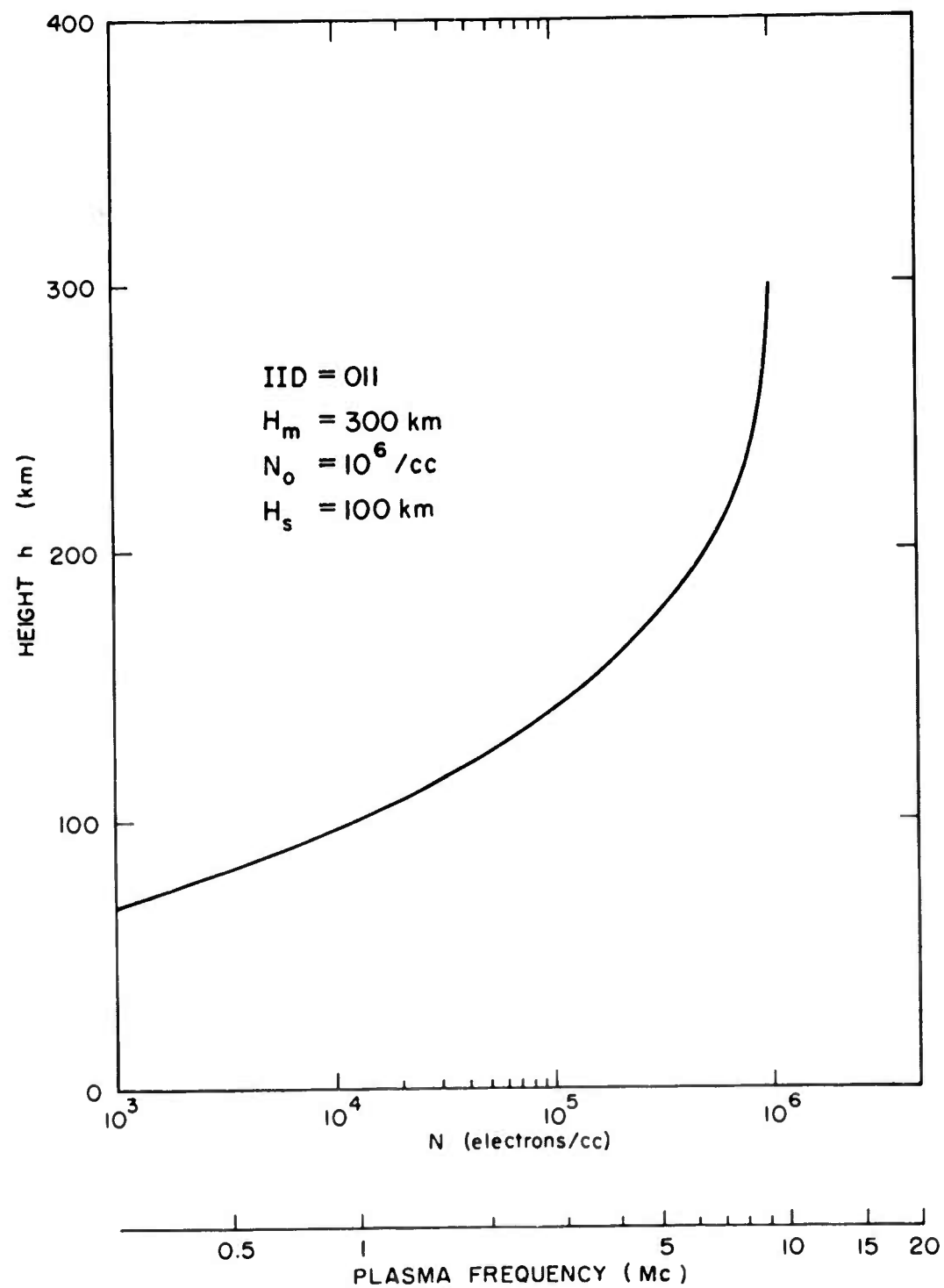


FIG. 2. ELECTRON-DENSITY DISTRIBUTION FOR CHAPMAN LAYER, IID 011.

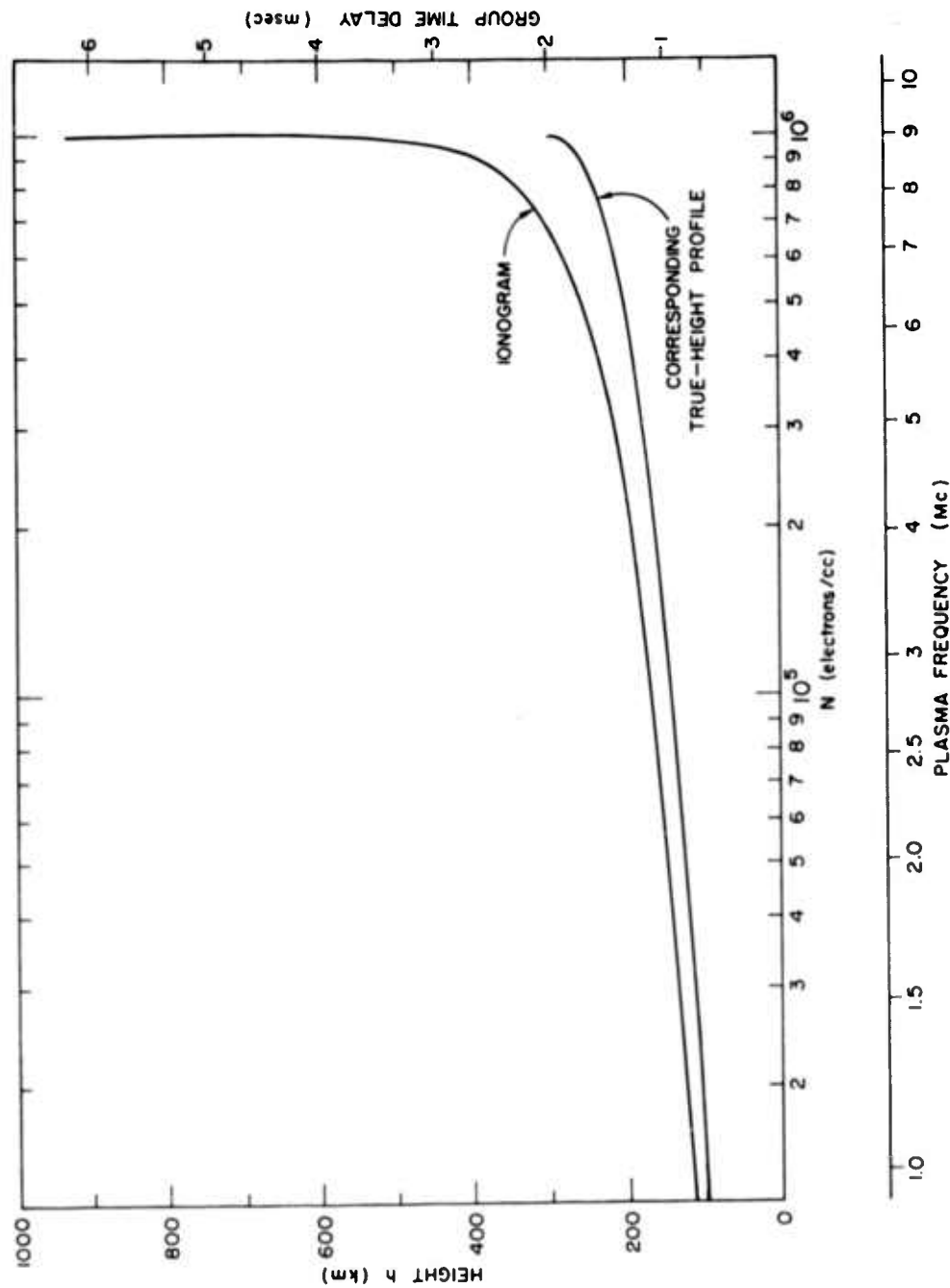
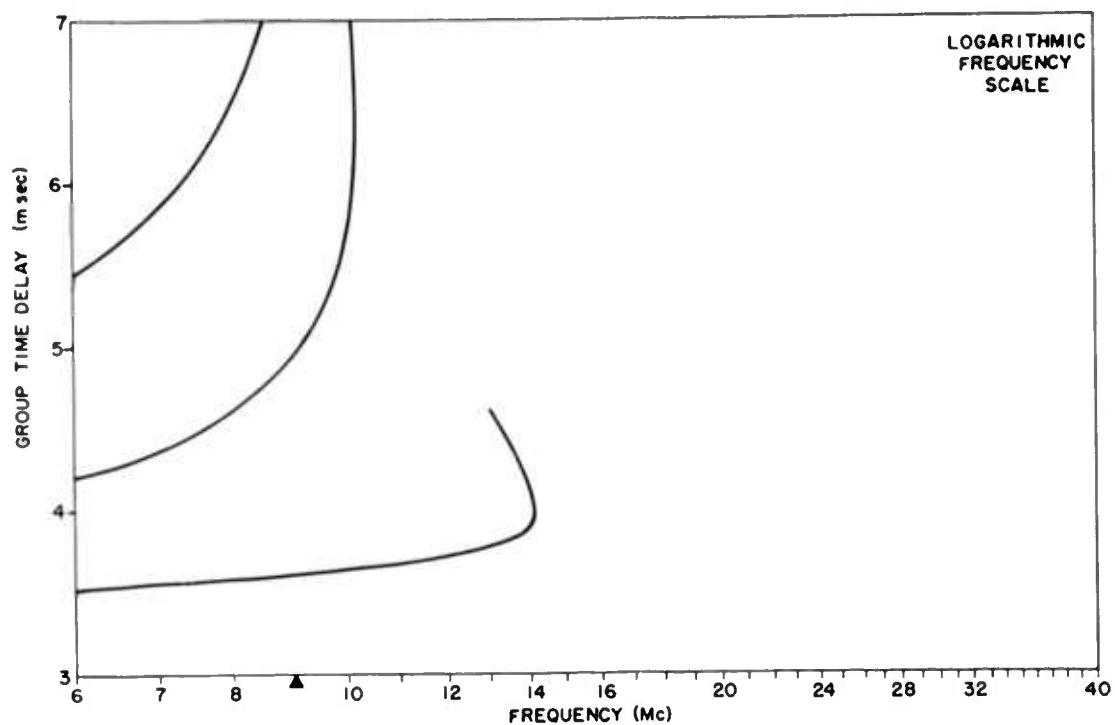
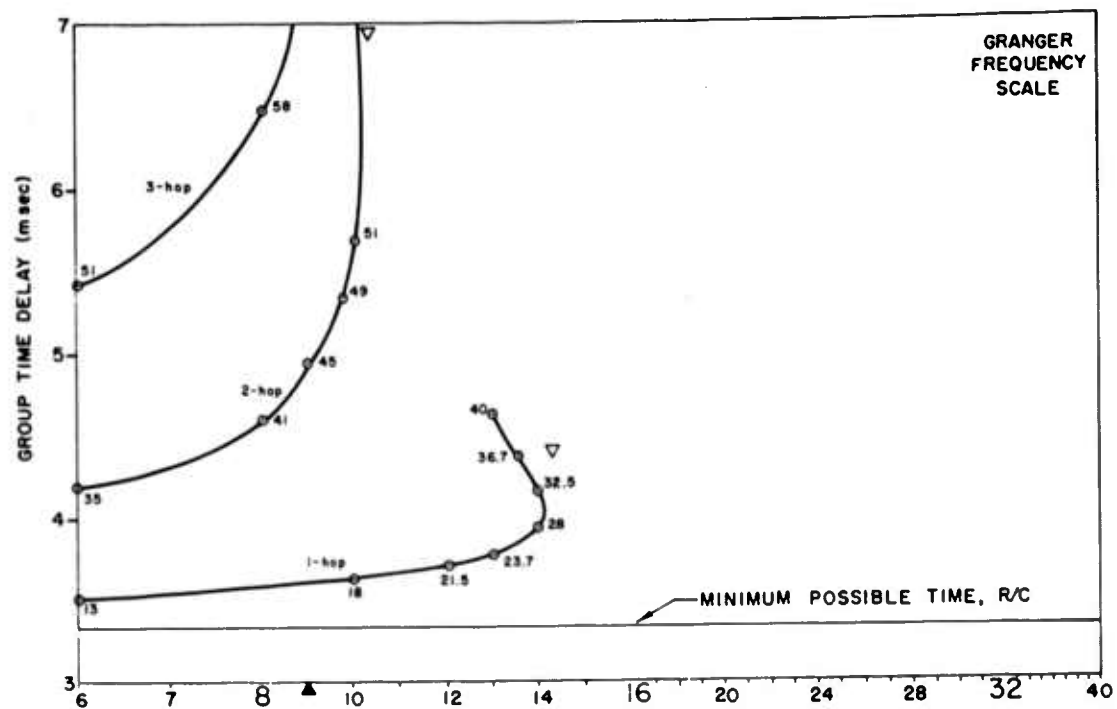
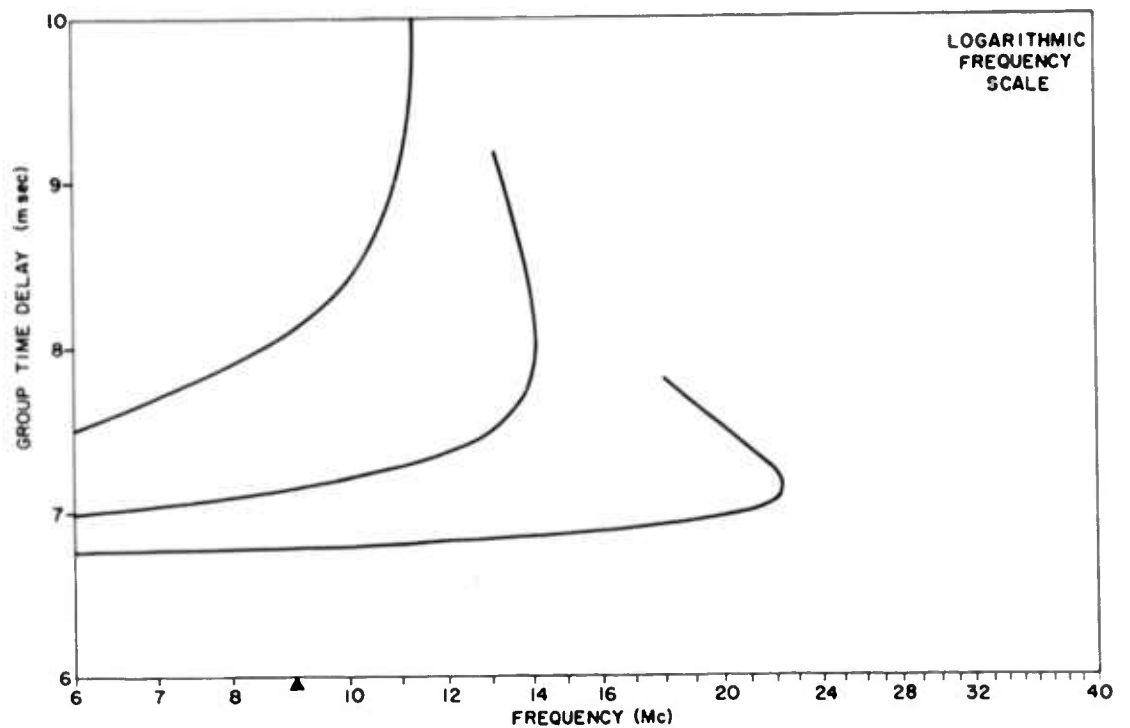
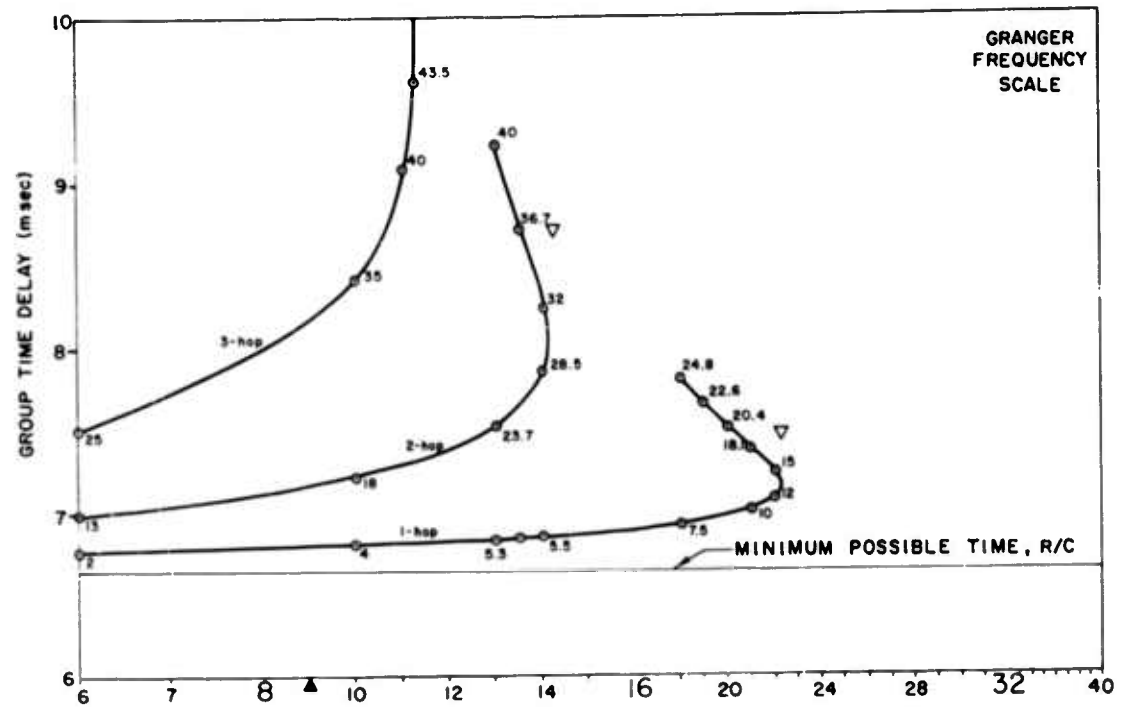


FIG. 3. IONOGRAM FOR 11D 011; SEPARATION DISTANCE, 0 km.



O11 at 1000 km

FIG. 4. IONOGRAM FOR IID O11; SEPARATION DISTANCE, 1000 km.



O11 at 2000 km

FIG. 5. IONOGRAM FOR IID O11; SEPARATION DISTANCE, 2000 km.

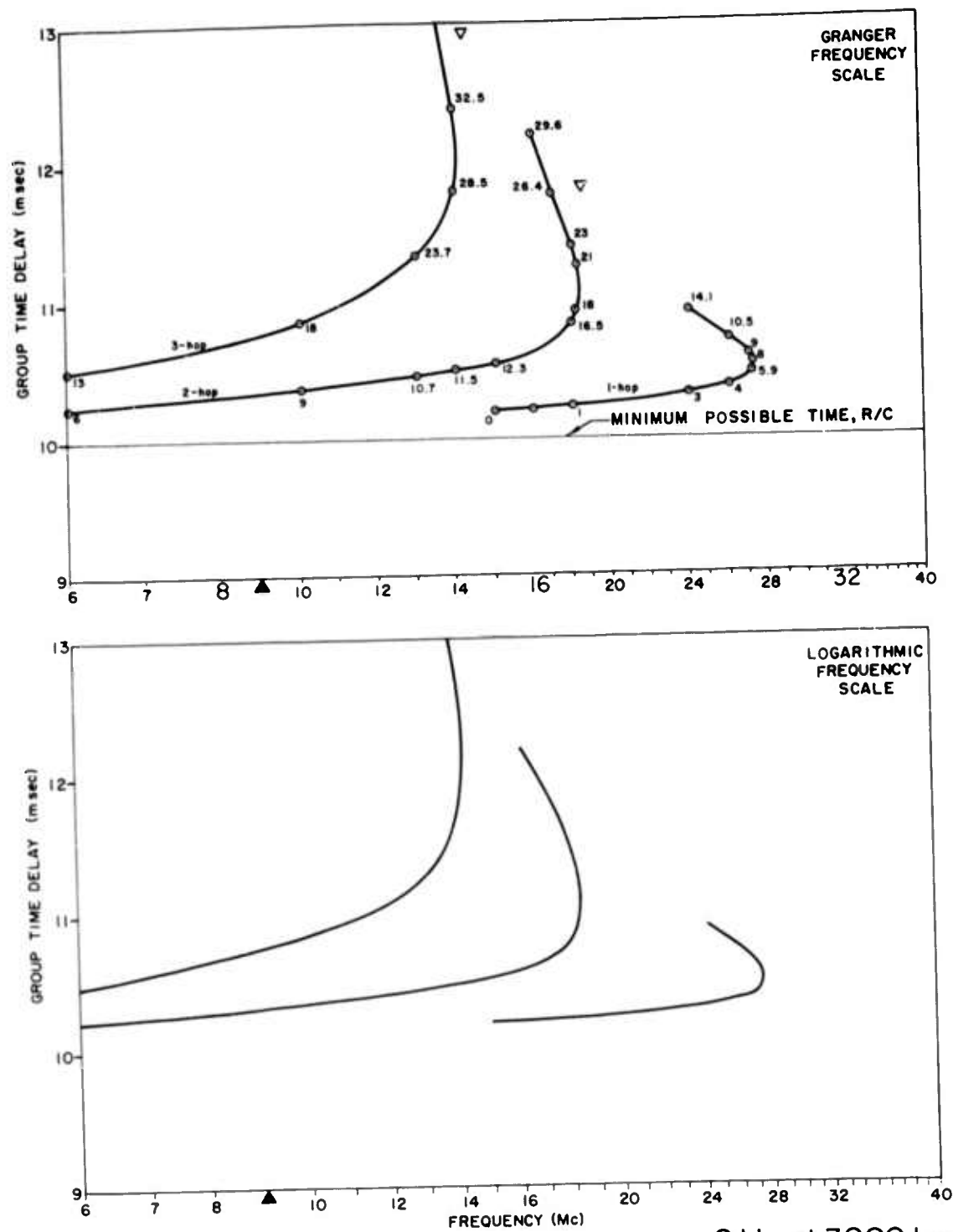
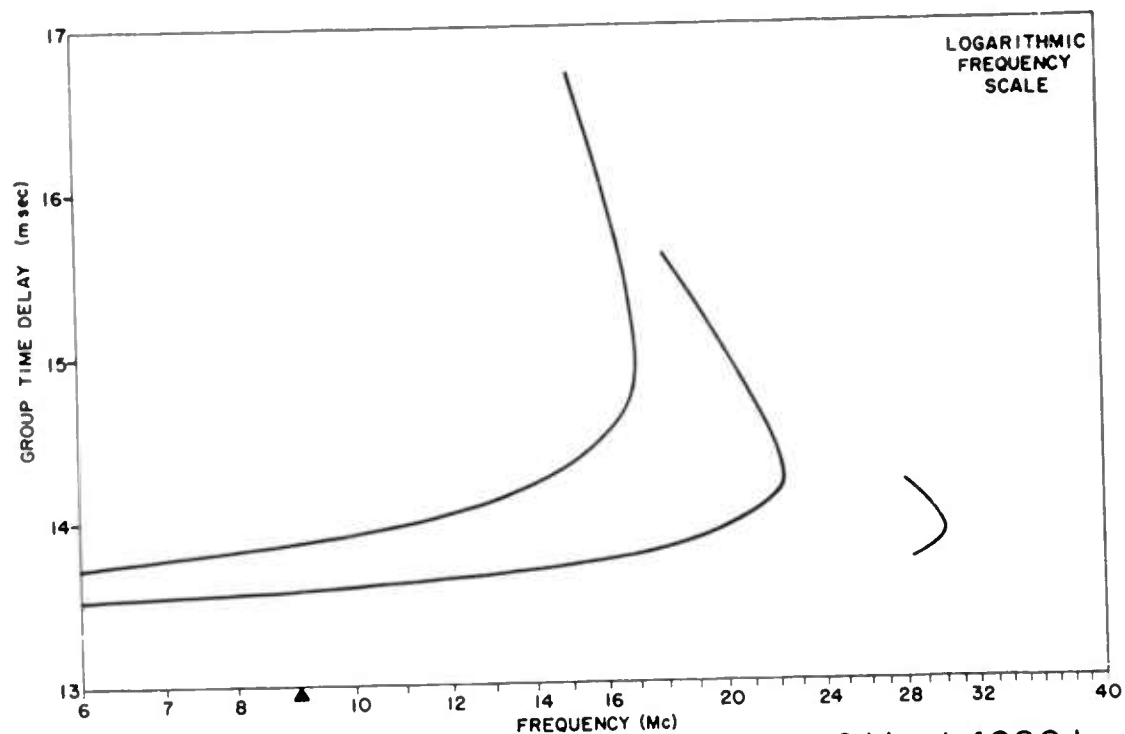
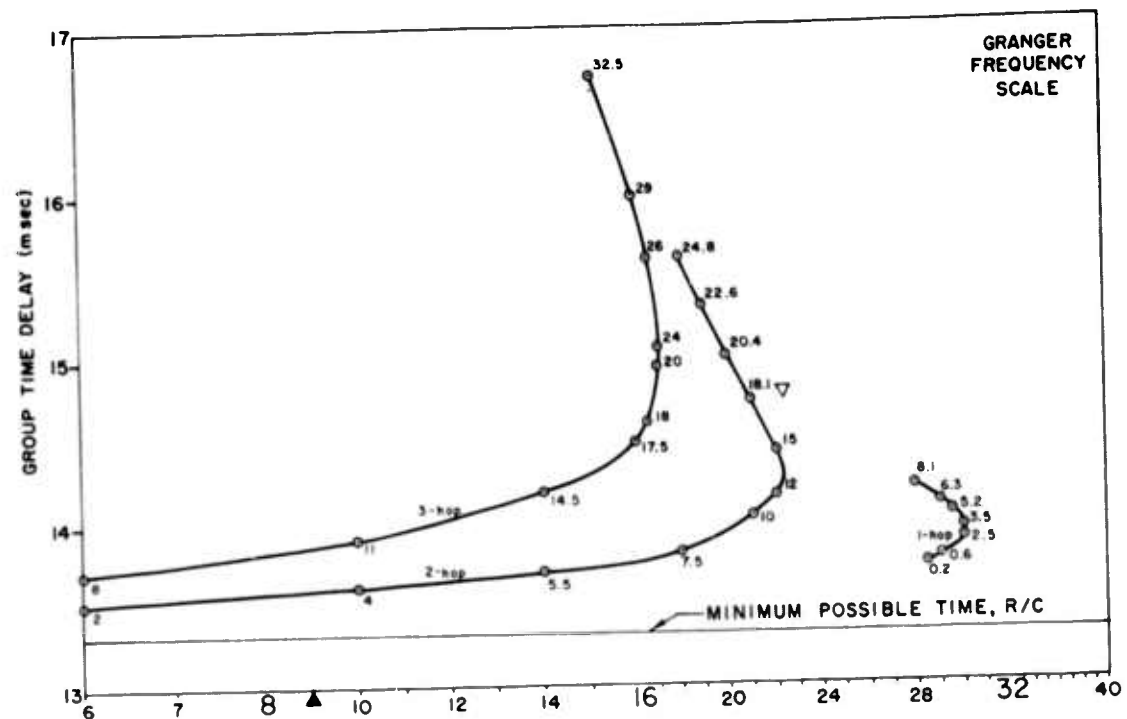
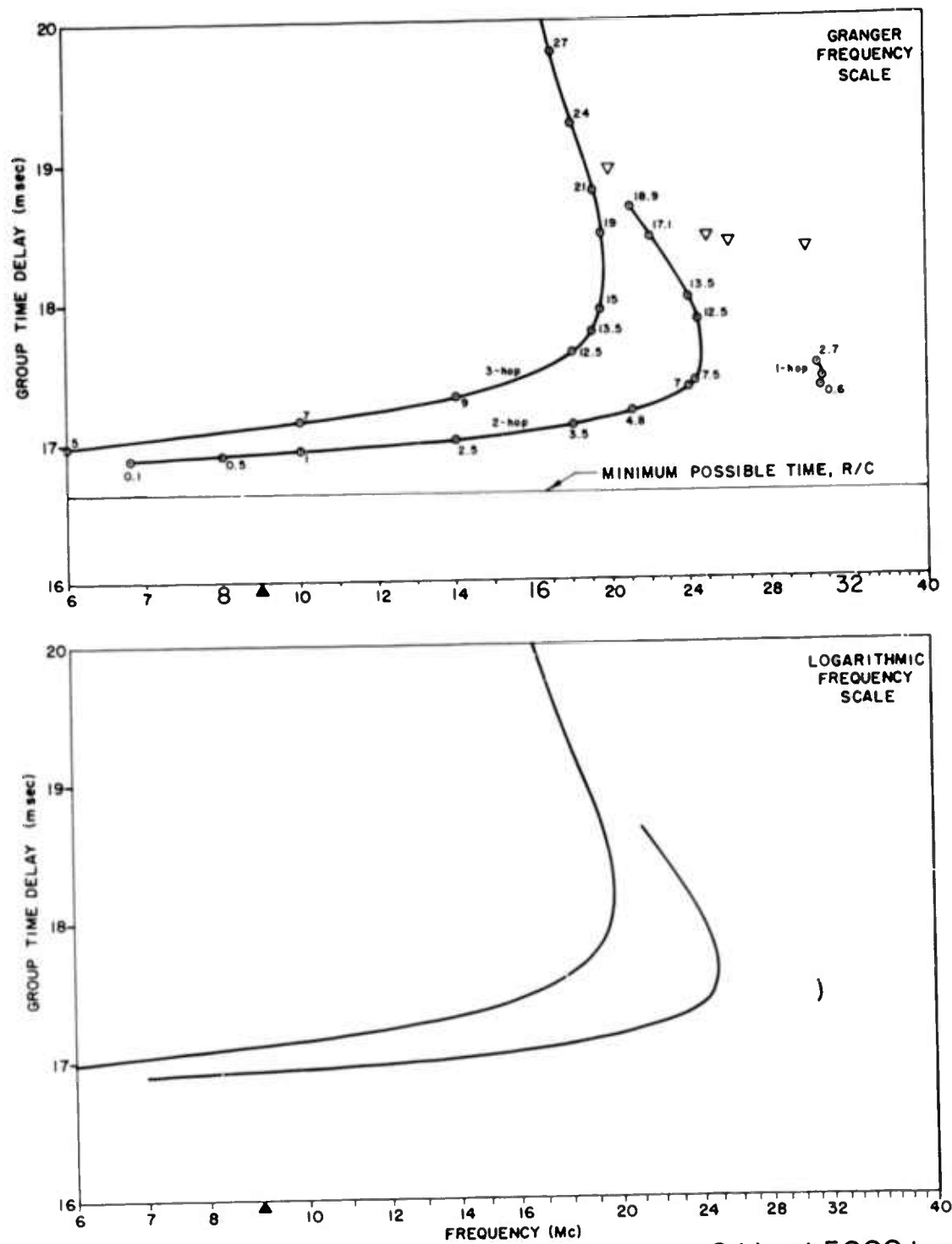


FIG. 6. IONOGRAM FOR IID 011; SEPARATION DISTANCE, 3000 km.



O11 at 4000 km

FIG. 7. IONOGRAM FOR IID O11; SEPARATION DISTANCE, 4000 km.



011 at 5000 km

FIG. 8. IONOGRAM FOR IID 011; SEPARATION DISTANCE, 5000 km.

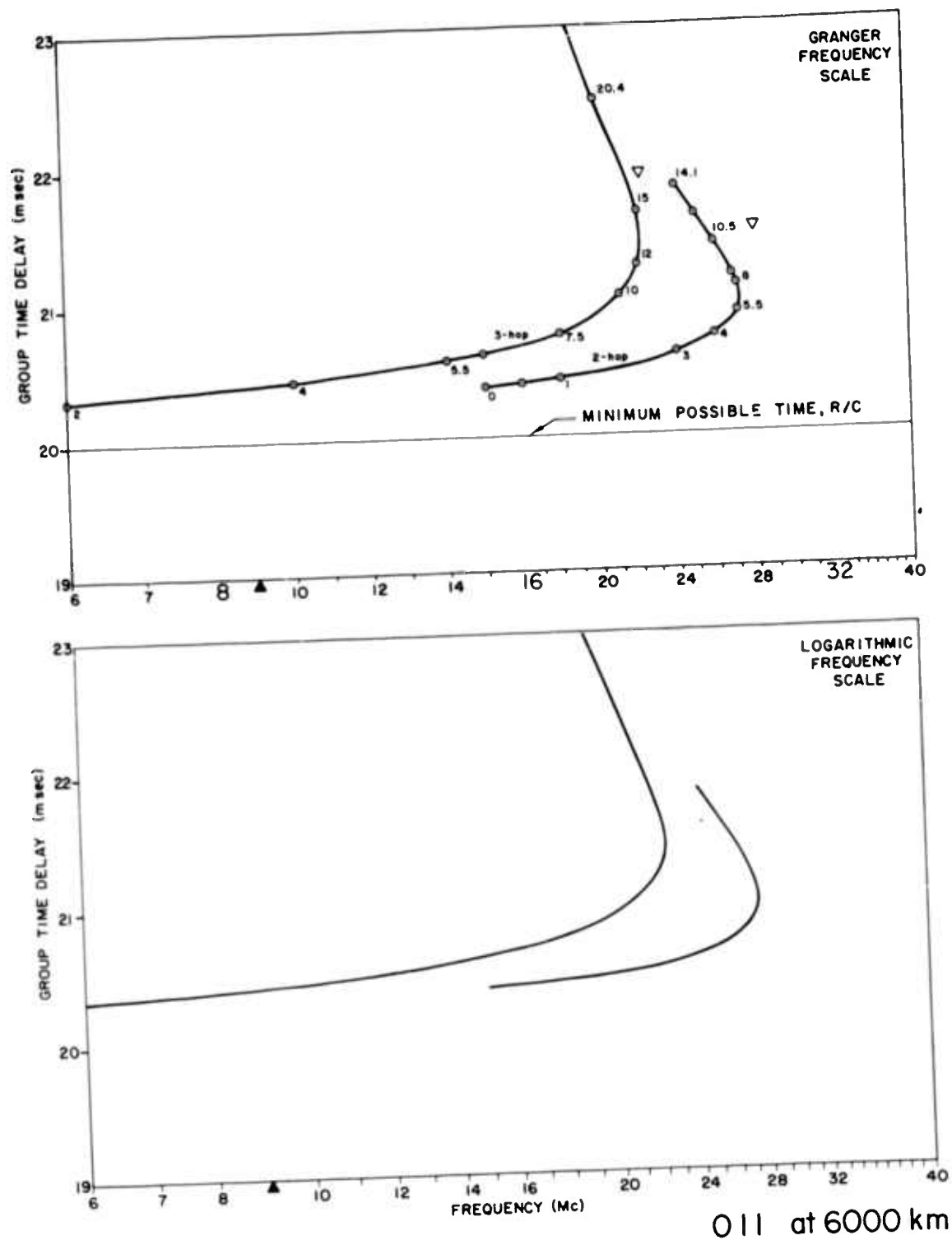


FIG. 9. IONOGRAM FOR IID 011; SEPARATION DISTANCE, 6000 km.

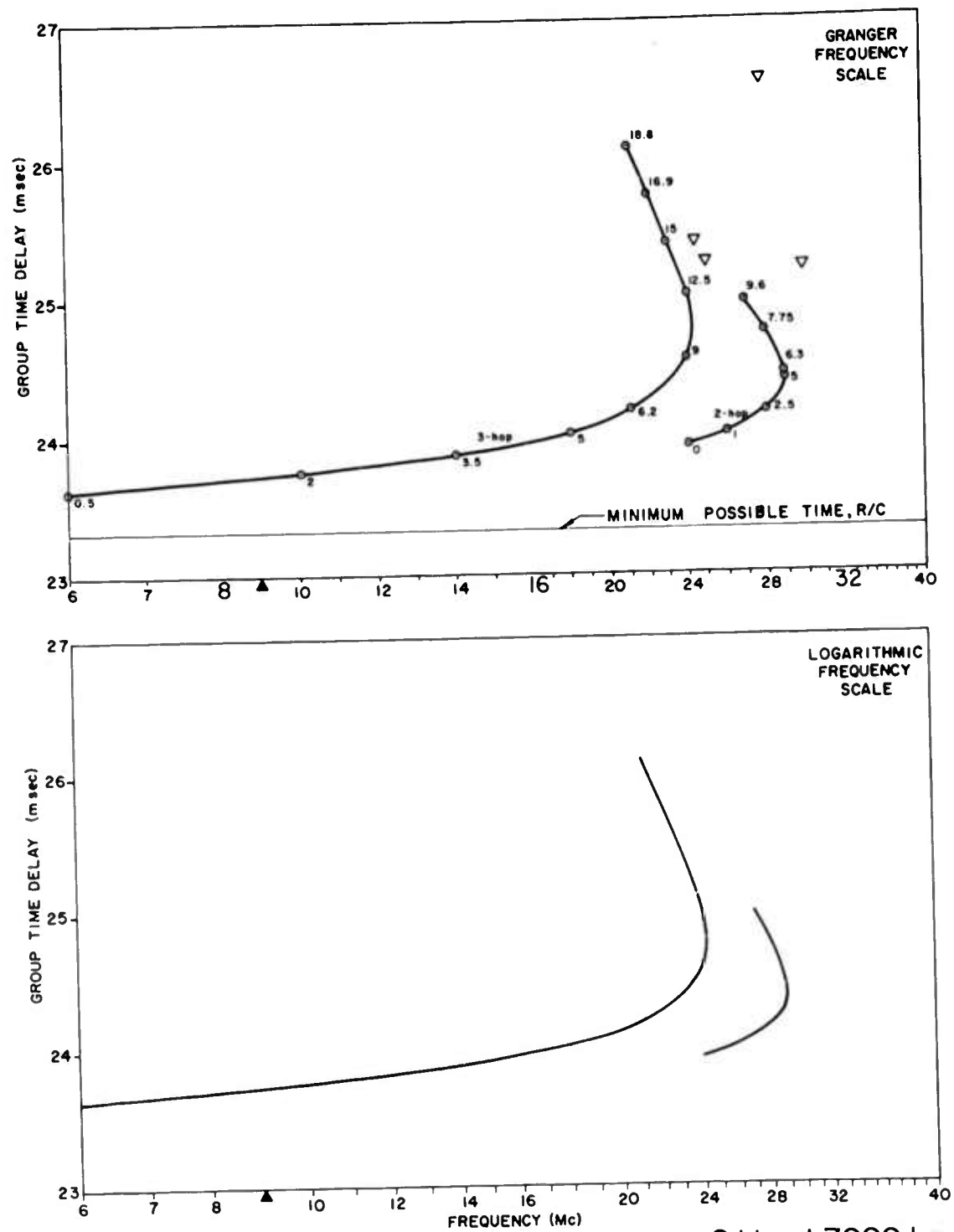


FIG. 10. IONOGRAM FOR IID O11; SEPARATION DISTANCE, 7000 km.

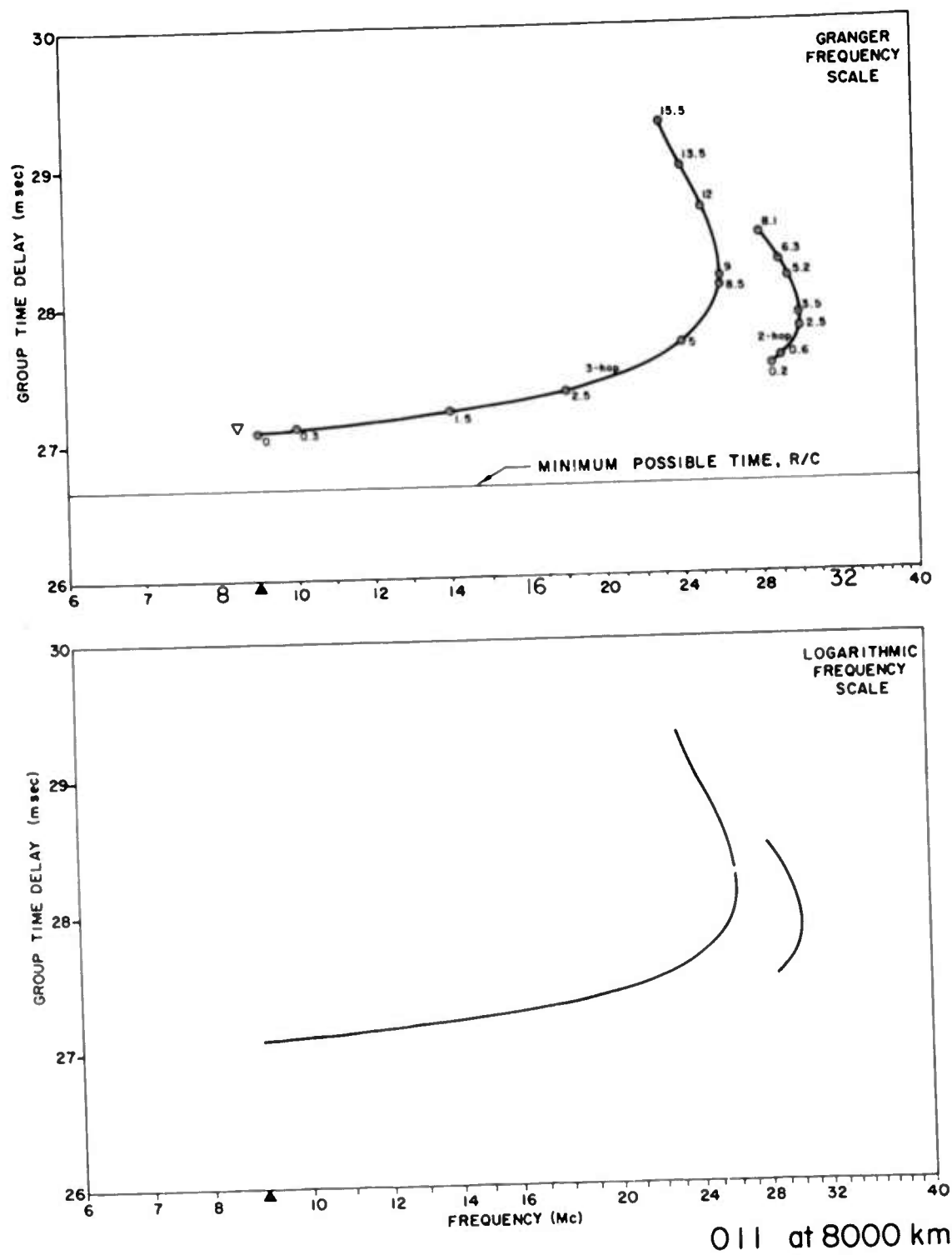


FIG. 11. IONOGRAM FOR 11D 011; SEPARATION DISTANCE, 8000 km.

B. WEAK AND STRONG E-LAYERS AT VARIOUS RANGES

In order to investigate the effect of an E layer on oblique ionograms, the electron-density distribution IID 011 was modified with a weak E layer (IID 012) and a strong E layer (IID 089) as shown in Fig. 12. These particular electron distributions were chosen subjectively with the idea that 012 is fairly typical and 089 is more prominent than the average E layer encountered in nature.

Ionograms for 012 were calculated at the same nine ranges presented on the Chapman layer 011 (Figs. 13 through 21), whereas, because 089 is atypical, its ionogram was calculated only at 0 and 3000 km (Figs. 22 and 23). Since 012 is identical to 011 in all respects except the addition of the E layer, the comparisons of these ionograms are particularly interesting. One can also compare the 3000-km ionograms for 011, 012, and 089 and see the effect of the degree of ionization in the E layer.

The ionograms calculated for Chapman layer 011 are repeated in red on the lower (logarithmic) presentations of these ionograms to permit a clearer visualization of the changes caused by the presence of the E layer. In addition, the 089 oblique ionogram shows (in blue) the corresponding trace obtained for IID 012.

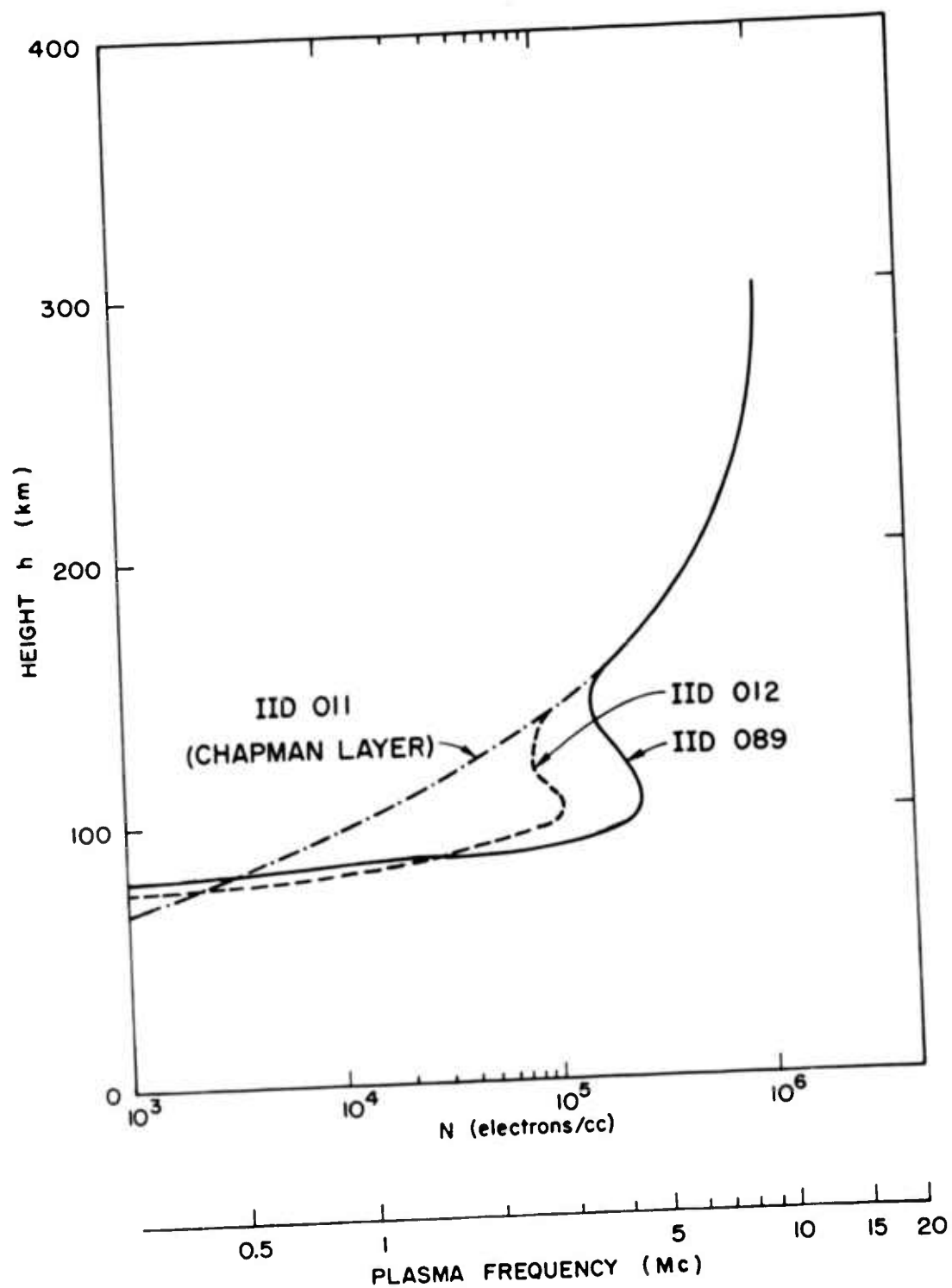


FIG. 12. ELECTRON-DENSITY DISTRIBUTIONS FOR IIDs 011, 012, AND 089.

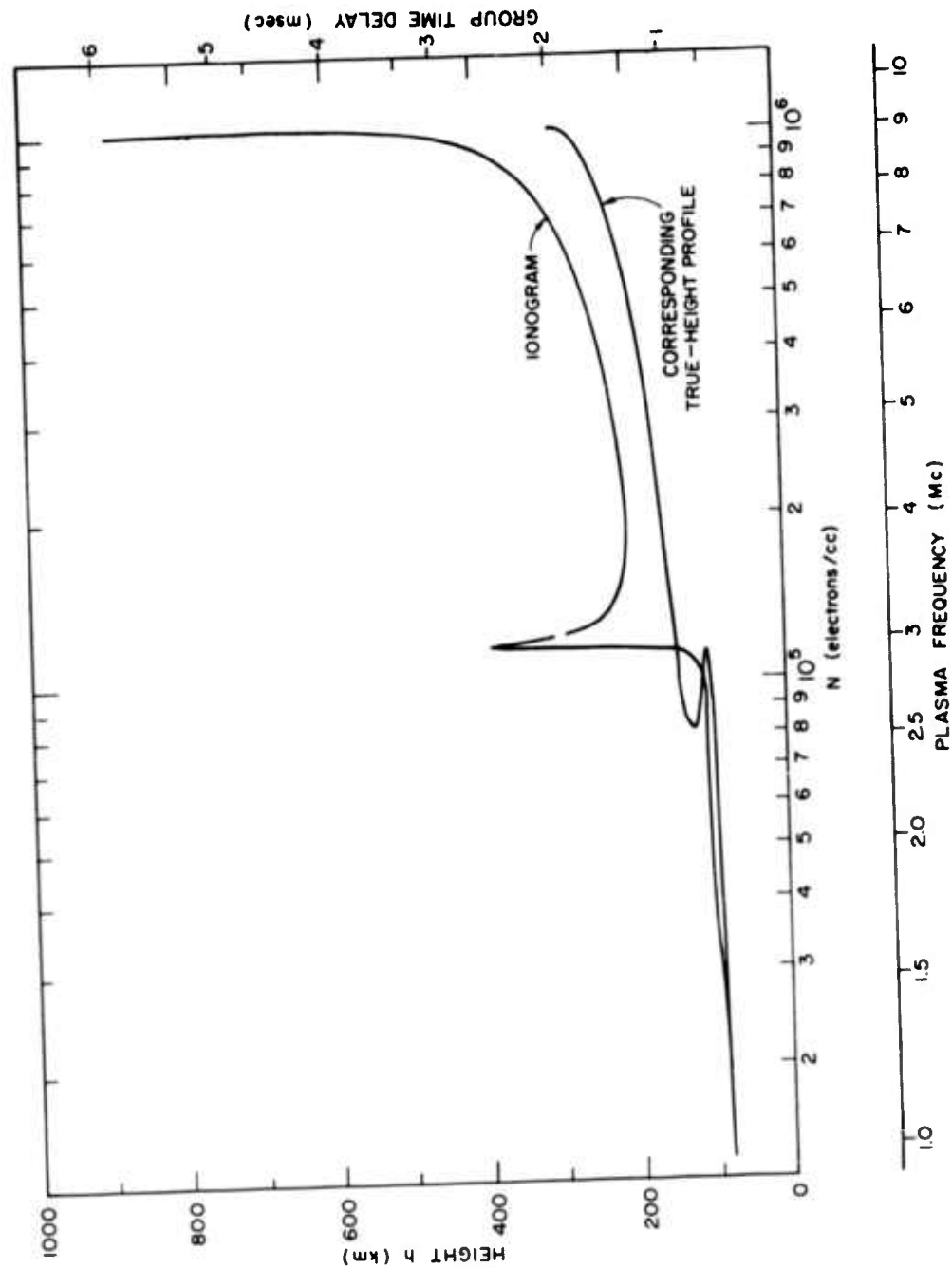
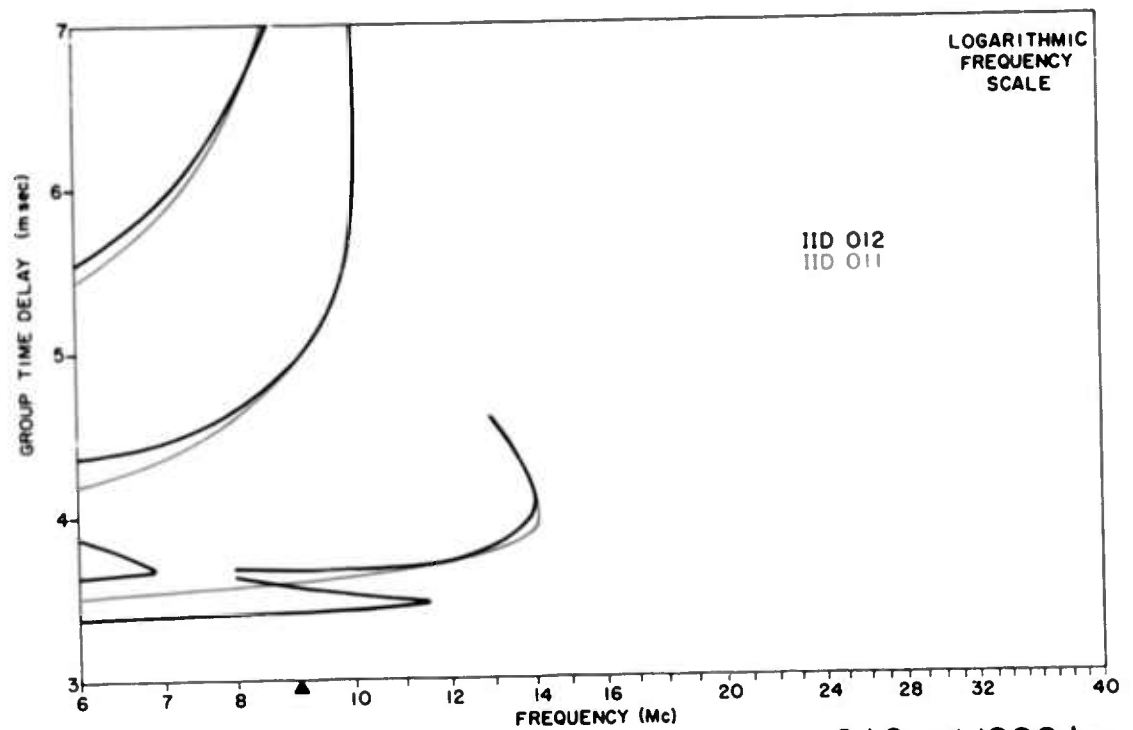
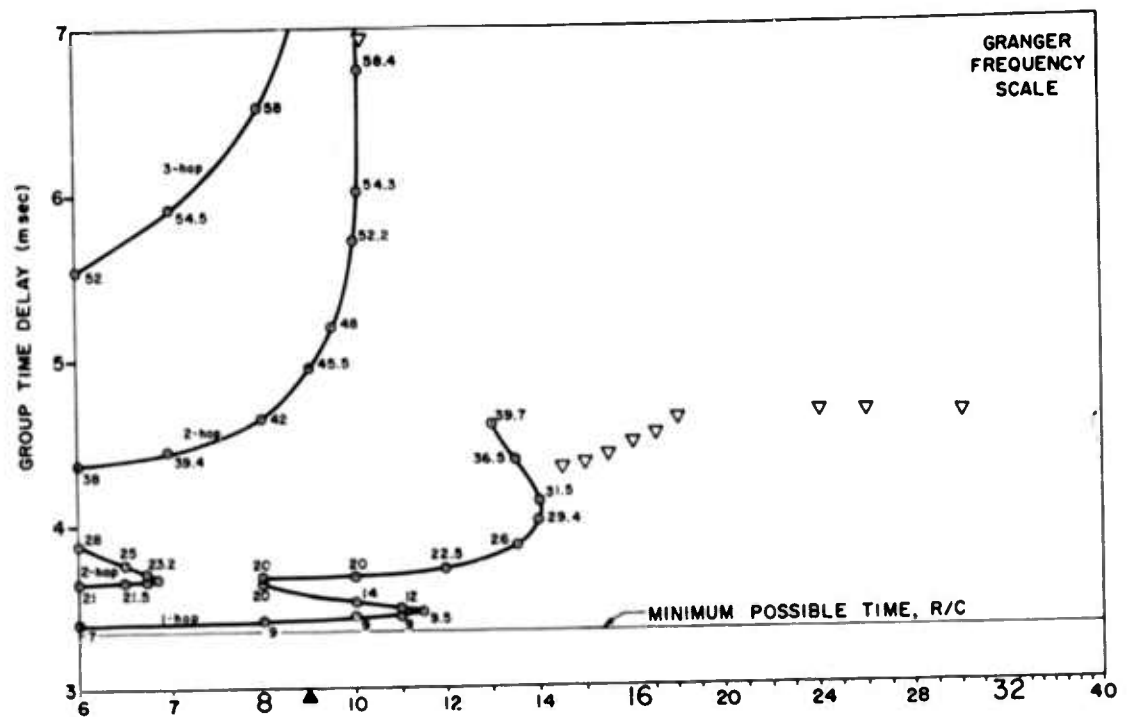


FIG. 13. IONOGRAM FOR I1D 012; SEPARATION DISTANCE, 0 km.



IID 012
IID 011

012 at 1000 km

FIG. 14. IONOGRAM FOR IID 012; SEPARATION DISTANCE, 1000 km.

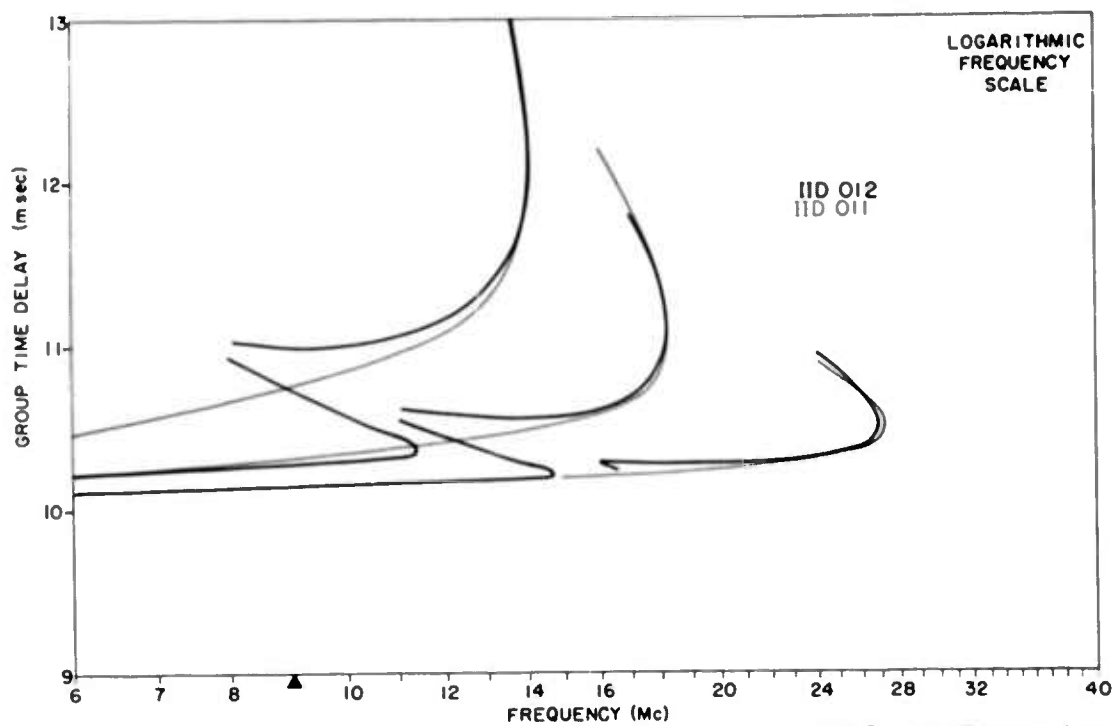
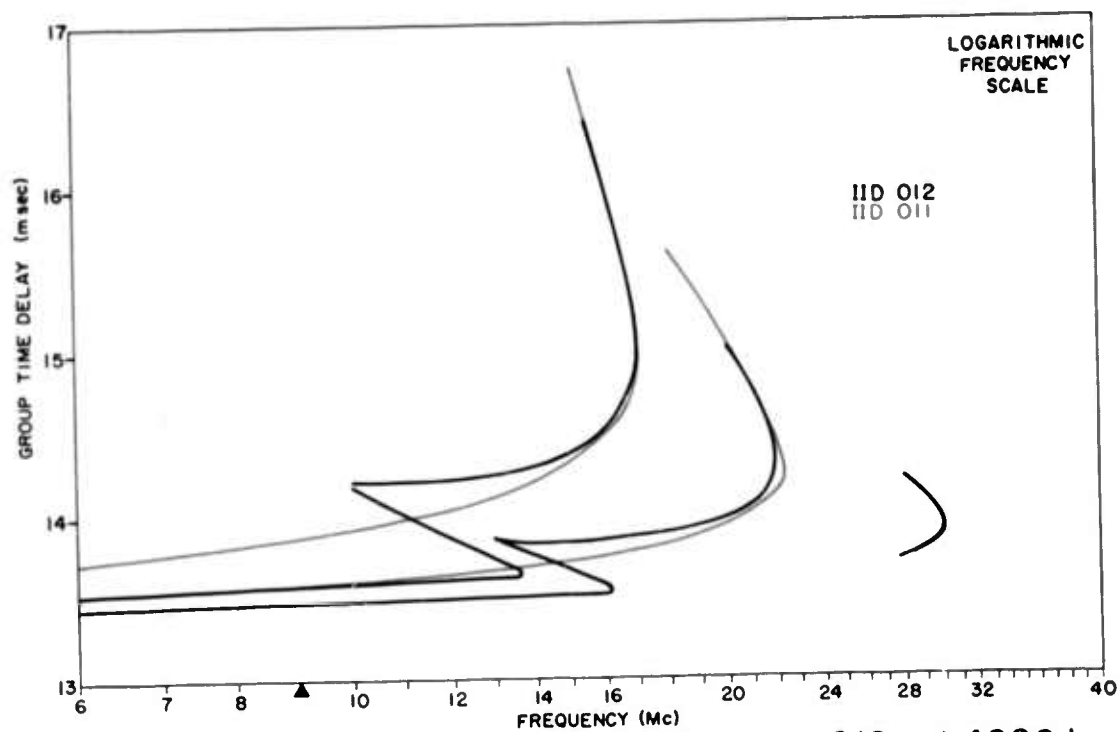


FIG. 16. IONOGRAM FOR IID 012; SEPARATION DISTANCE, 3000 km.



SEL-64-106

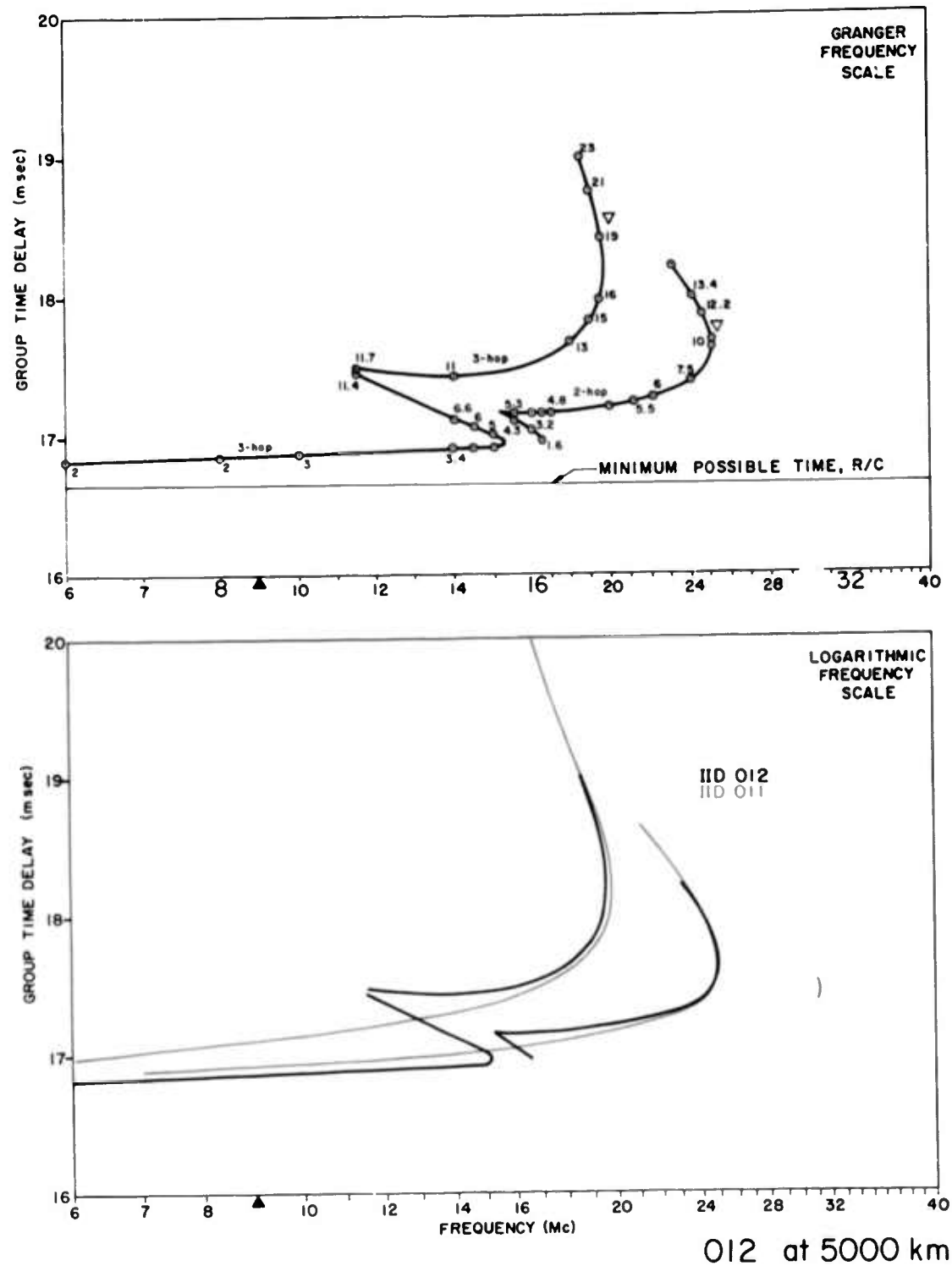


FIG. 18. IONOGRAM FOR IID 012; SEPARATION DISTANCE, 5000 km.

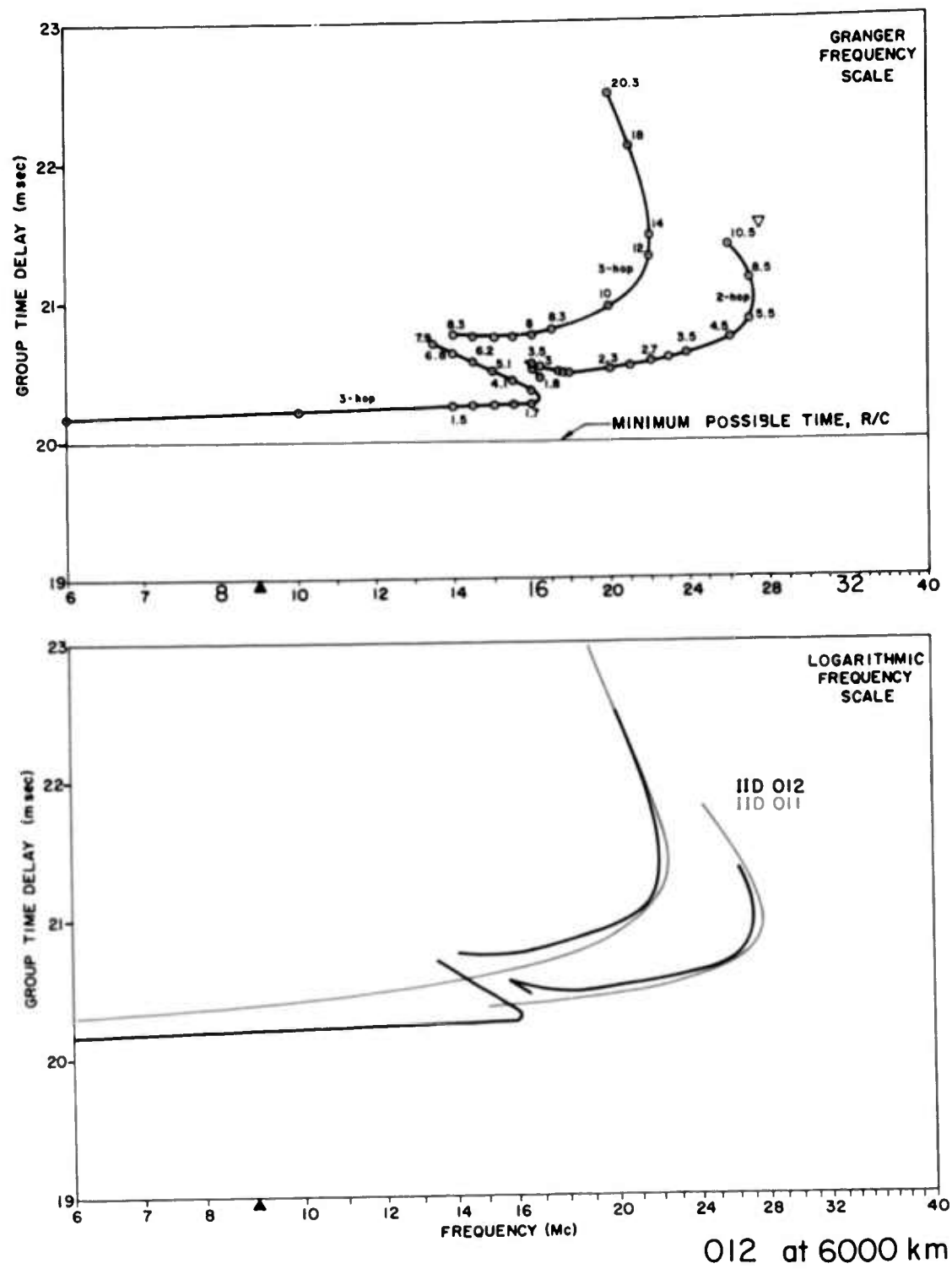


FIG. 19. IONOGRAM FOR IID 012; SEPARATION DISTANCE, 6000 km.

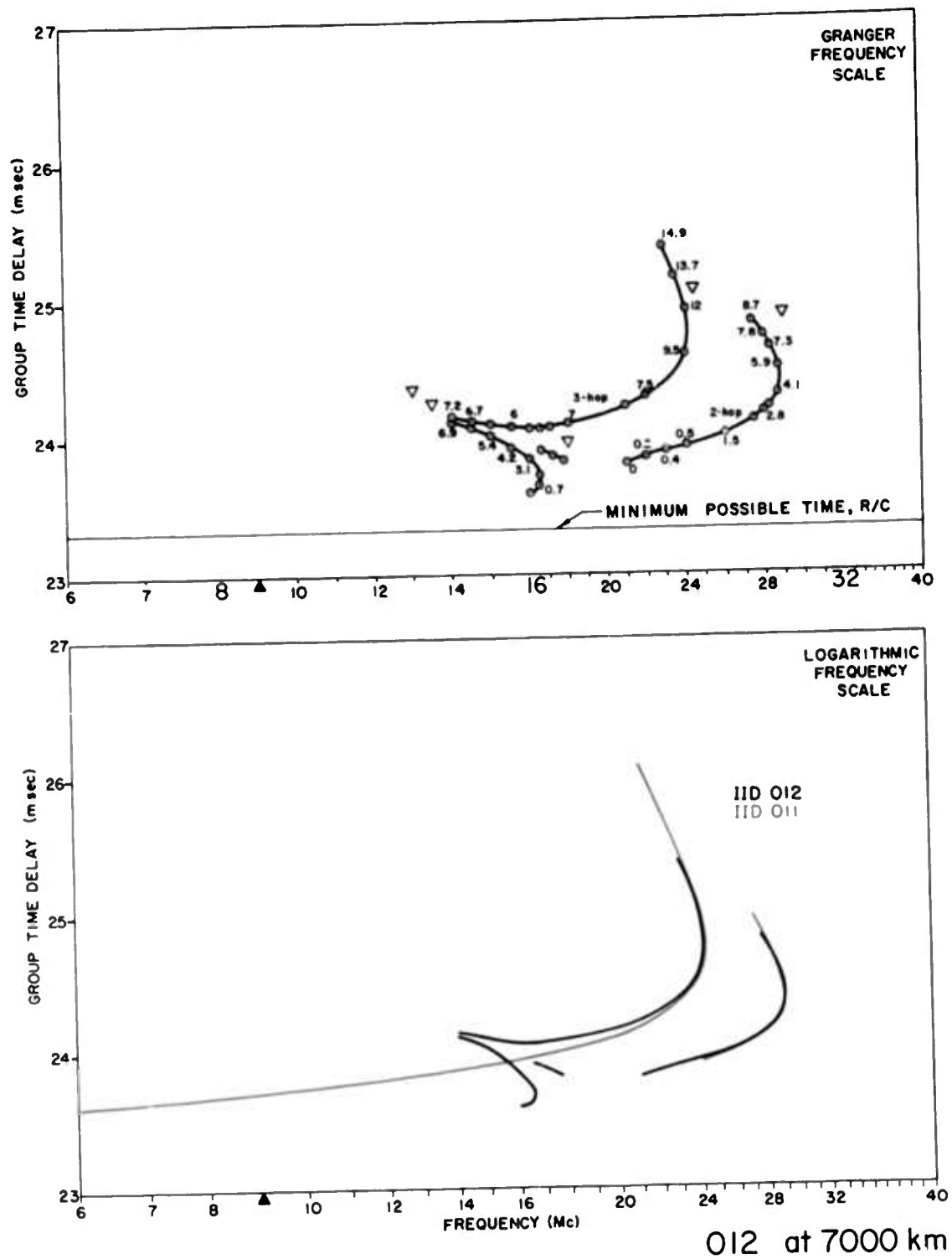


FIG. 20. IONOGRAM FOR IID 012; SEPARATION DISTANCE, 7000 km.

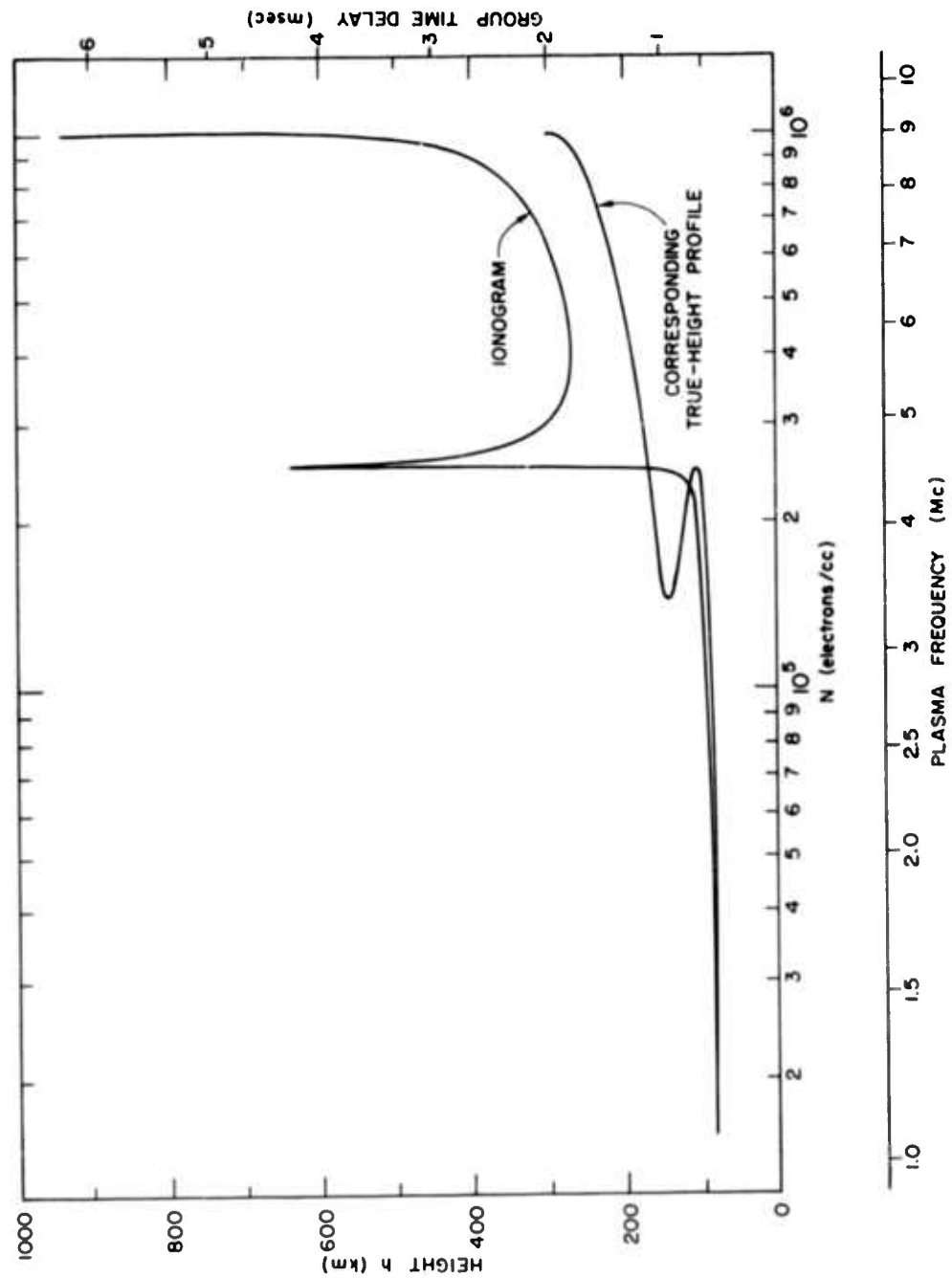


FIG. 22. IONOGRAM FOR 11D 089; SEPARATION DISTANCE, 0 km.

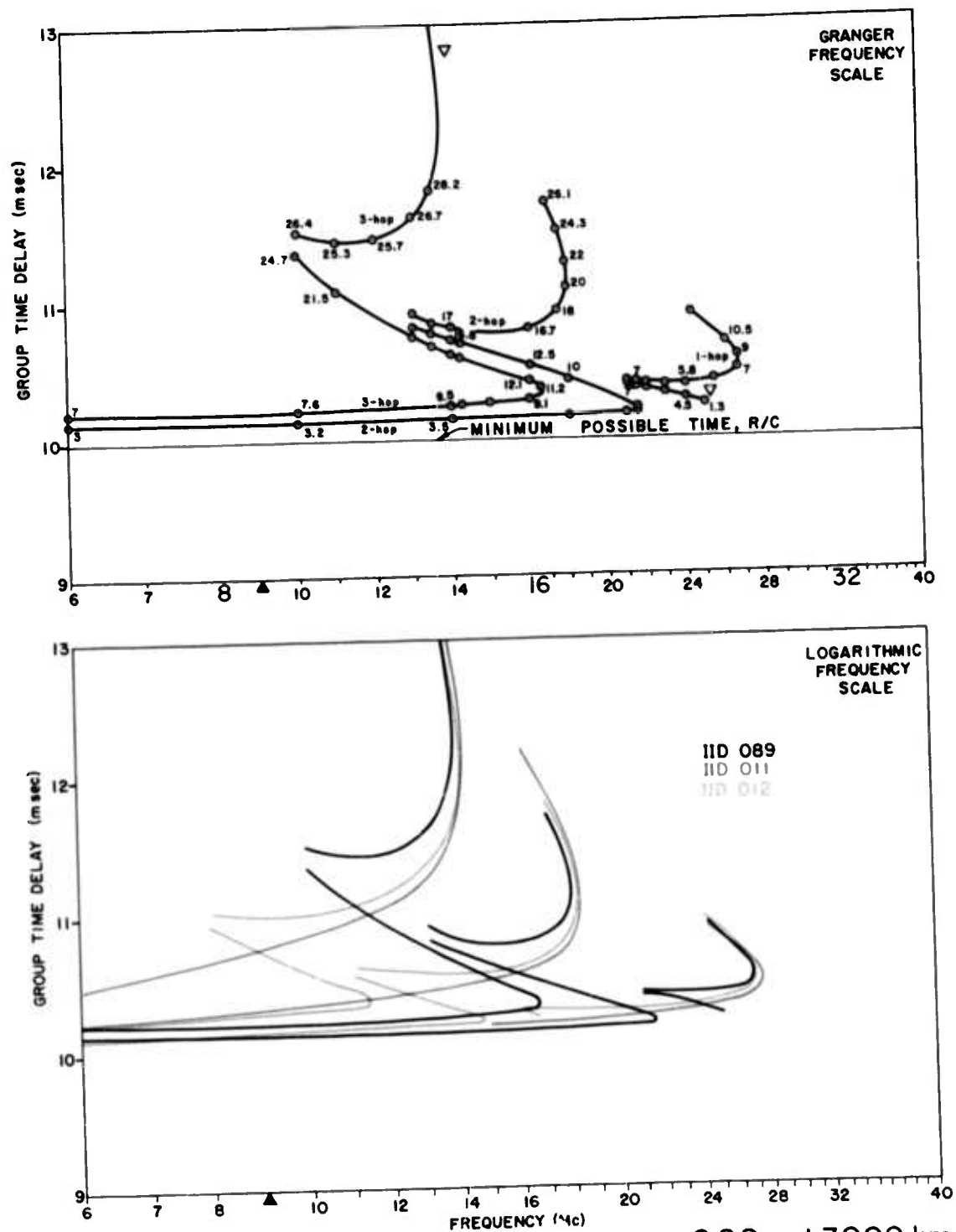


FIG. 23. IONOGRAM FOR IID 089; SEPARATION DISTANCE, 3000 km.

C. CHANGES IN LAYER HEIGHT

The effect of changes in the height of the maximum electron density in a Chapman layer is examined here. The oblique ionograms are calculated only for a separation distance of 3000 km. Two new ionospheres were generated, with H_m 's selected so that their heights bracketed the value used for IID 011. Also, in order to maintain the similarity to 011, it was decided to maintain the ratio $H_m/H_s = 3$. This ratio resulted in the following:

<u>IID</u>	<u>H_m (km)</u>	<u>H_s (km)</u>
053	200	66.7
011	300	100
054	400	133.3

The maximum electron density for the new ionospheres is still 10^6 per cc, as it was for 011. These new electron-density distributions are shown together with 011 in Fig. 24. The 3000-km ionograms calculated using these new ionospheres are shown on Figs. 25 and 26. For comparison purposes, the appropriate oblique ionogram for ionosphere 011 is repeated in red on the logarithmic presentations that follow.

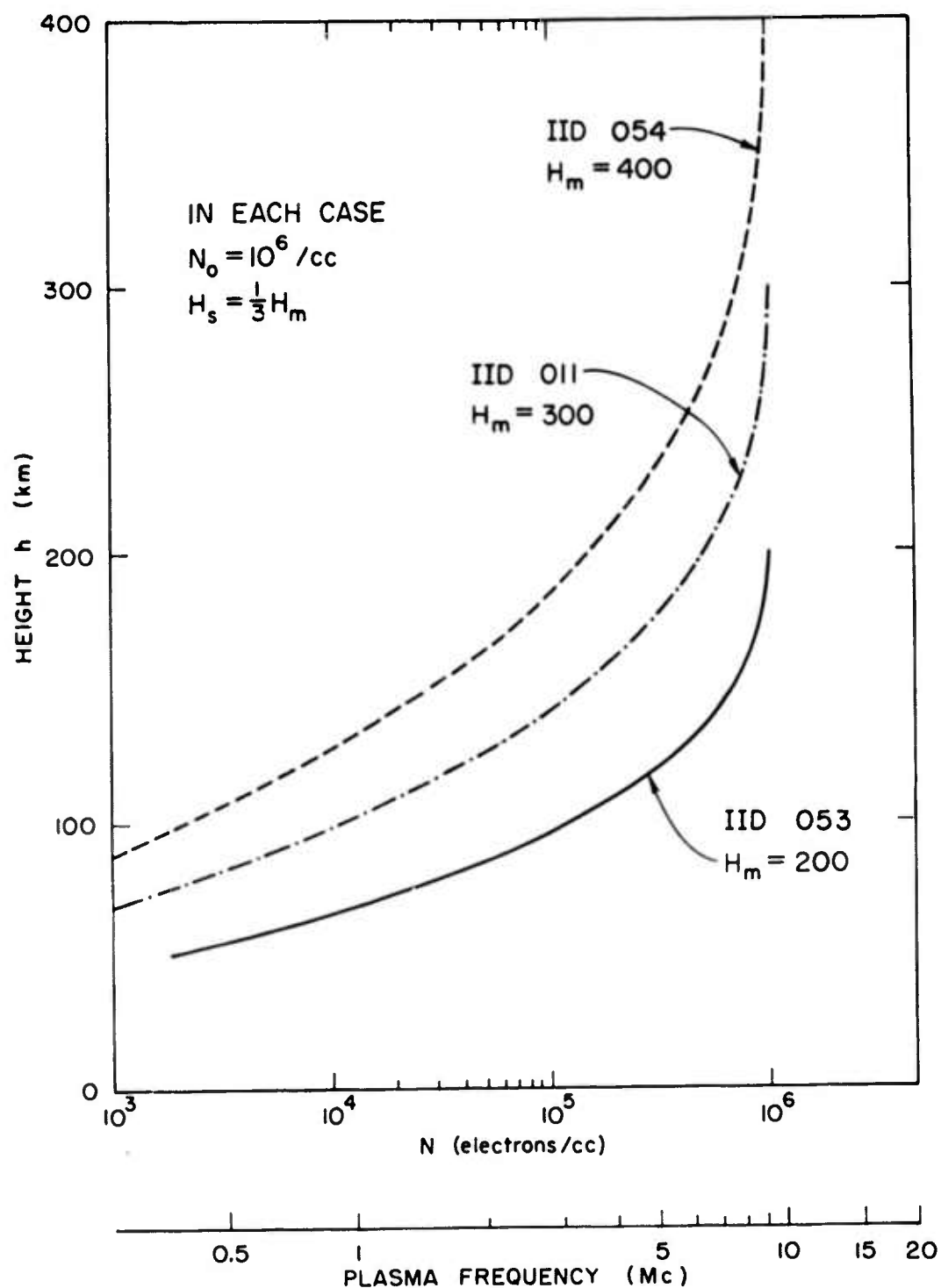


FIG. 24. ELECTRON-DENSITY DISTRIBUTIONS FOR IIDs 011, 053, AND 054.

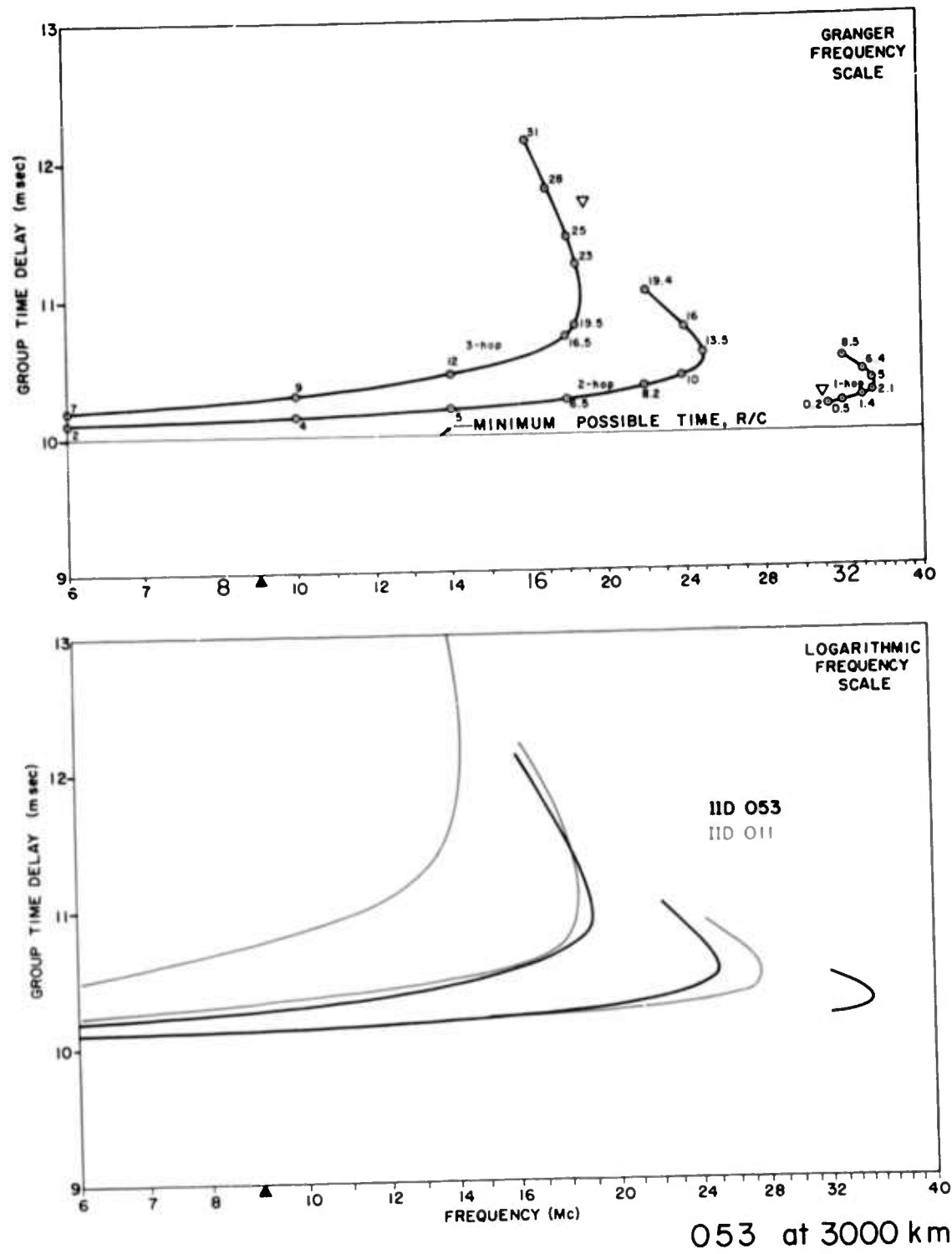
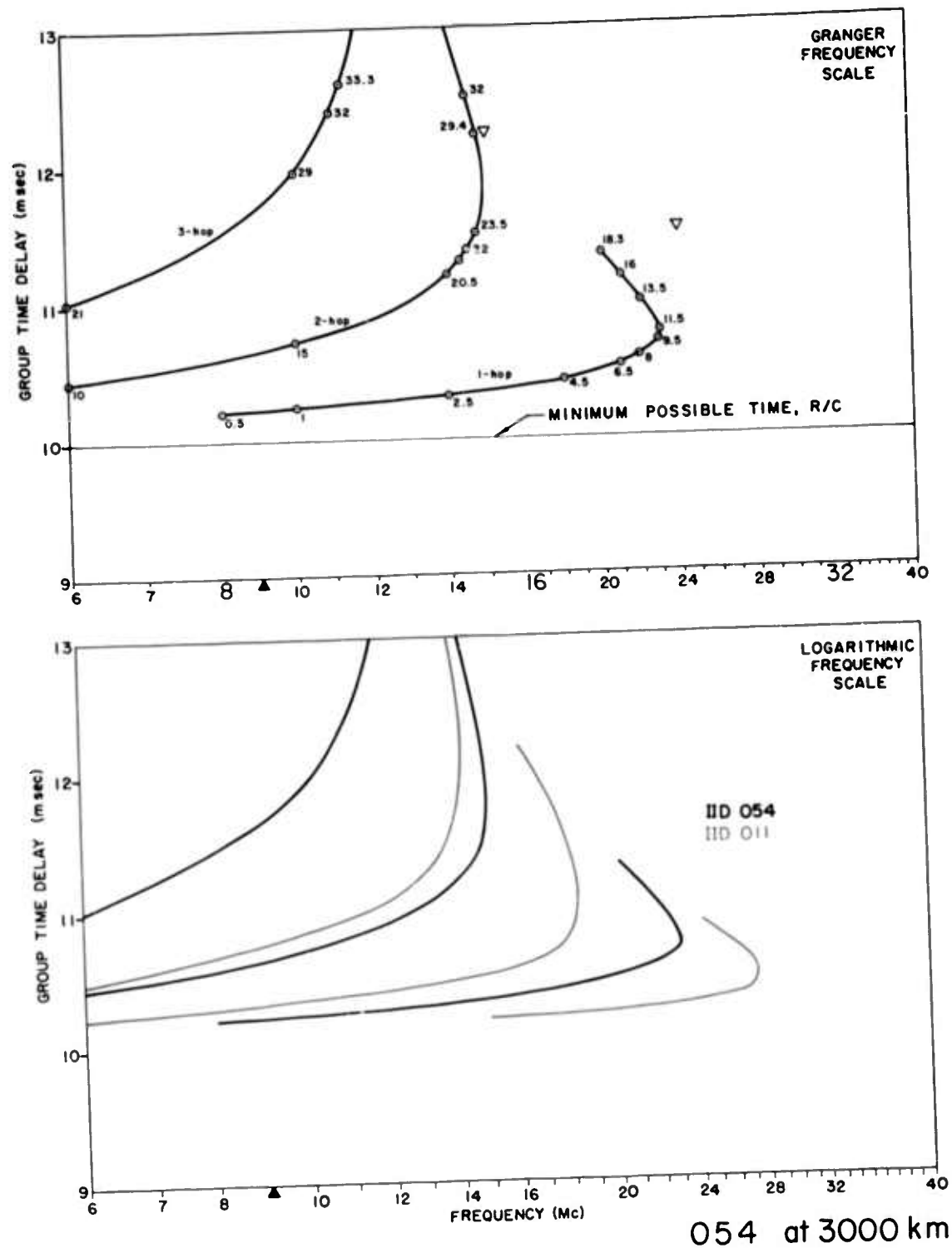


FIG. 25. IONOGRAM FOR IID 053; SEPARATION DISTANCE, 3000 km;
LOW CHAPMAN LAYER.



D. CHANGES IN SCALE HEIGHT

The effect of changes in the scale height of a Chapman layer (when the height of the maximum density is fixed) is now examined. In order to do this, two new ionospheres were generated, again bracketing the "standard" Chapman layer. The values chosen were as follows:

<u>IID</u>	<u>H_m (km)</u>	<u>H_s (km)</u>
055	300	80
011	300	100
056	300	120

These ionospheres are shown on Fig. 27 for comparison. The new ionograms, generated for a 3000-km separation distance only, are shown in Figs. 28 and 29. Again, these figures show the corresponding oblique ionogram for IID 011 in red on the logarithmic presentations.

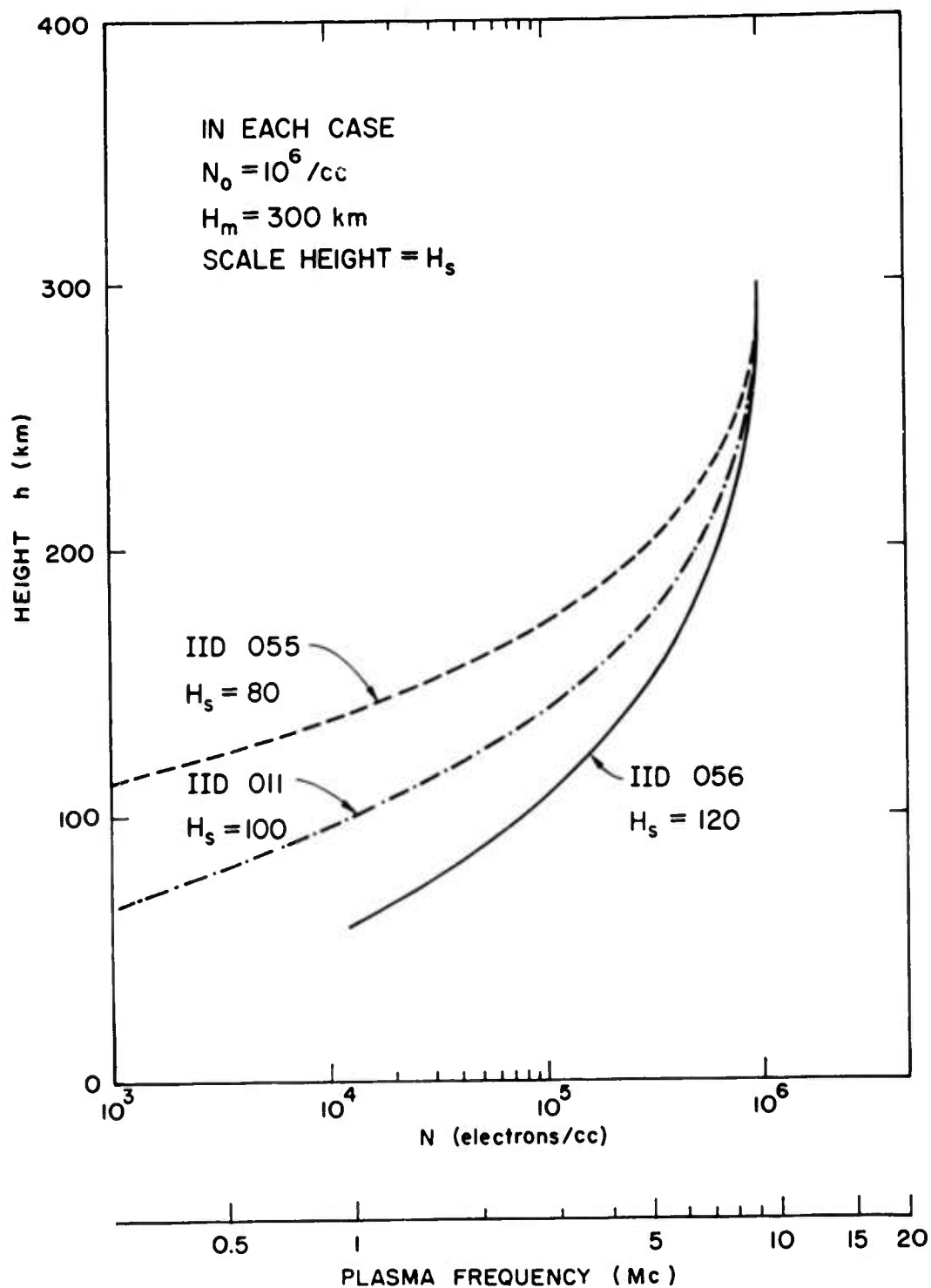


FIG. 27. ELECTRON-DENSITY DISTRIBUTIONS FOR IIDs 011, 055, AND 056.

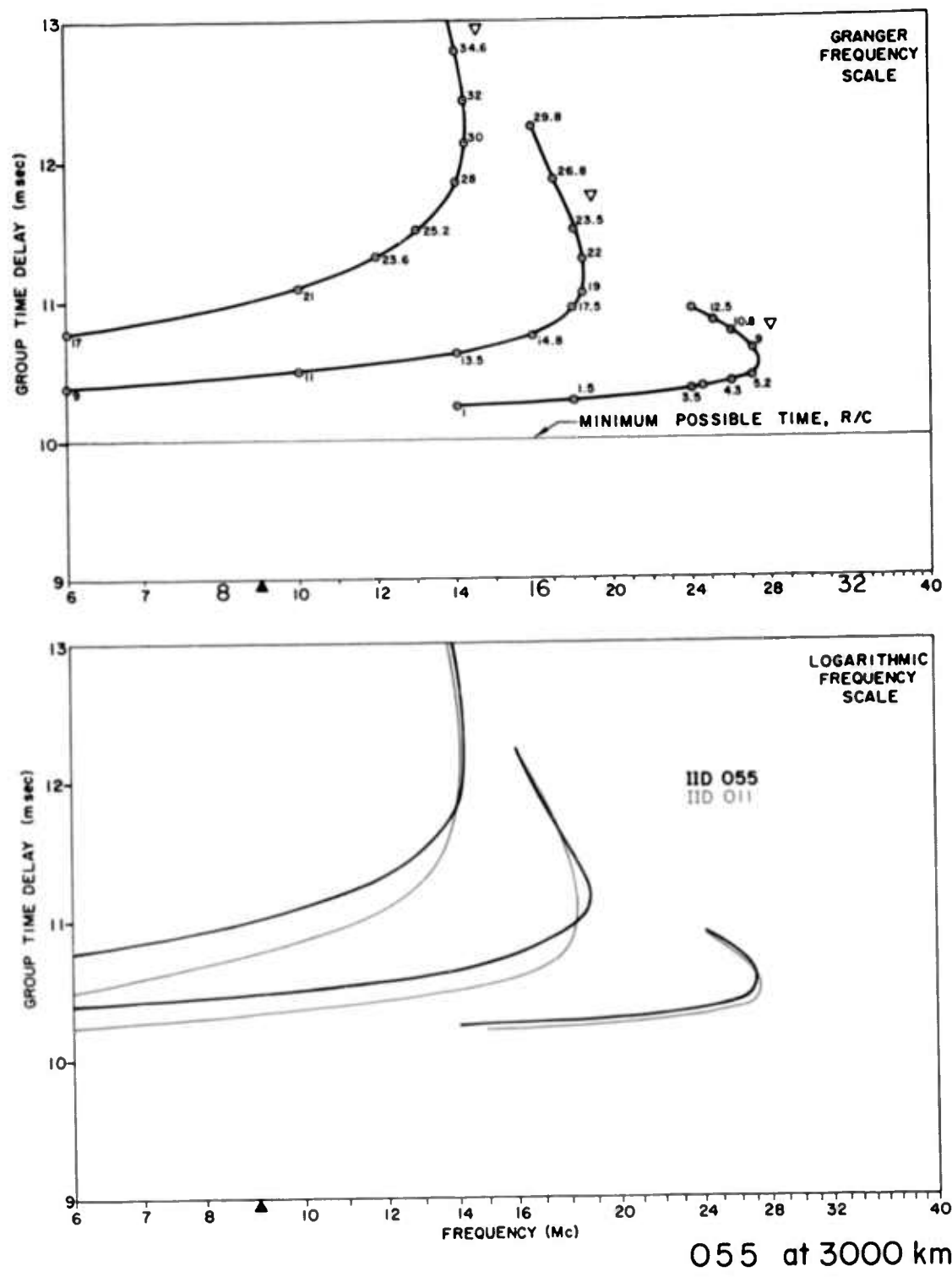


FIG. 28. IONOGRAM FOR IID 055; SEPARATION DISTANCE, 3000 km;
SMALL SCALE HEIGHT.

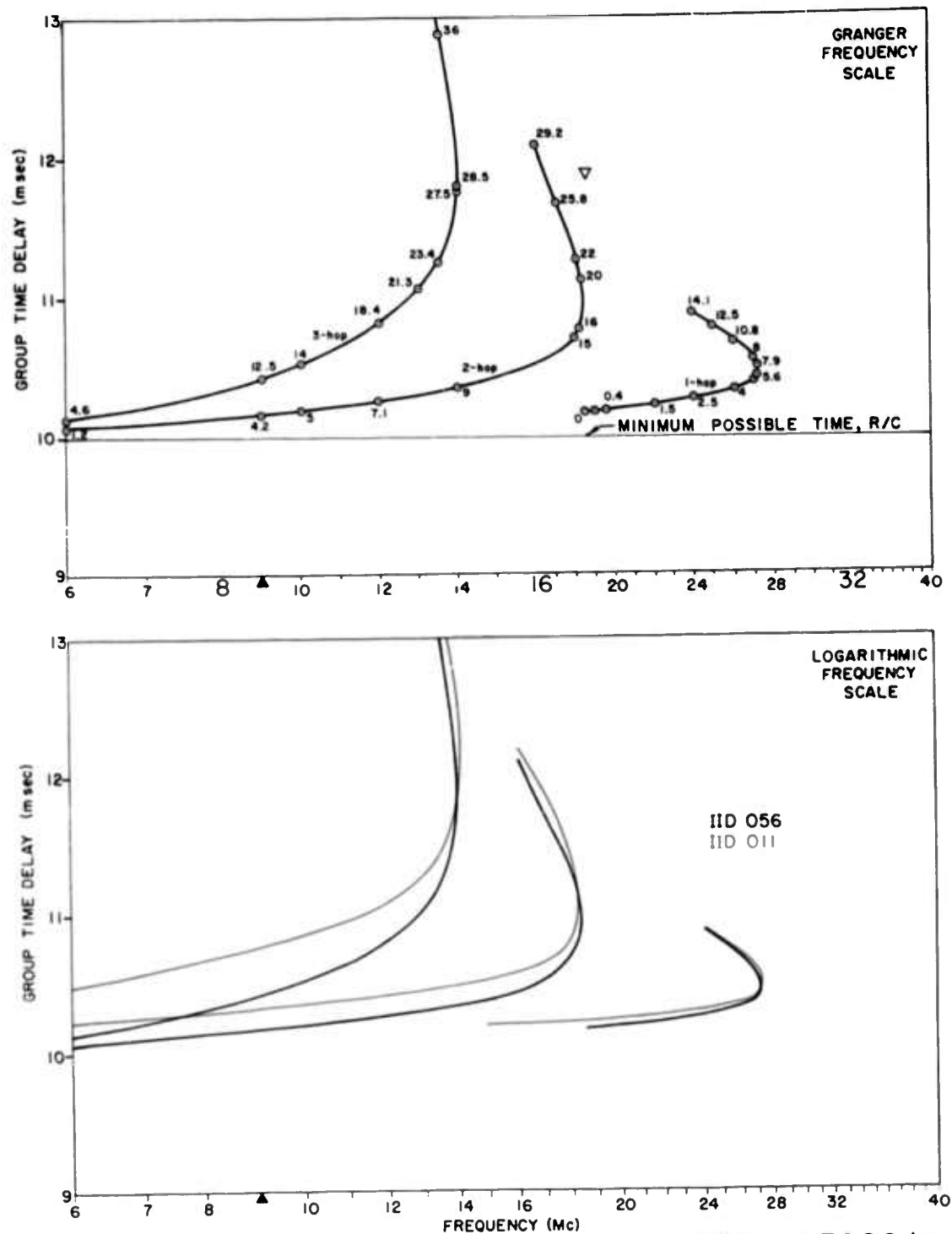


FIG. 29. IONOGRAM FOR IID 056; SEPARATION DISTANCE, 3000 km; LARGE SCALE HEIGHT.

E. HORIZONTAL GRADIENTS WITHIN A CHAPMAN LAYER

To investigate the effect of horizontal gradients on synthetic ionograms, a tilted ionosphere was generated according to the following specifications: directly above the transmitter, the electron-density distribution varies with altitude like that of IID 011, except that $N_0 = 2 \times 10^6$, exactly twice the electron density that was present in IID 011. If one traveled 4000 km from the transmitter in the direction of the receiver and then measured the electron-density distribution, one would again find a Chapman layer, except that then $N_0 = \frac{1}{2} \times 10^6$. Thus the electron-density distribution is fixed above two points along the path.

In order to specify the method of variation from one extreme to the other, it was decided to make electron density a linear function of range between 0 and 4000 km and then nontilted beyond 4000. This rather complicated distribution is labeled IID = 093. A similar ionosphere (IID 094) was generated, but in it the electron-density profiles at the two end points of the path were switched. Another way of looking at this is to think of a 4000-km separation distance between transmitter and receiver with the tilted ionosphere existing only between them. Then, for IID 093, the transmitter is under the most dense ionosphere and the receiver is under the least dense ionosphere. For IID 094, the transmitter and receiver positions are switched.

It is interesting to note that reciprocity should apply, and indeed it does, for if the reader will examine the 4000-km ionograms, he will see that they are indeed identical, even though different raytracings were used to generate them. The takeoff angles, however, are different because the takeoff angles for one ionogram are the landing angles of the other.

The electron-density distributions of the end points of these two ionograms are shown on Fig. 30. Vertical-incidence ionograms are not shown because they would be identical in form to those of Fig. 3, except for this scale shift, which has been discussed. For each of these two ionospheres three ionograms are given, in Figs. 31 through 36.

The logarithmic presentation of each ionogram also shows, in red, the ionogram that would be obtained if one calculated on the basis of the electron-density profile above the path midpoint without any horizontal tilt.

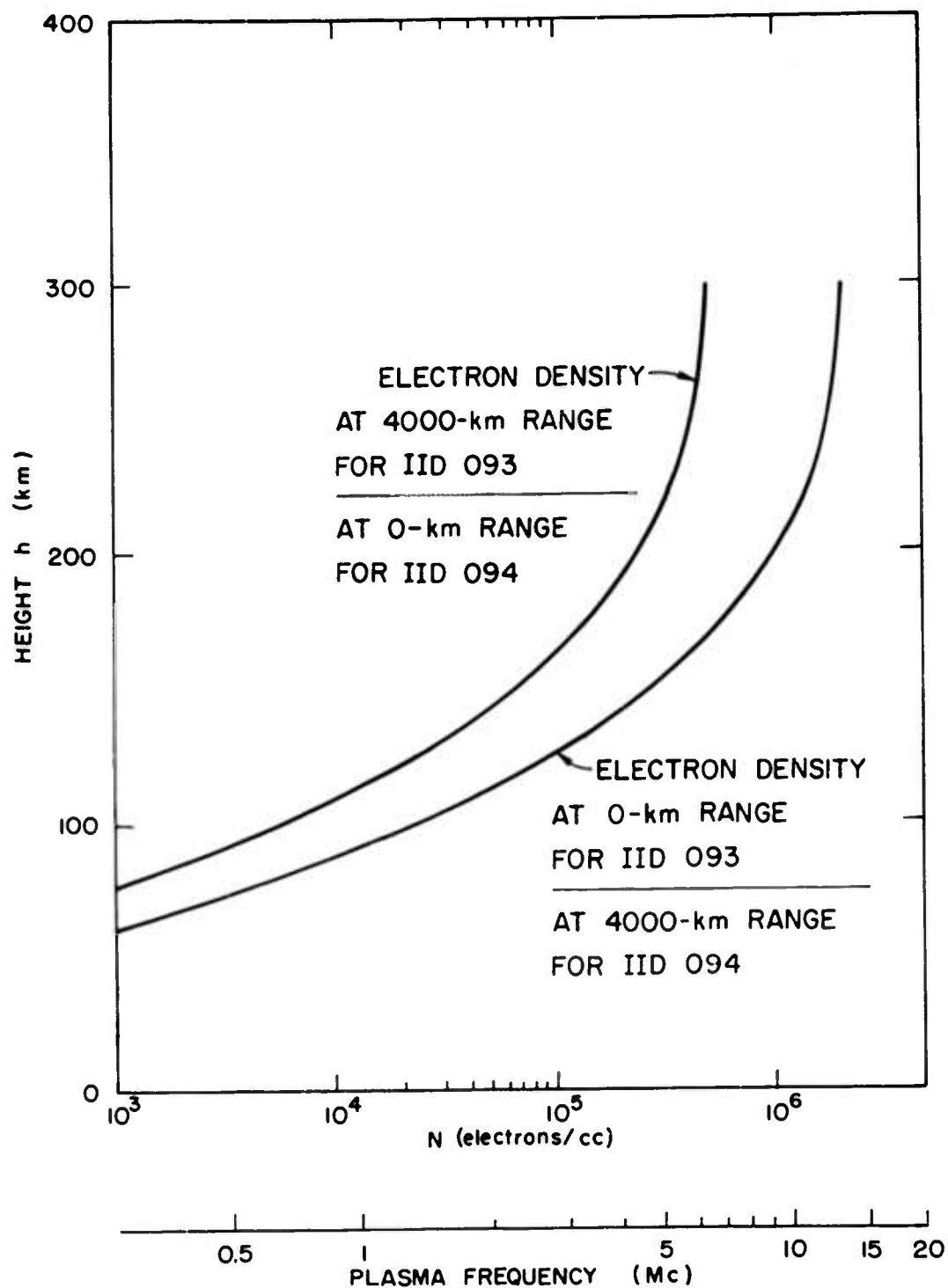
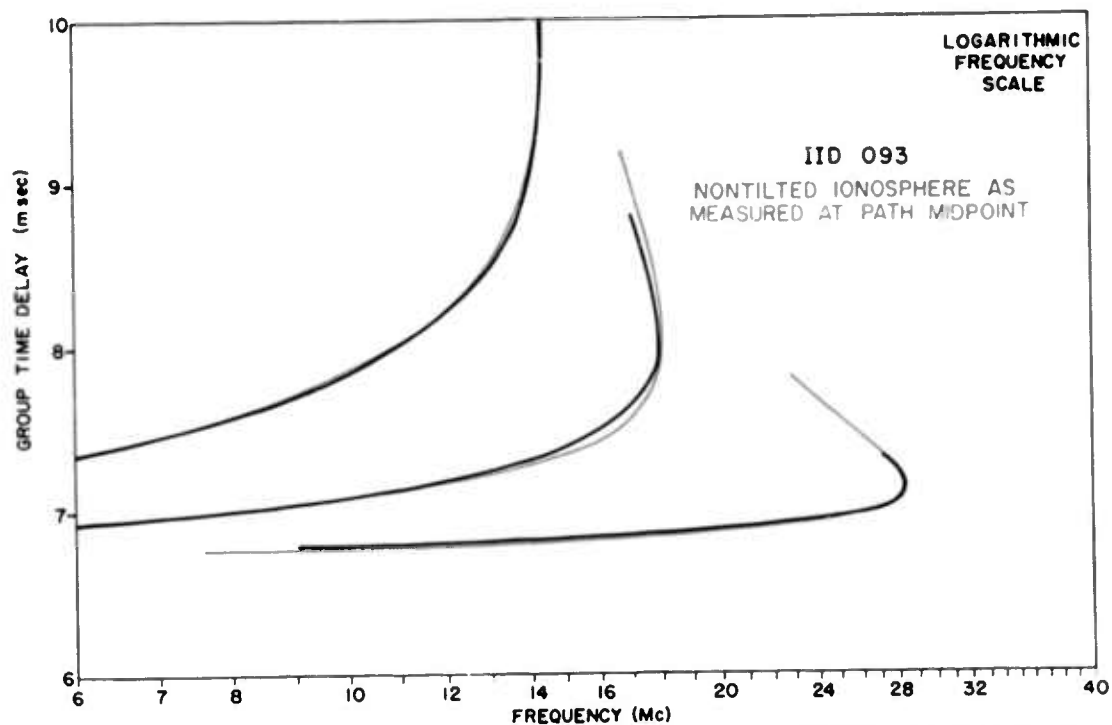
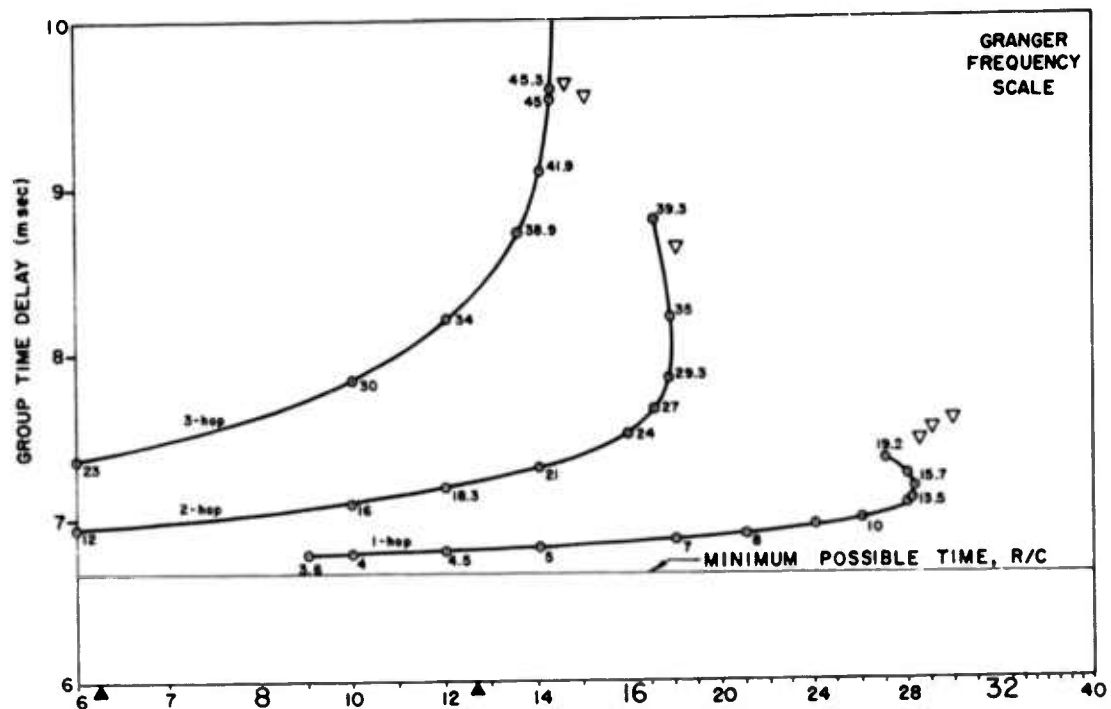


FIG. 30. ELECTRON DENSITIES AT PATH ENDPOINTS FOR IIDs 093 AND 094.



093 at 2000 km

FIG. 31. IONOGRAM FOR IID 093; SEPARATION DISTANCE, 2000 km.

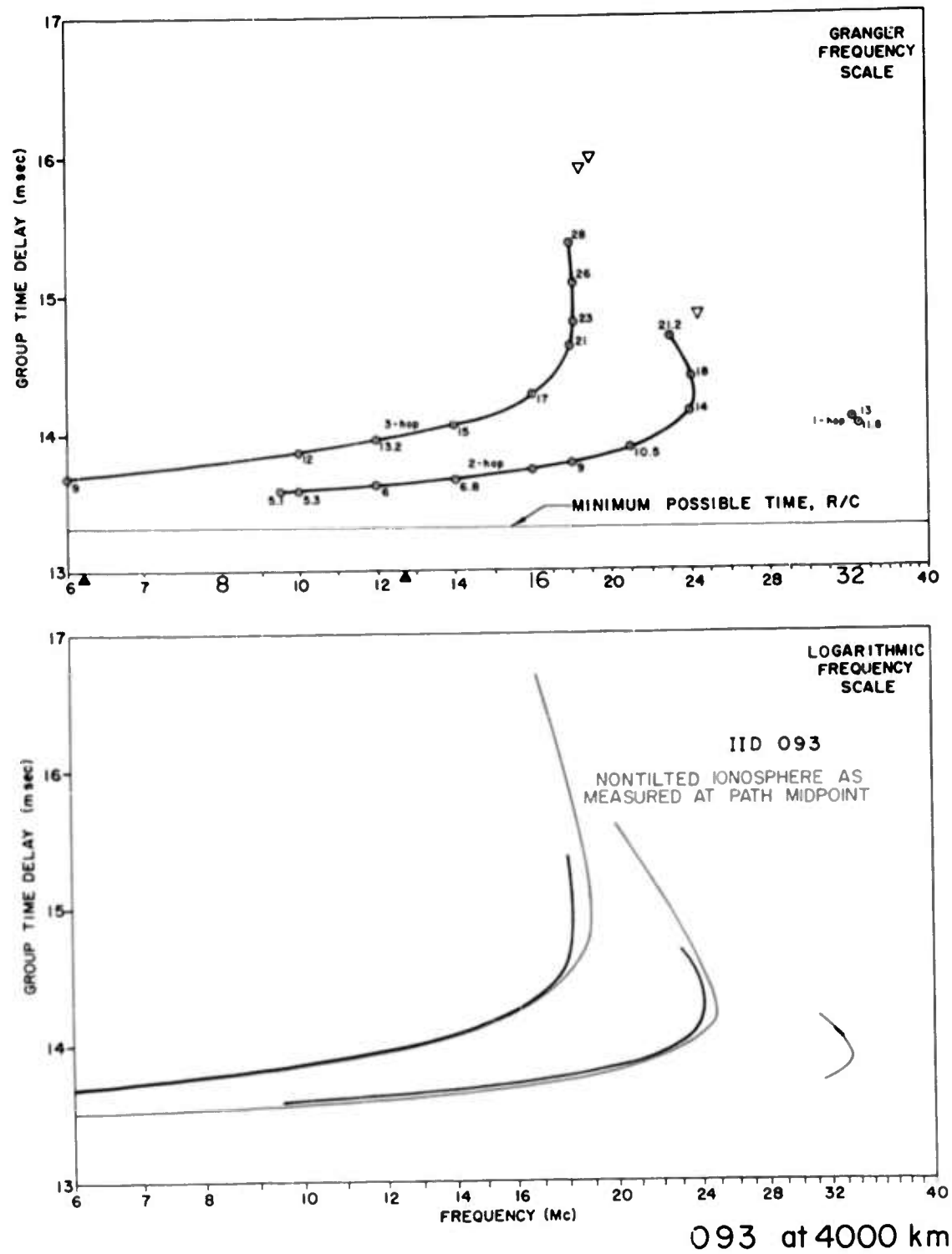


FIG. 32. IONOGRAM FOR IID 093; SEPARATION DISTANCE, 4000 km.

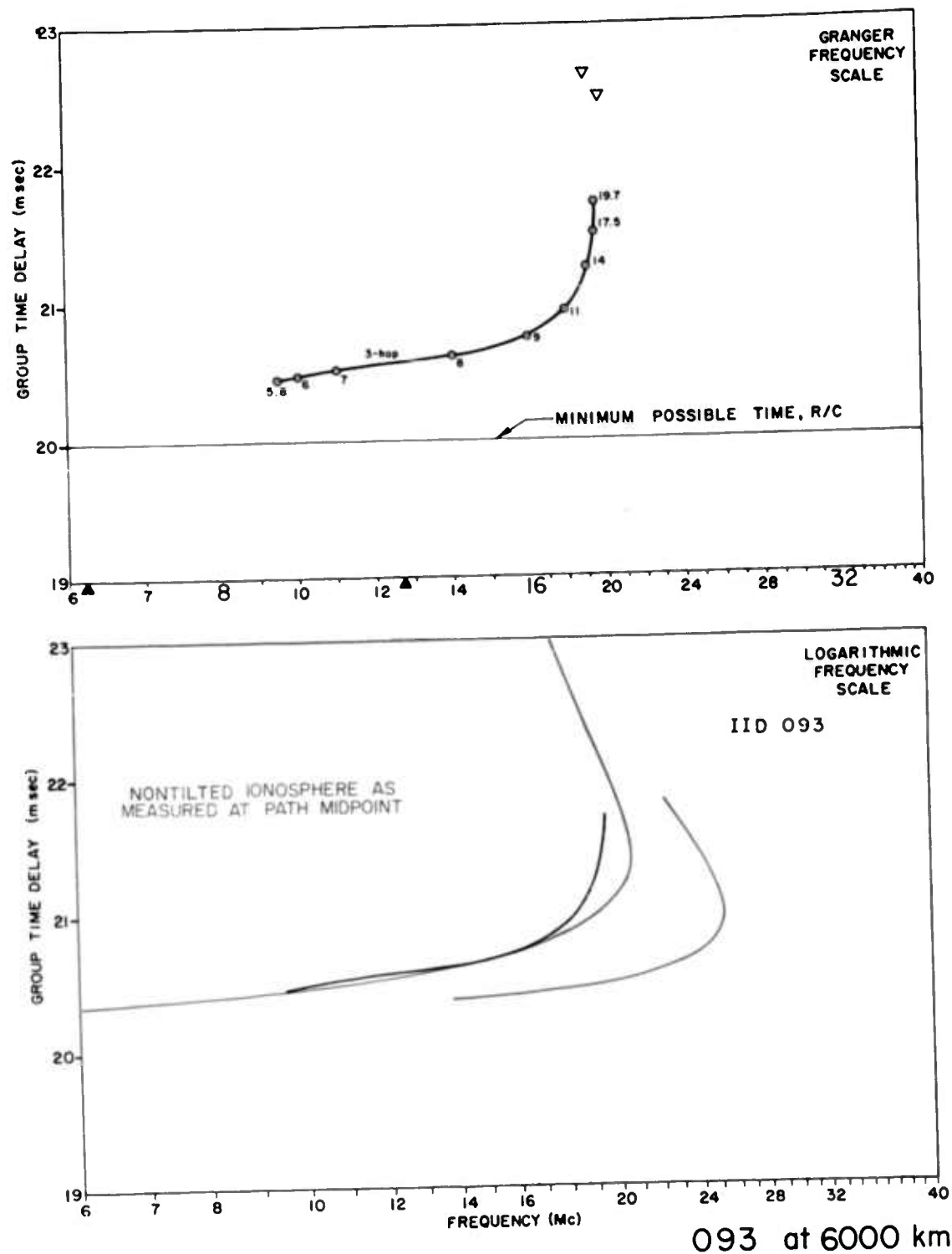
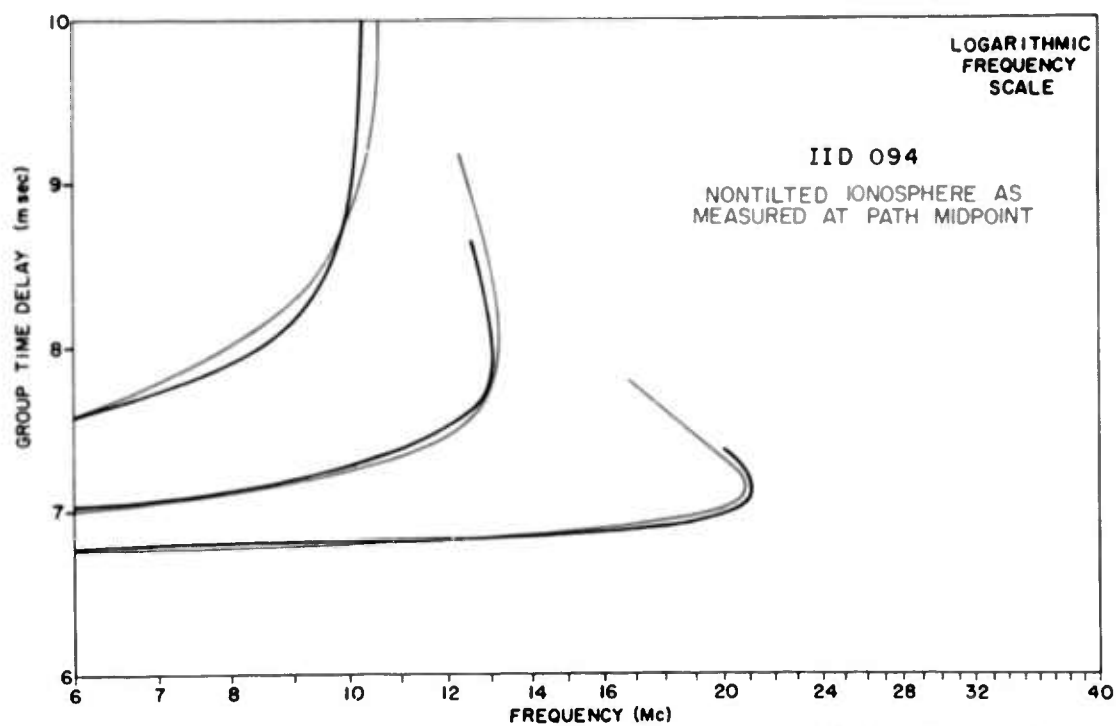
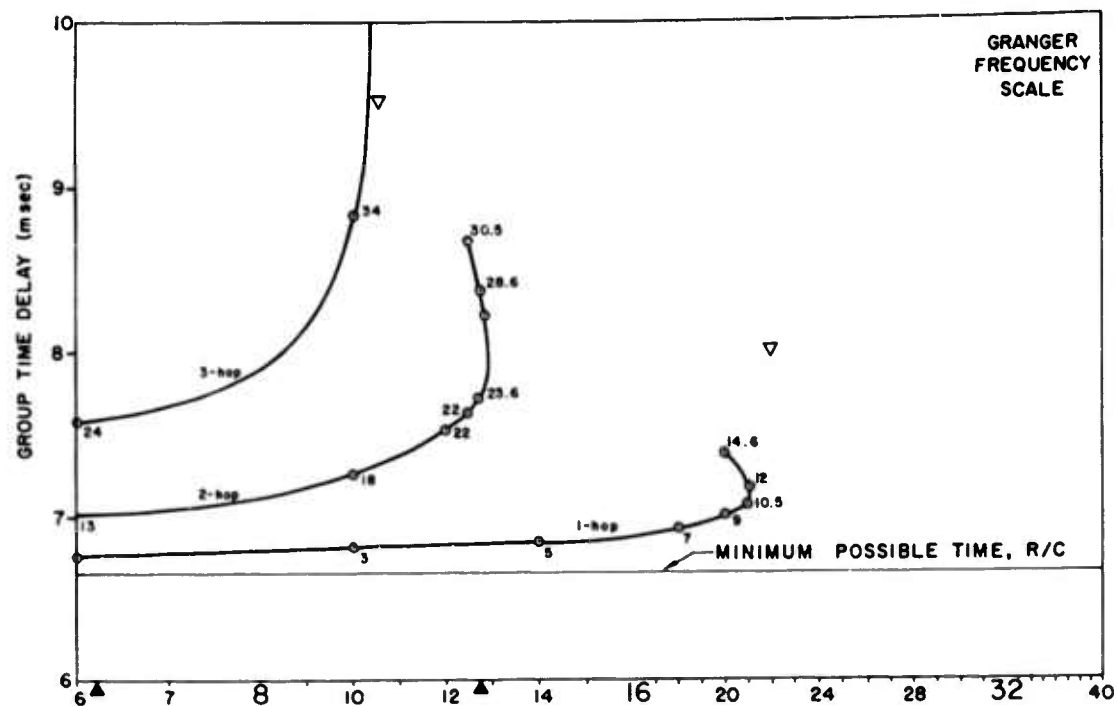
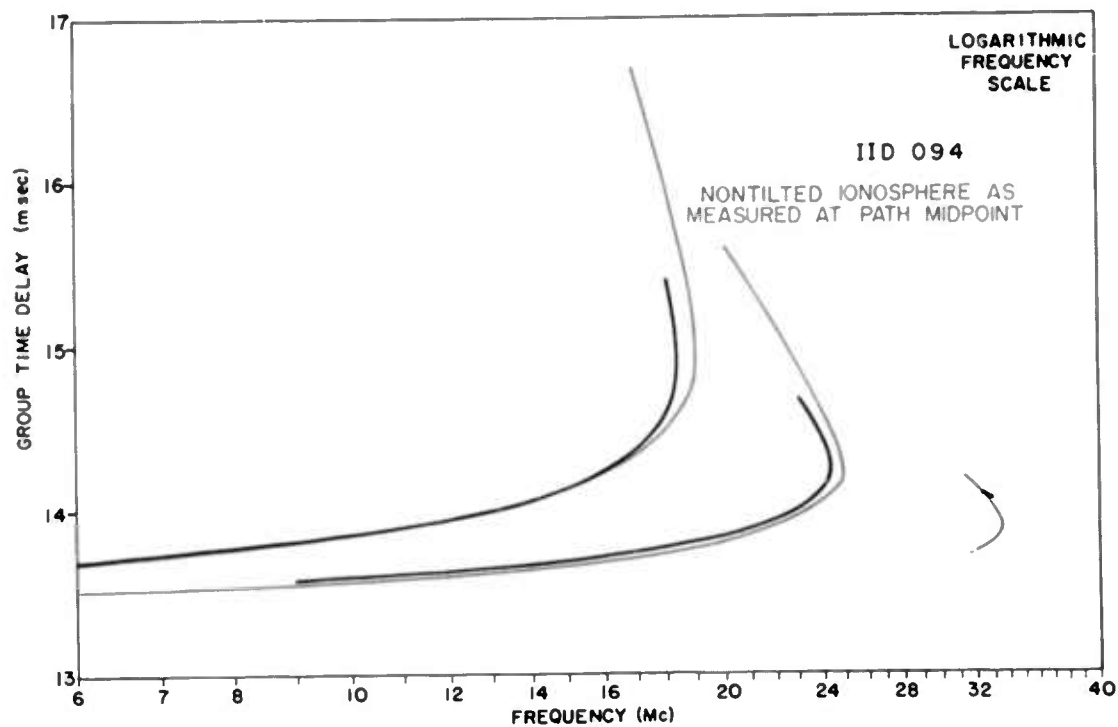
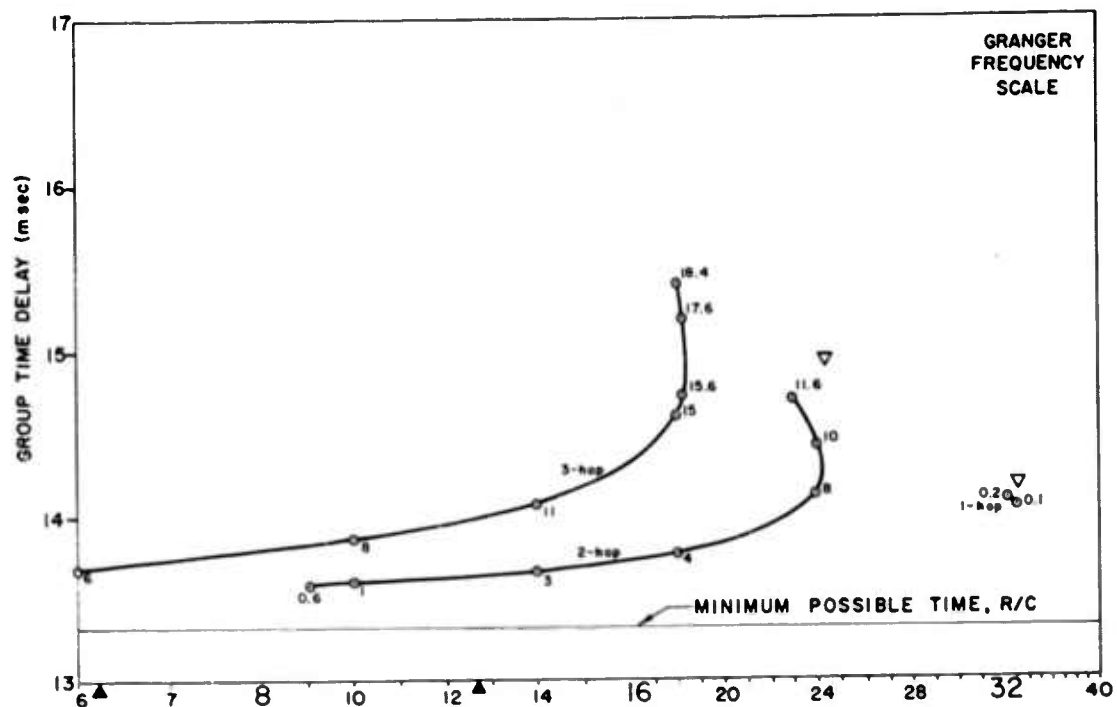


FIG. 33. IONOGRAM FOR IID 093; SEPARATION DISTANCE, 6000 km.



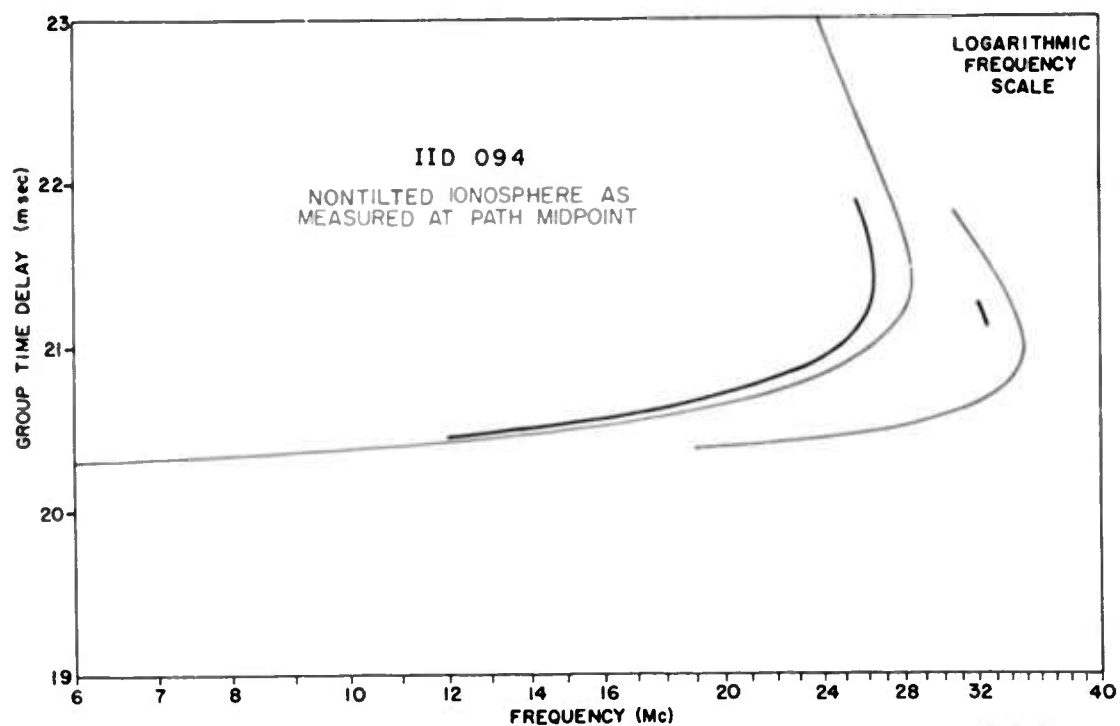
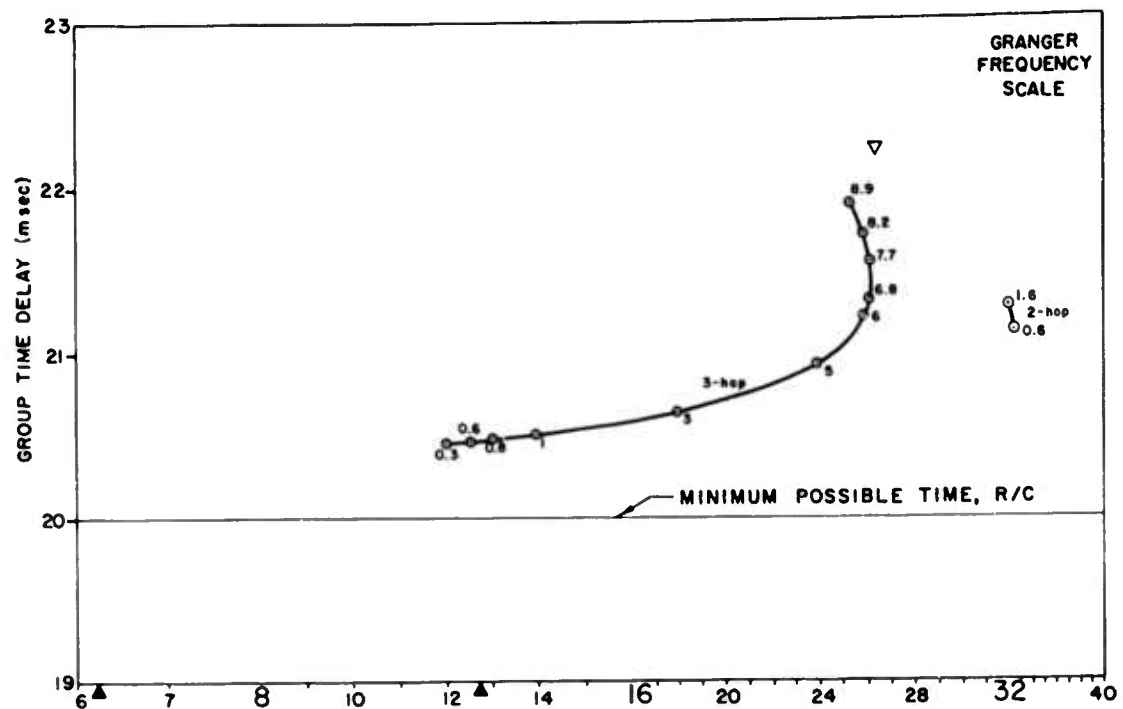
094 at 2000 km

FIG. 34. IONOGRAM FOR IID 094; SEPARATION DISTANCE, 2000 km.



094 at 4000 km

FIG. 35. IONOGRAM FOR IID 094; SEPARATION DISTANCE, 4000 km.



094 at 6000 km

FIG. 36. IONOGRAM FOR IID 094; SEPARATION DISTANCE, 6000 km.

F. TWO PARABOLIC LAYERS AT VARIOUS RANGES

Parabolic layers are of interest in raytracing primarily because they constitute a special case in which raypaths can be solved analytically without the use of a digital computer or its associated limitations. Consequently, a parabolic layer can be put into the digital-computer program and the results can be checked by analytic methods. However, it should be appreciated that in nature the electron-density distribution is not very similar to any parabolic layer except perhaps near the nose of the curve; the usefulness of the parabolic concept is primarily mathematical.

Some time ago the author was requested to make synthetic ionograms for two particular parabolic layers at four specified ranges. The results are presented here because they are of fairly general interest and because they do show what oblique ionograms would look like if parabolic layers actually did exist. Also, others may wish to use them to check analytical techniques for raytracing.

The two parabolic layers, IID 111 and 124, are shown on Fig. 37, together with the various parameters that characterize them. Each has been used to calculate synthetic ionograms at ranges of 0, 1375, 1833, 2750, and 5500 km to four hops. These results are presented on Figs. 38 through 47. The ionograms calculated for IID 111 are repeated in red on the logarithmic presentations of the 124 oblique ionograms in order to facilitate comparison. It can be seen that the differences between these ionograms are due solely to an increase in the height of the 124 layer.

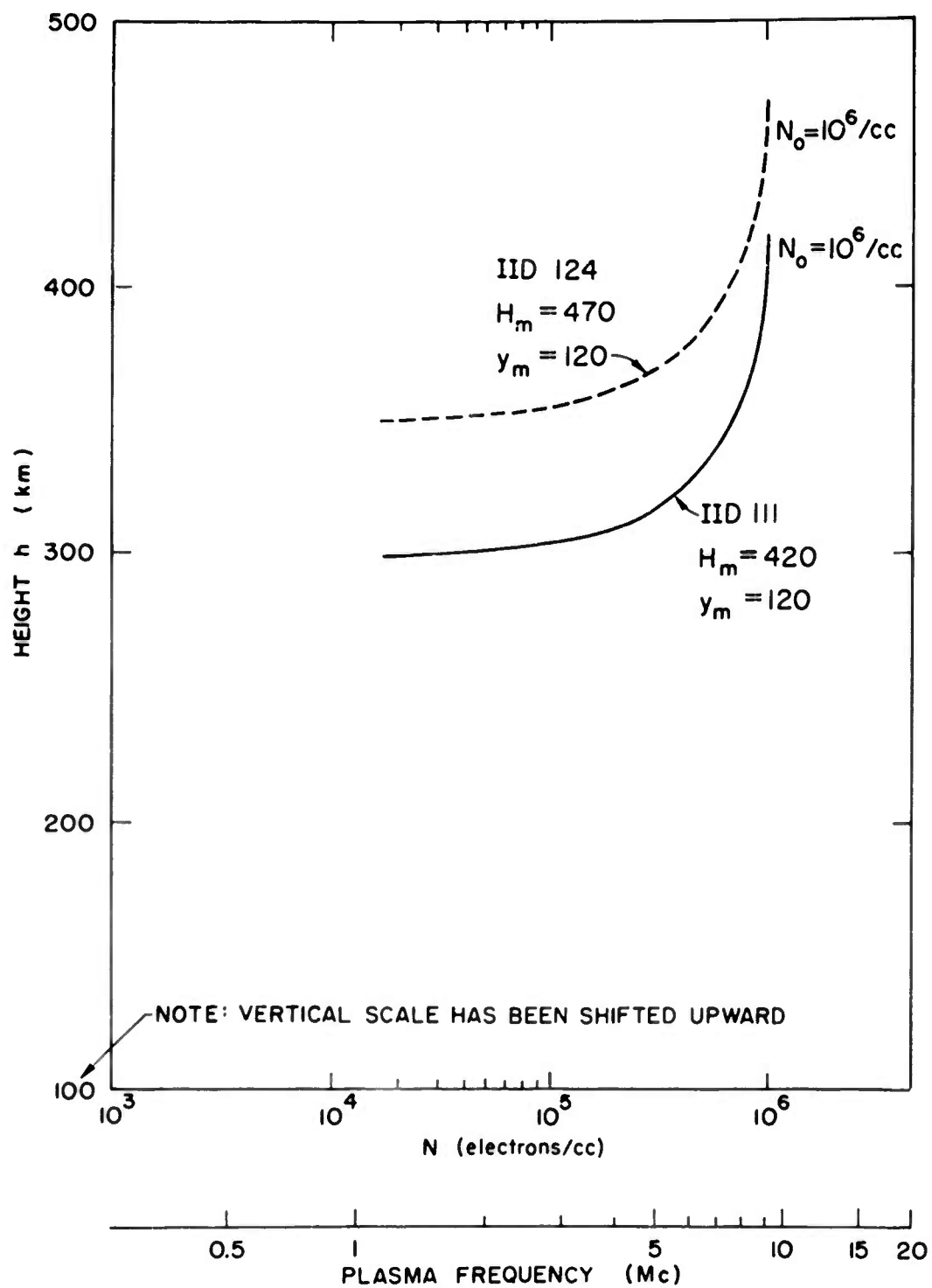


FIG. 37. ELECTRON DENSITIES IN TWO PARABOLIC LAYERS--IIDs 111 AND 124.

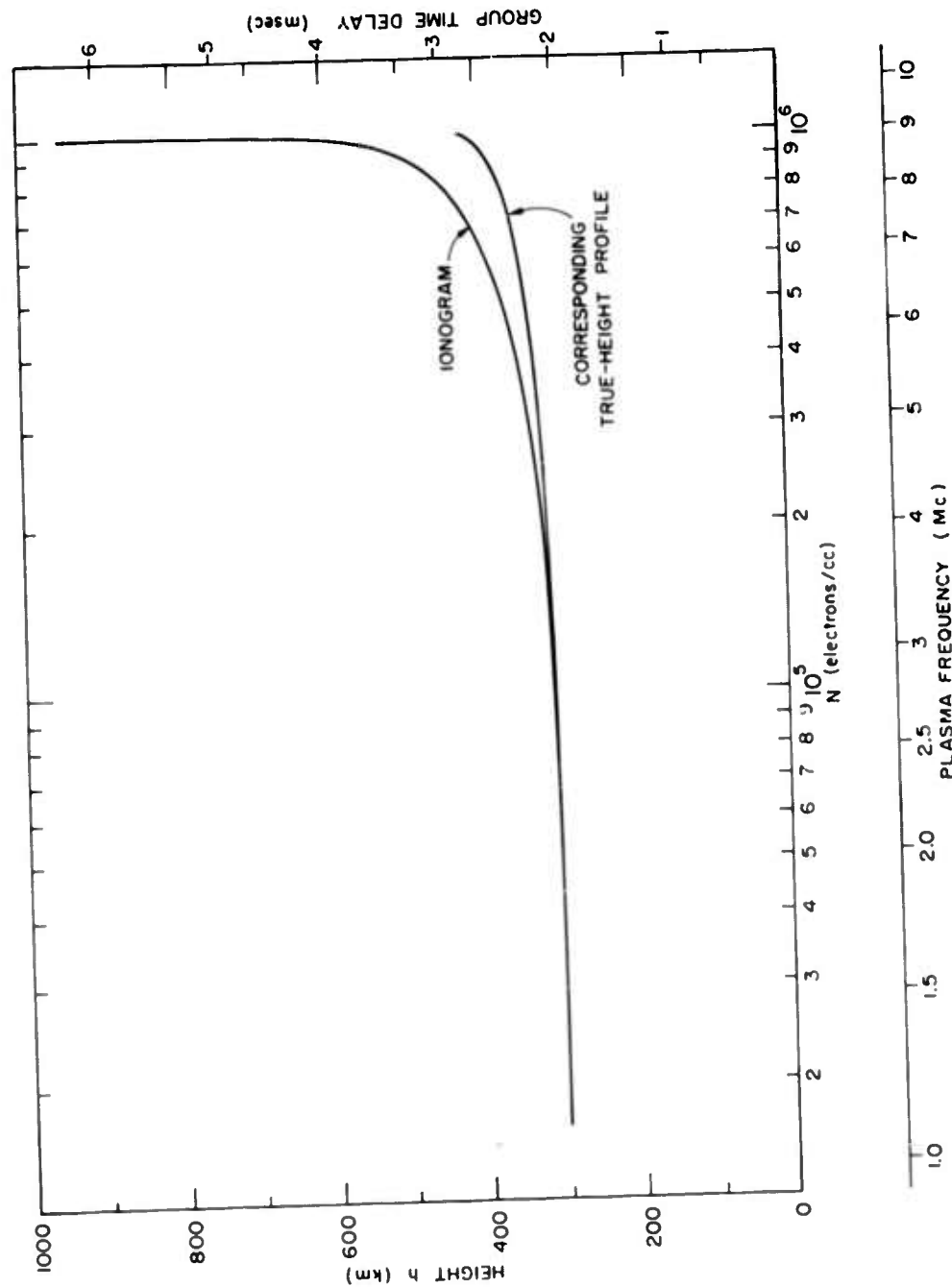
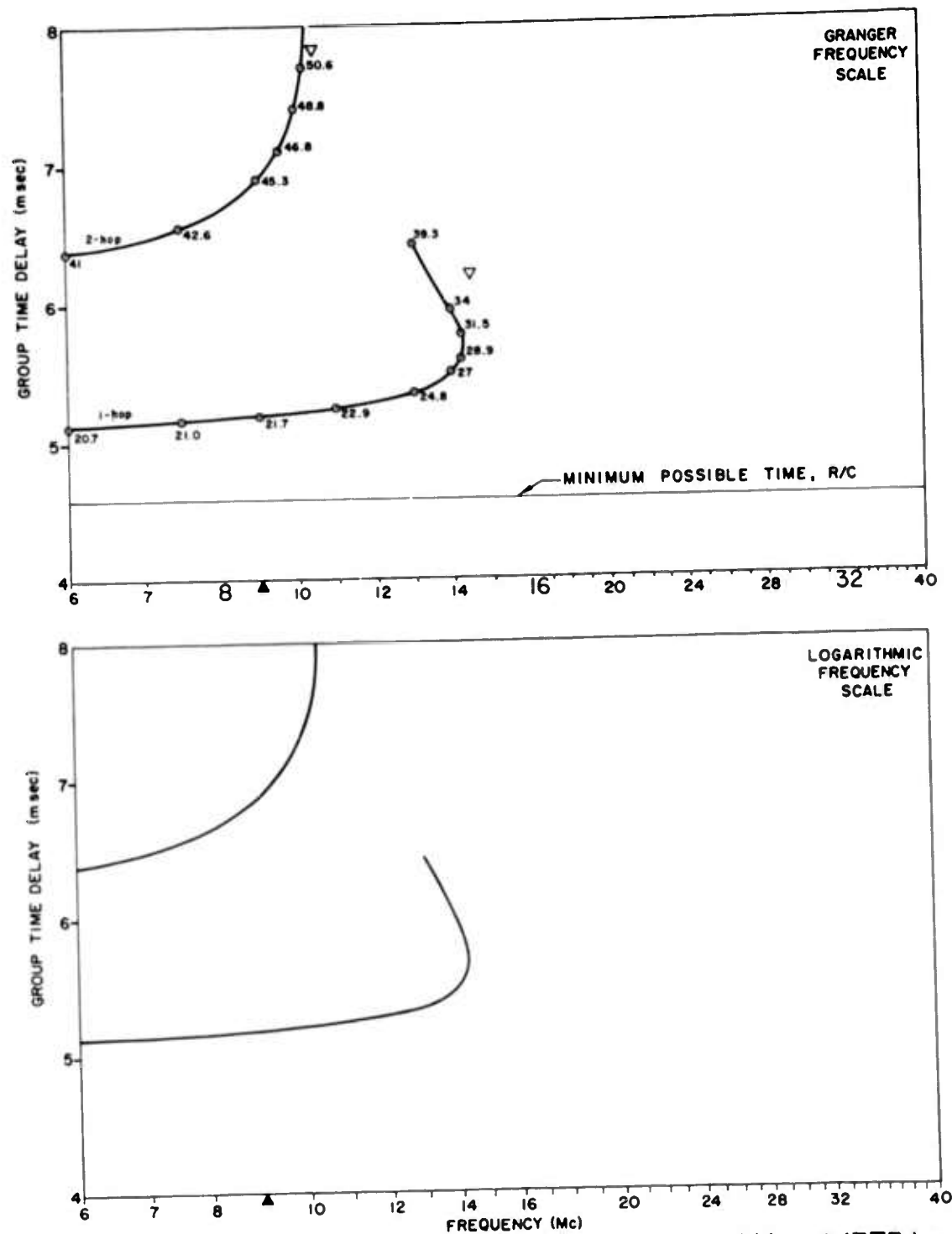
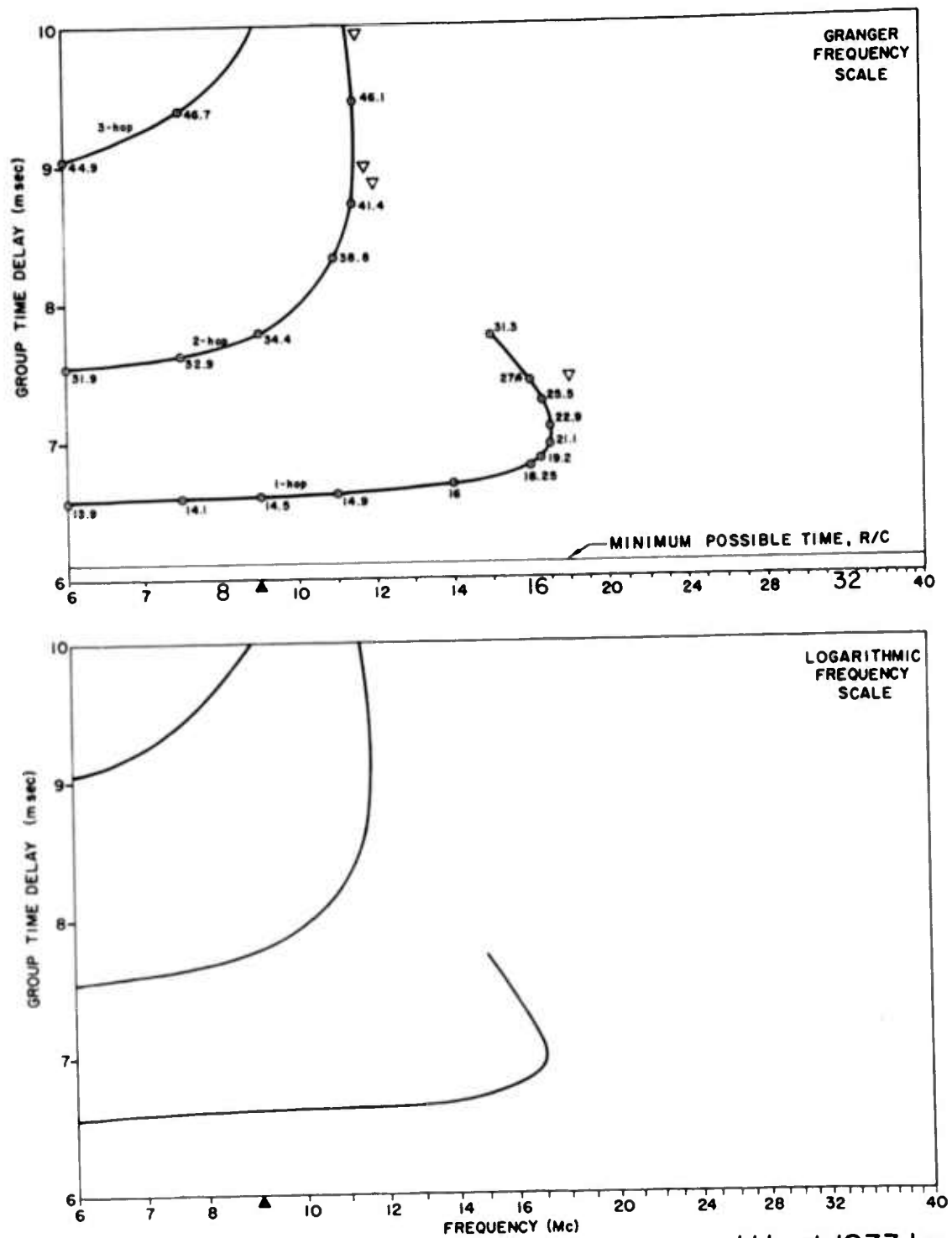


FIG. 38. IONOGRAM FOR IID 111; SEPARATION DISTANCE, 0 km.



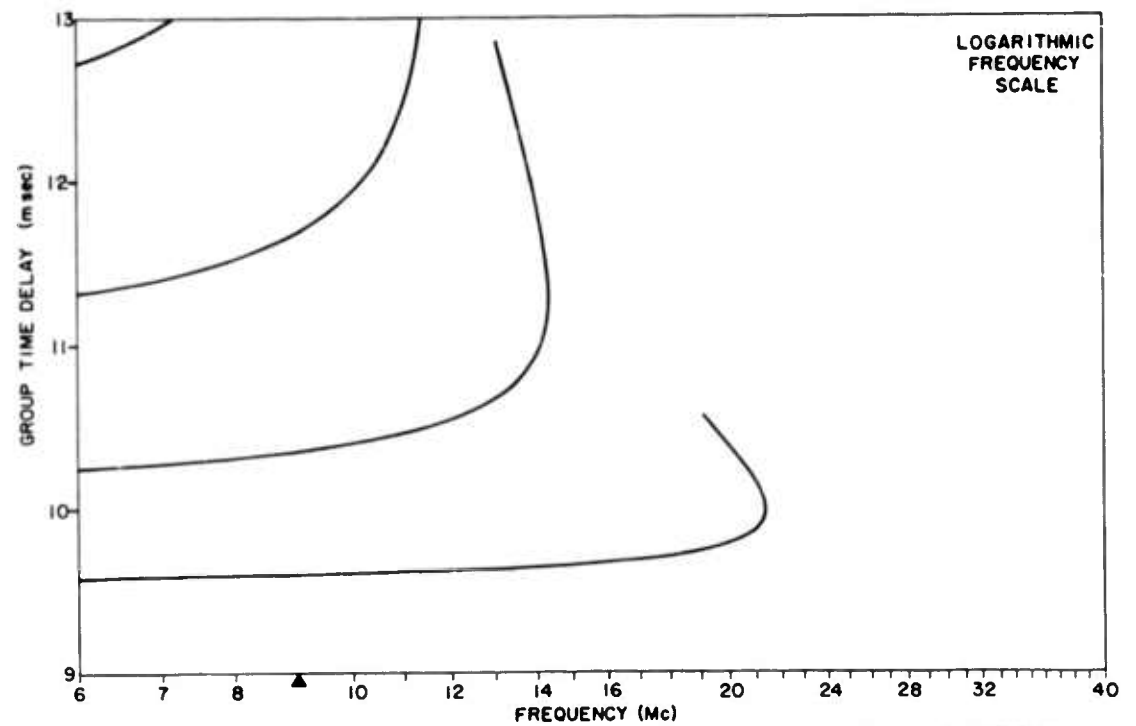
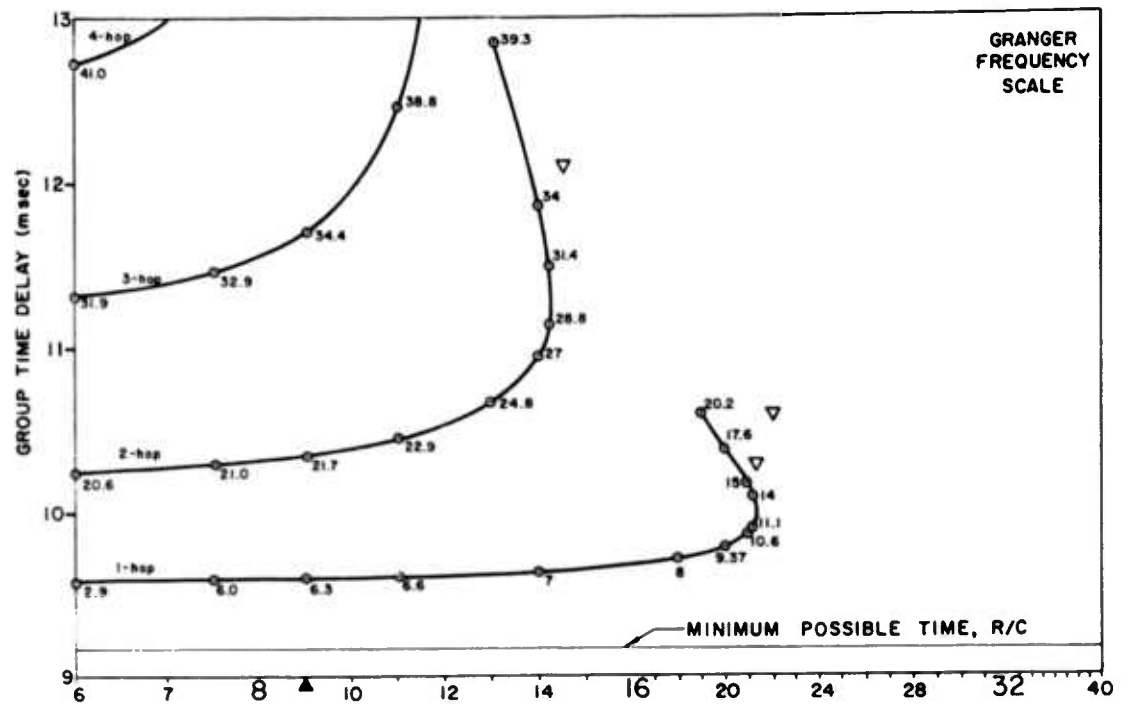
III at 1375 km

FIG. 39. IONOGRAM FOR IID 111; SEPARATION DISTANCE, 1375 km.



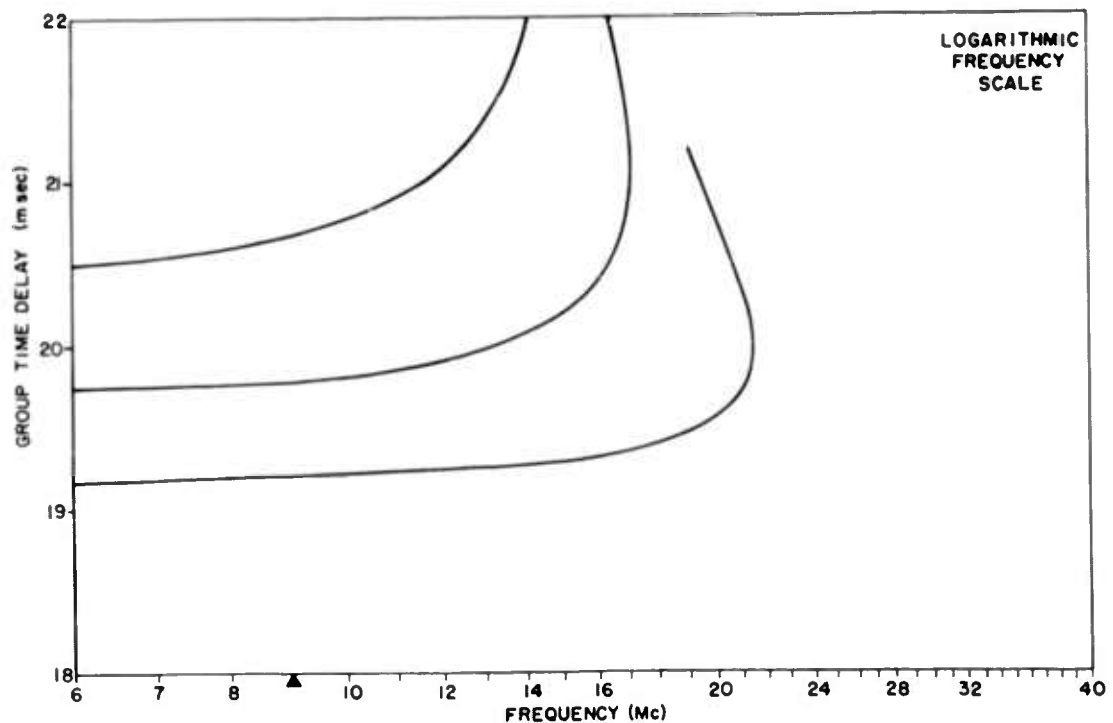
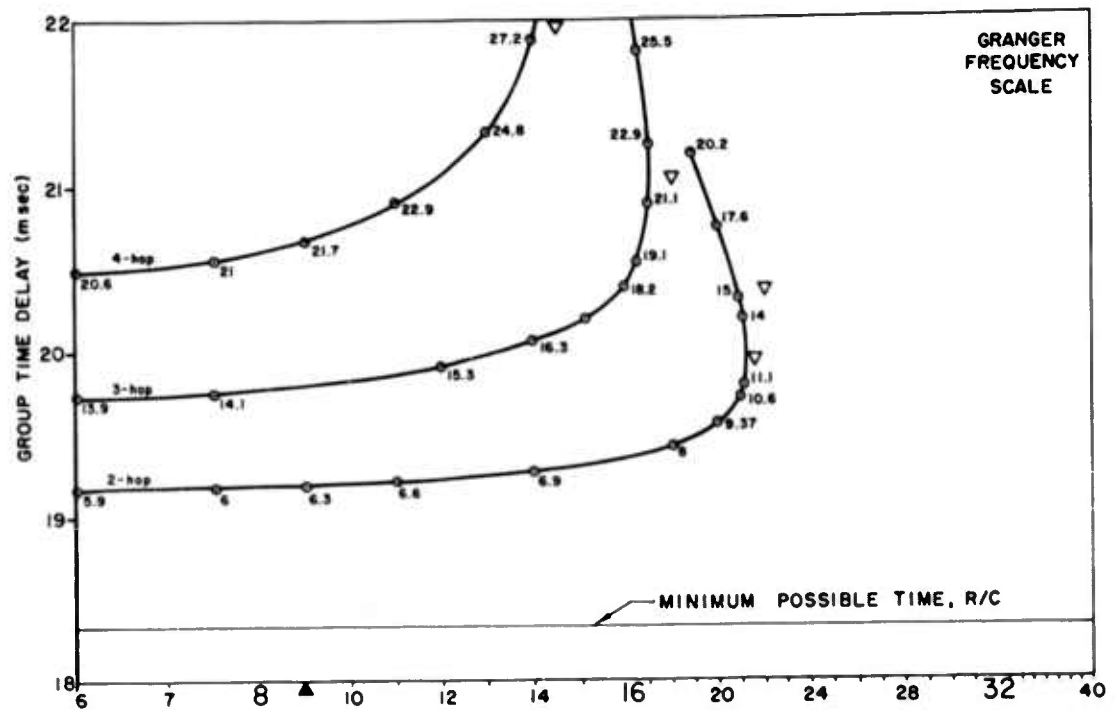
111 at 1833 km

FIG. 40. IONOGRAM FOR IID 111; SEPARATION DISTANCE, 1833 km.



III at 2750 km

FIG. 41. IONOGRAM FOR IID 111; SEPARATION DISTANCE, 2750 km.



III at 5500 km

FIG. 42. IONOGRAM FOR IID 111; SEPARATION DISTANCE, 5500 km.

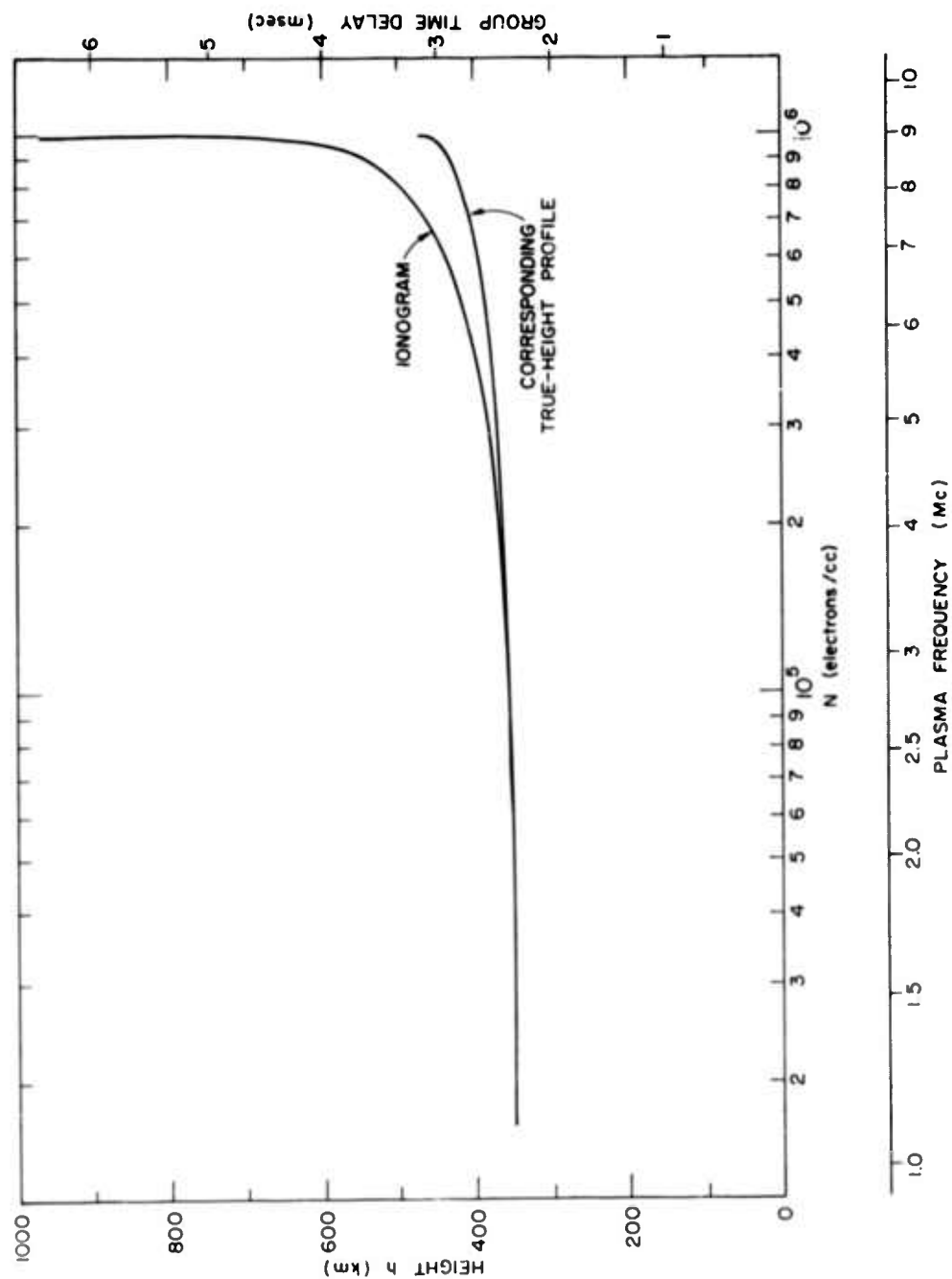
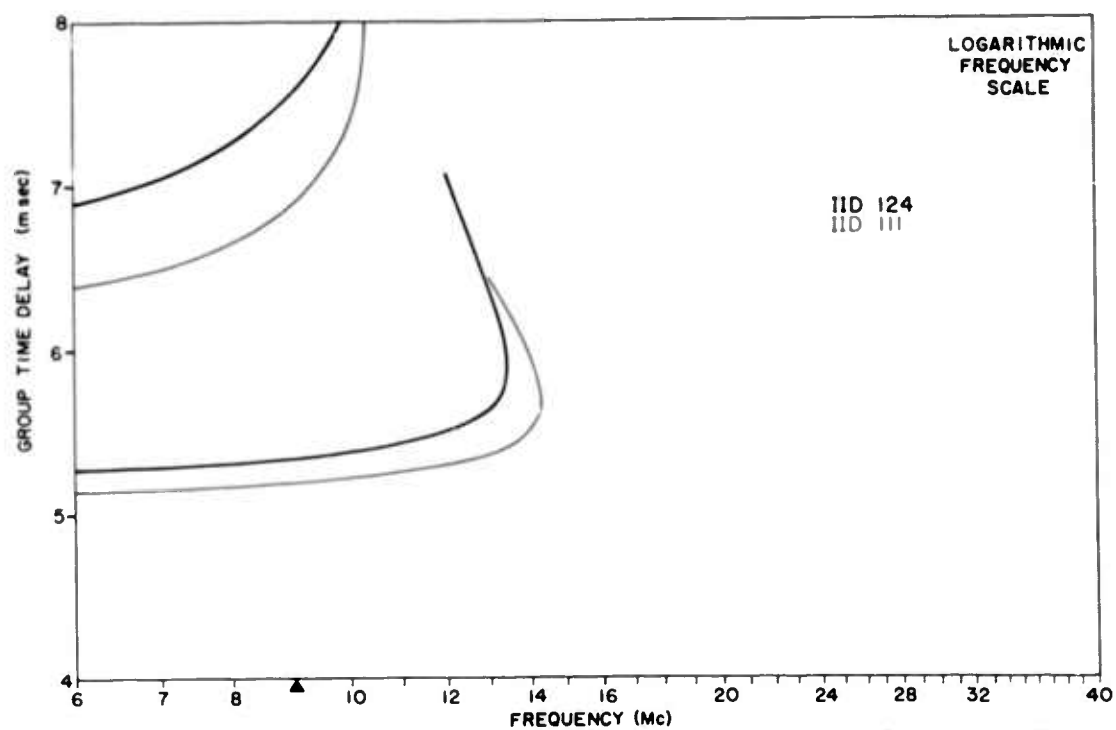
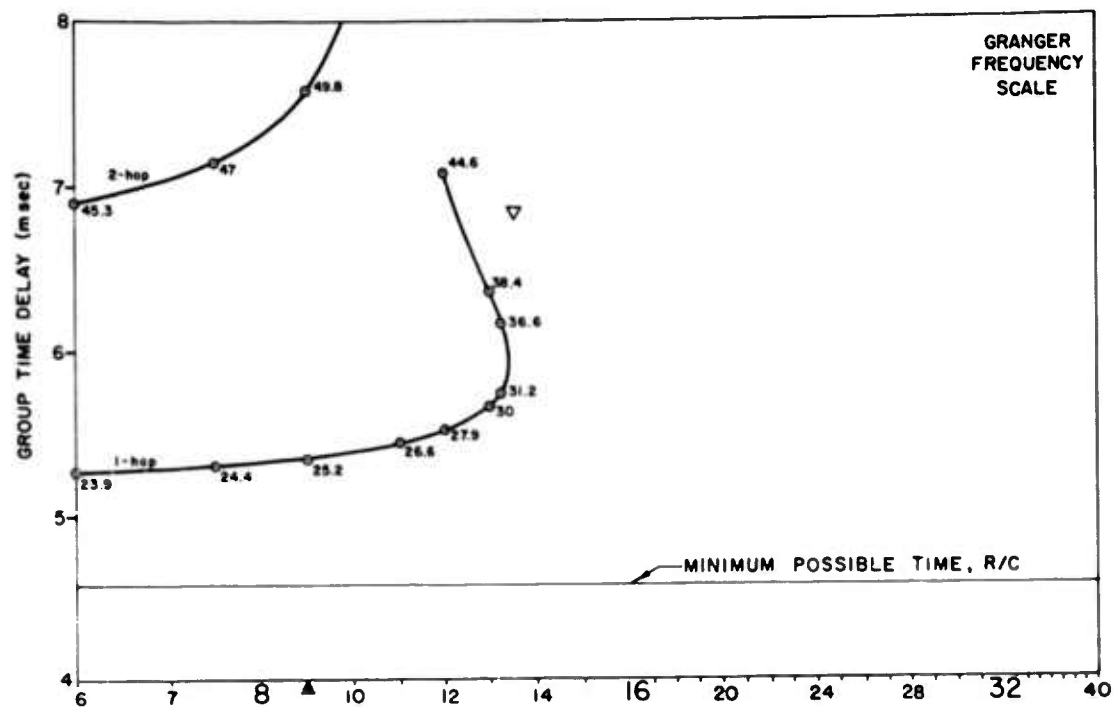
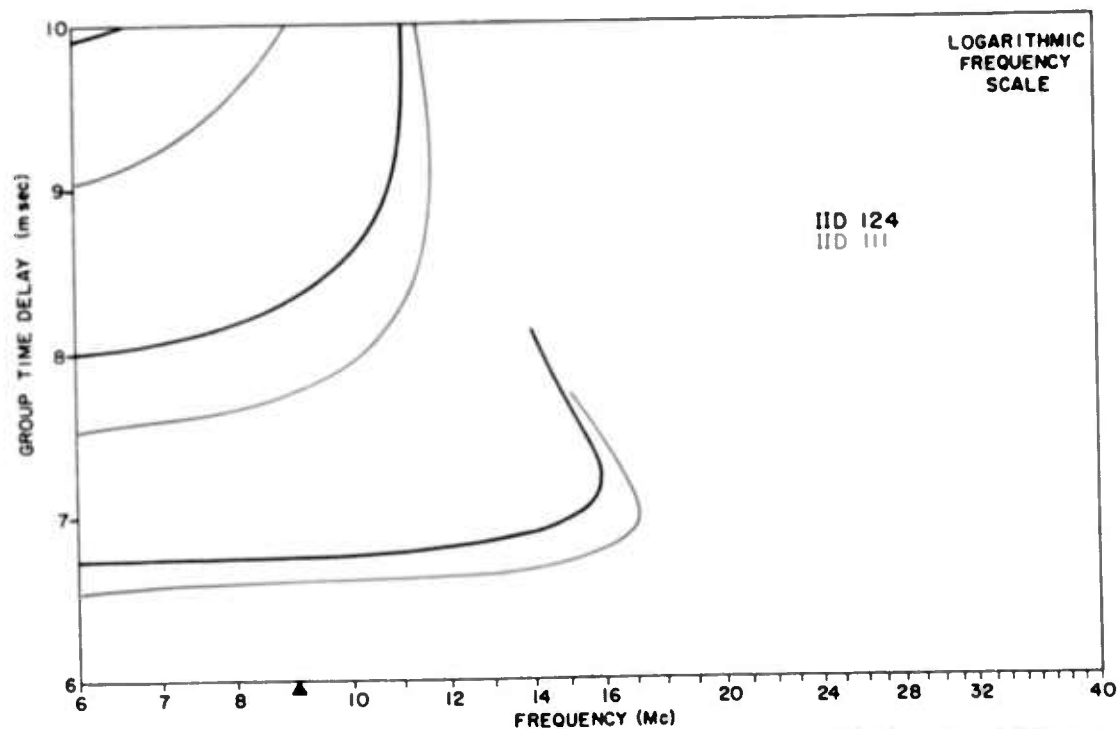
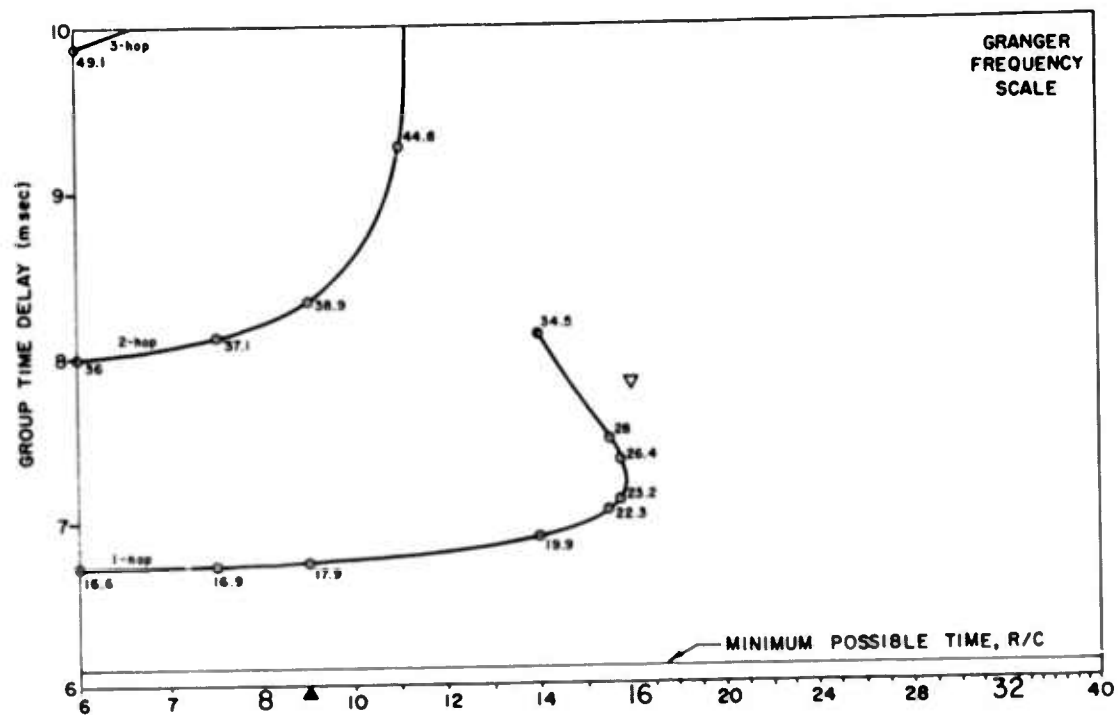


FIG. 43. IONOGRAM FOR IID 124; SEPARATION DISTANCE, 0 km.



124 at 1375 km

FIG. 44. IONOGRAM FOR IID 124; SEPARATION DISTANCE, 1375 km.



124 at 1833 km

FIG. 45. IONOGRAM FOR IID 124; SEPARATION DISTANCE, 1833 km.

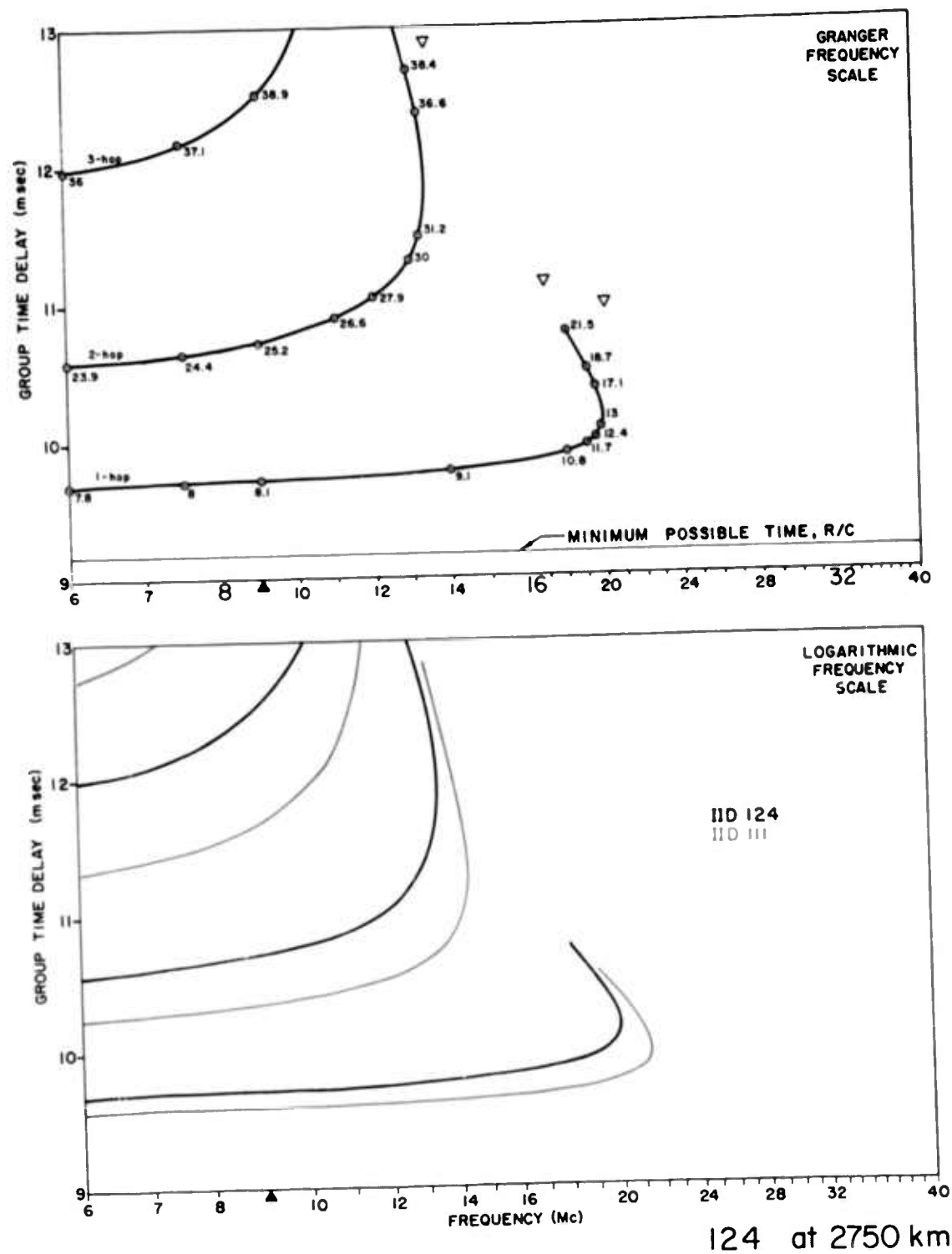
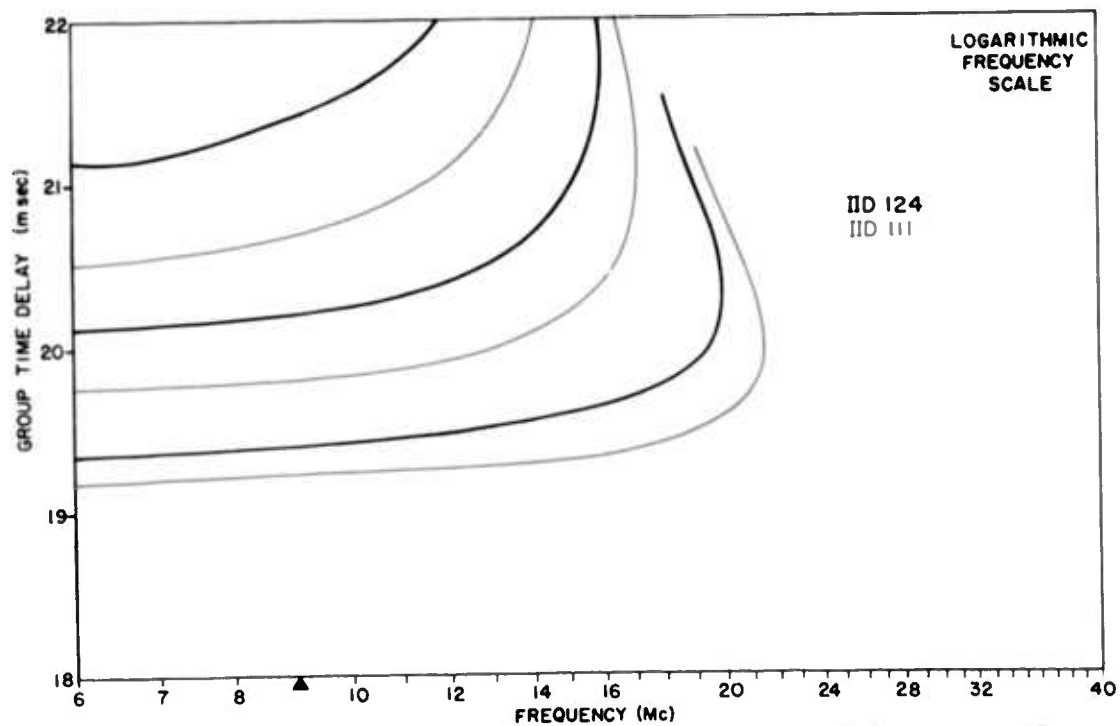
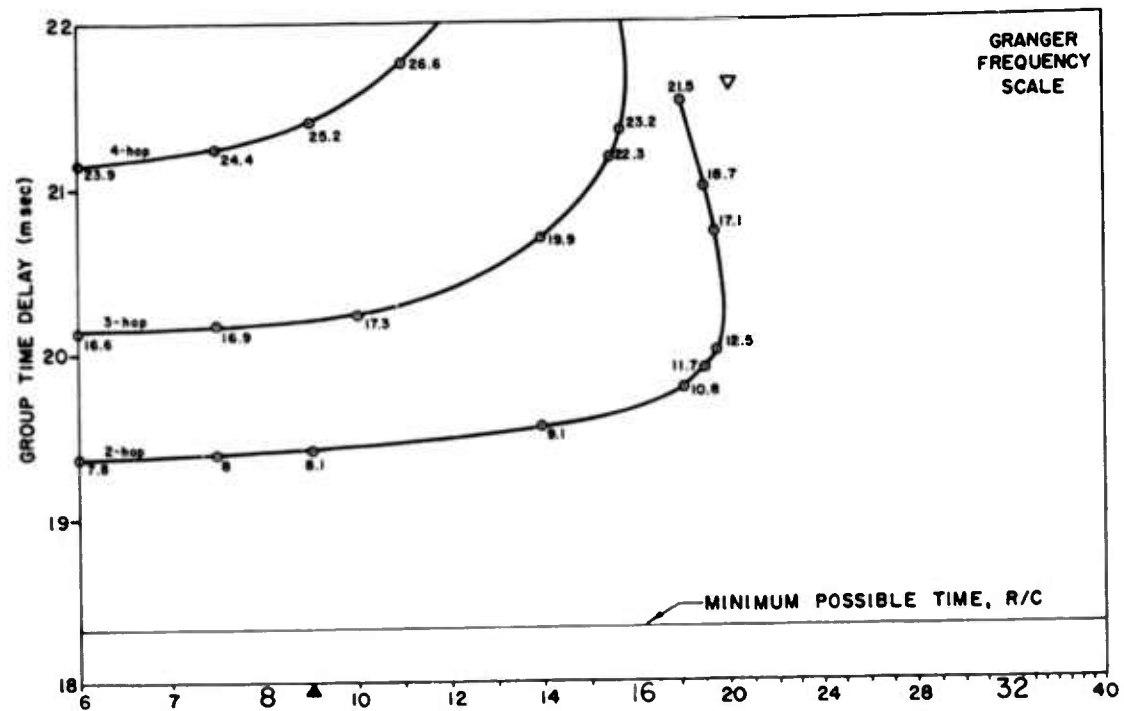


FIG. 46. IONOGRAM FOR IID 124; SEPARATION DISTANCE, 2750 km.



124 at 5500 km

FIG. 47. IONOGRAM FOR IID 124; SEPARATION DISTANCE, 5500 km.

G. AN UNUSUAL EXAMPLE

At the time the ionograms just presented were requested, a very unusual example was also requested; it is presented here. Although the electron-density distribution is irregular, the features found on the resulting ionograms are exaggerated examples of features that seem to be present on actual oblique ionograms.

The electron-density distribution shown on Fig. 48 was generated from sections of parabolic layers. The resulting five ionograms at various ranges are presented in Figs. 49 through 53. In particular, notice the behavior of the lower raytraces in the upper layer. The exaggerated way in which the range of these traces decreases as the frequency increases seems to be characteristic of some echoes seen on experimental traces and is apparently due to the long interval of height in which there is no change in electron density. The phenomenon is due to Pederson rays in the lower layer which are reflected from the upper layer. As the frequency increases, the retardation decreases but the ray trajectories remain relatively stable with the consequent apparent decrease in the range of the echoes.

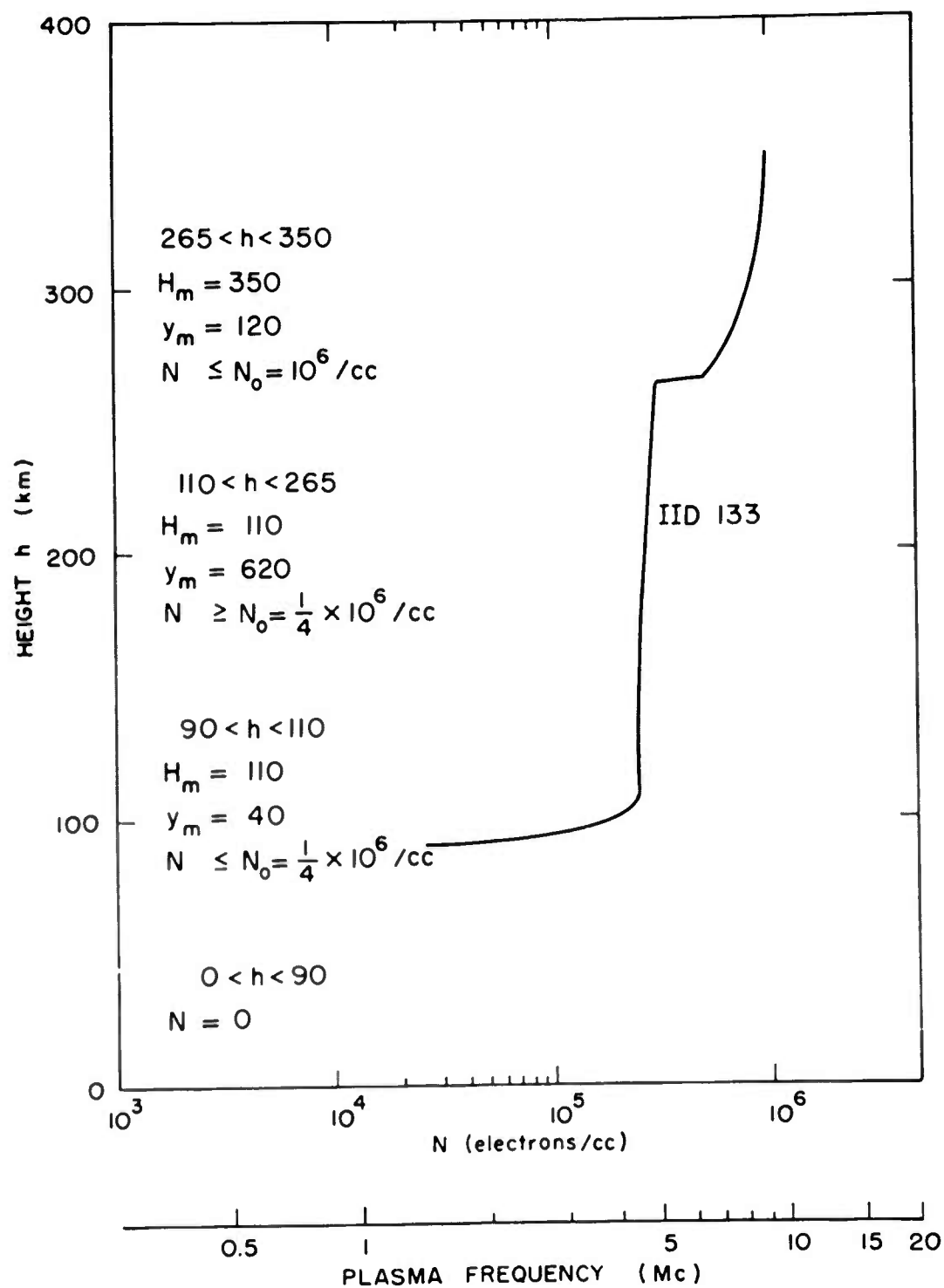


FIG. 48. ELECTRON-DENSITY DISTRIBUTIONS FOR IID 133.

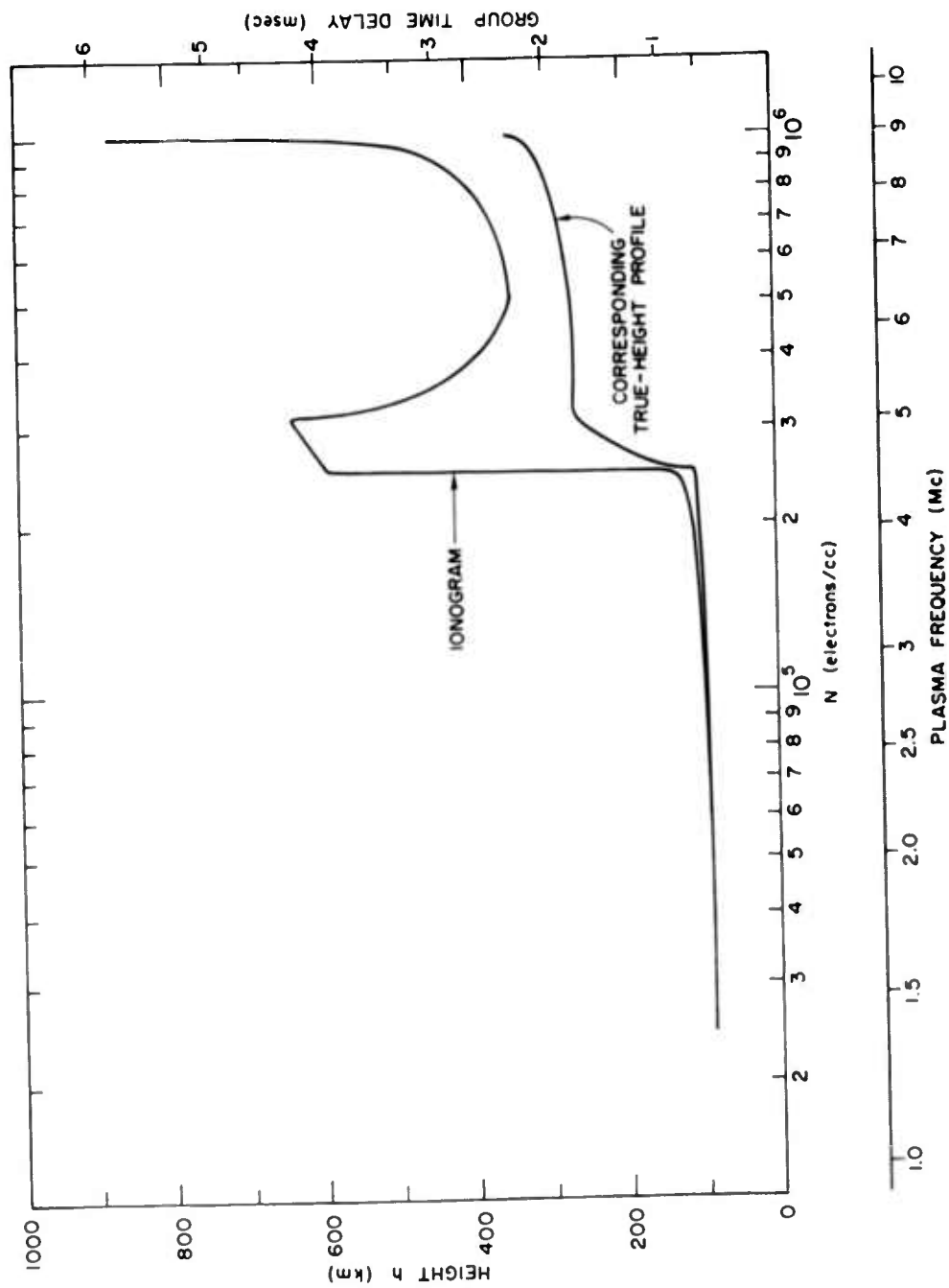
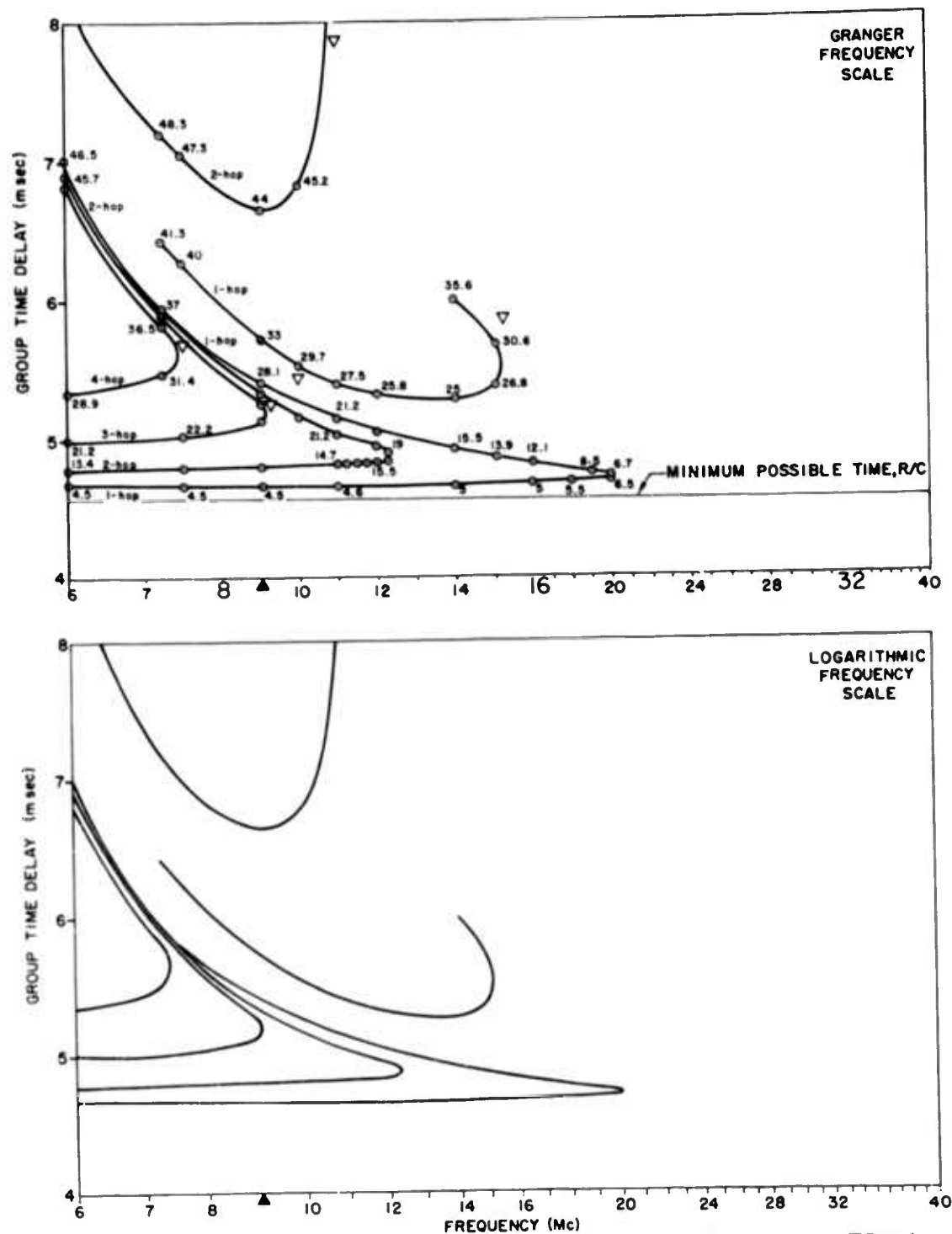
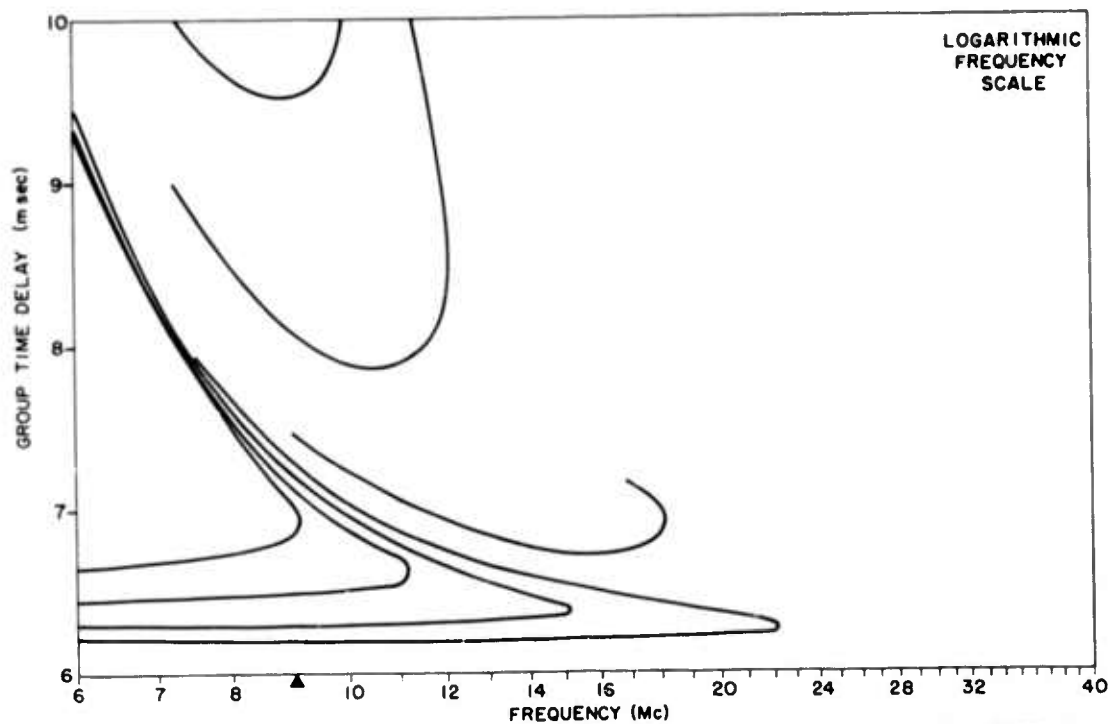
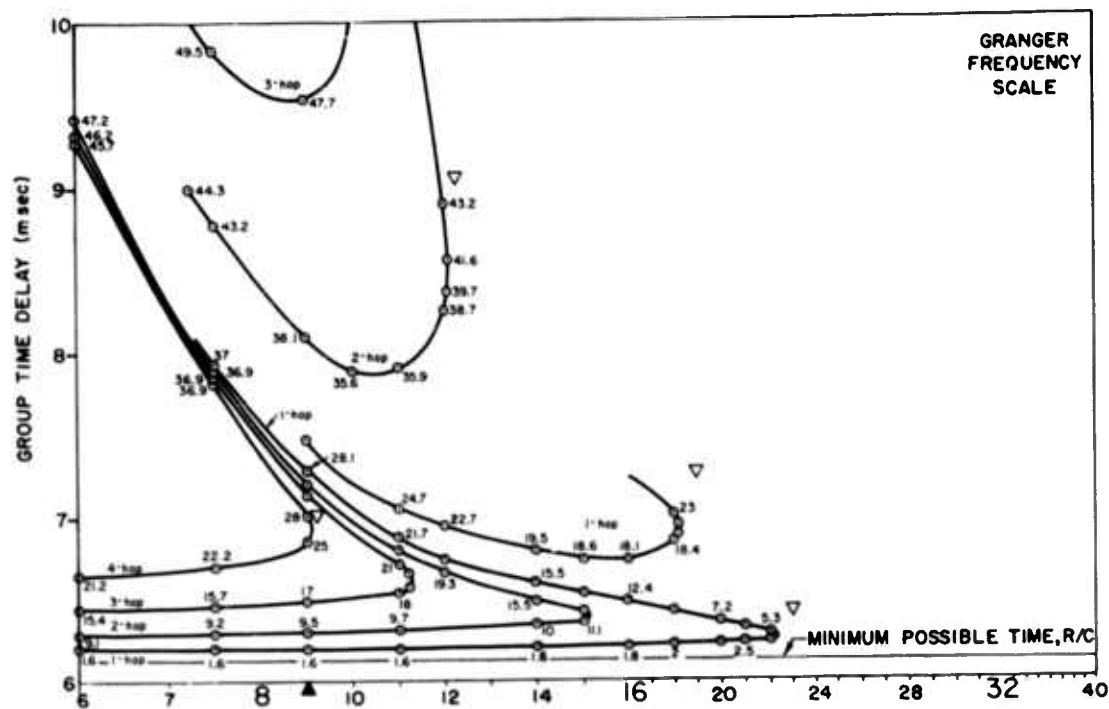


FIG. 49. IONOGRAM FOR IID 133; SEPARATION DISTANCE, 0 km.



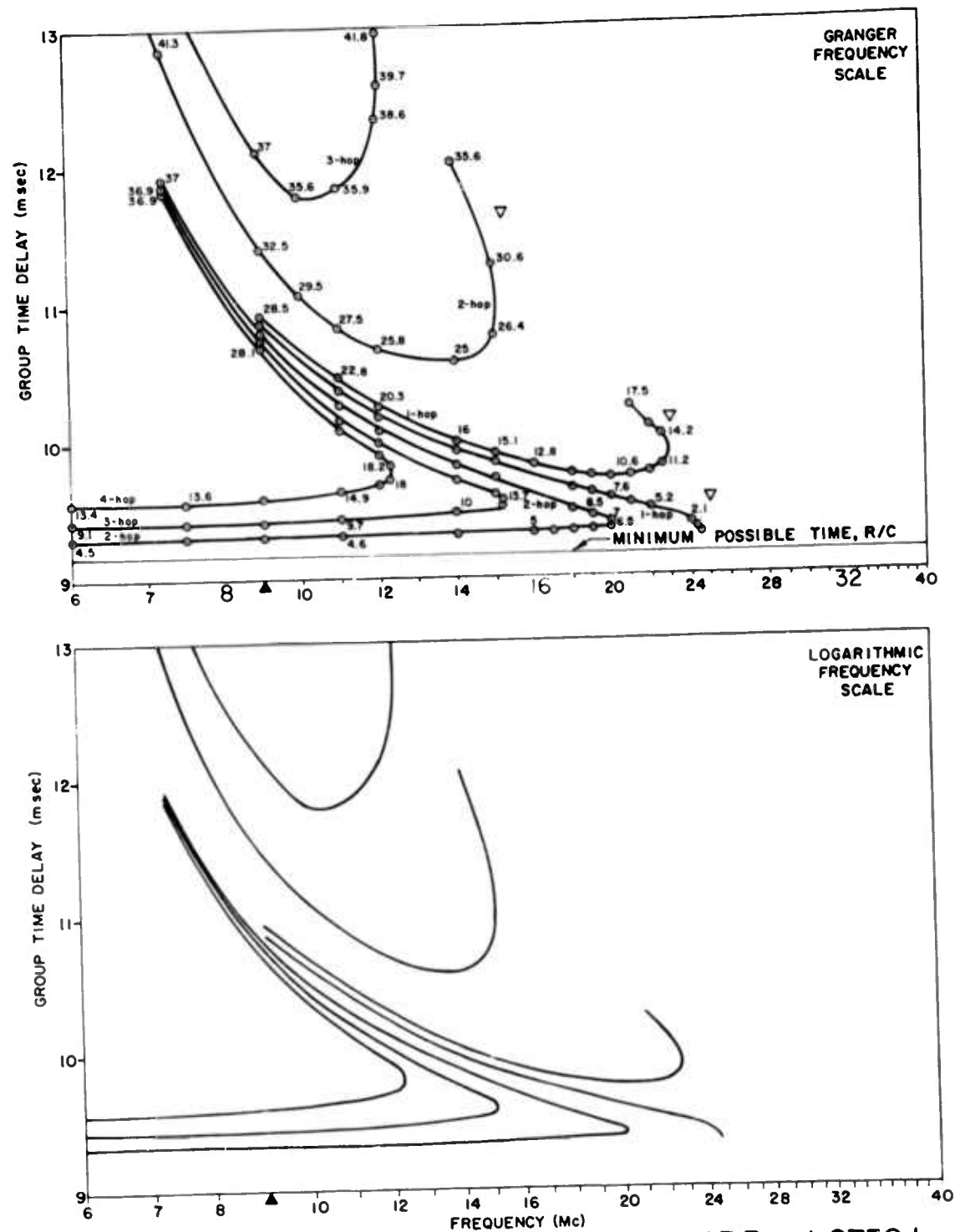
133 at 1375 km

FIG. 50. IONOGRAM FOR IID 133; SEPARATION DISTANCE, 1375 km.



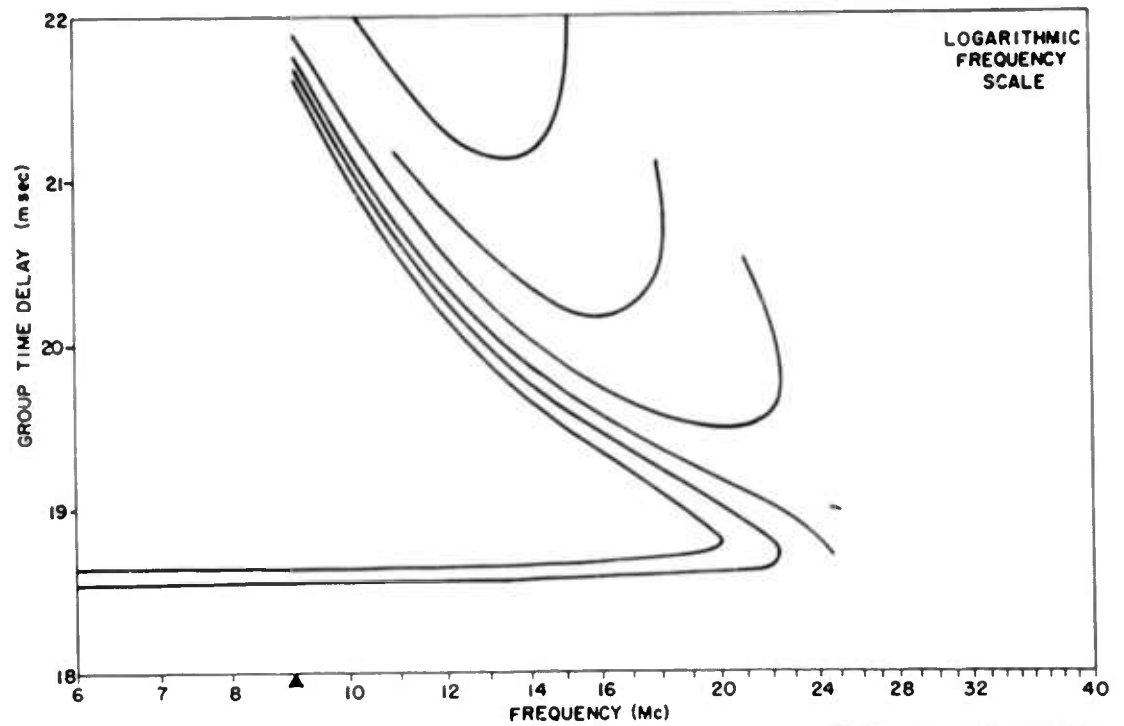
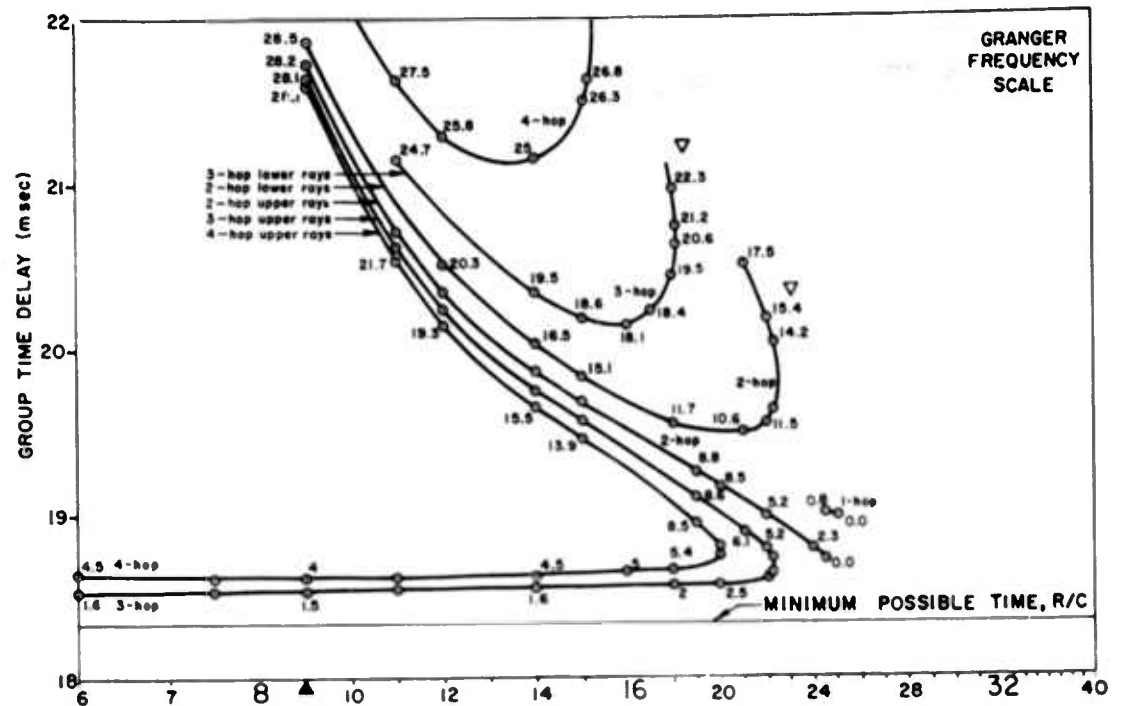
133 at 1833 km

FIG. 51. IONOGRAM FOR IID 133; SEPARATION DISTANCE, 1833 km.



133 at 2750 km

FIG. 52. IONOGRAM FOR IID 133; SEPARATION DISTANCE, 2750 km.



133 at 5500 km

FIG. 53. IONOGRAM FOR IID 133; SEPARATION DISTANCE, 5500 km.

VI. EXAMPLES SHOWING DETAILS OF SYNTHESIS

To provide some insight into the reason for various features on the ionograms, the three brief sections of this chapter show the nature of the calculation that resulted in some of the structures presented. The first example is classically simple, the second example is more complex but more interesting, and the third points out an unexpected phenomenon.

A. DETAILS OF THE NOSE OF IID 111 TWO-HOP ECHO

Reference to Fig. 40 will show that the two-hop echo has a very flat nose. The small open triangles at 11.6 and 11.75 Mc show that raytracing was done and that no propagation path existed at those two frequencies. The situation is more clearly revealed by Fig. 54, in which the takeoff angles and two-hop ground ranges of the various pertinent rays are shown. Notice the vertical line through a ground range of 1833 km. Propagation paths are known to exist at that range whenever the curves on the graph intersect the vertical line.

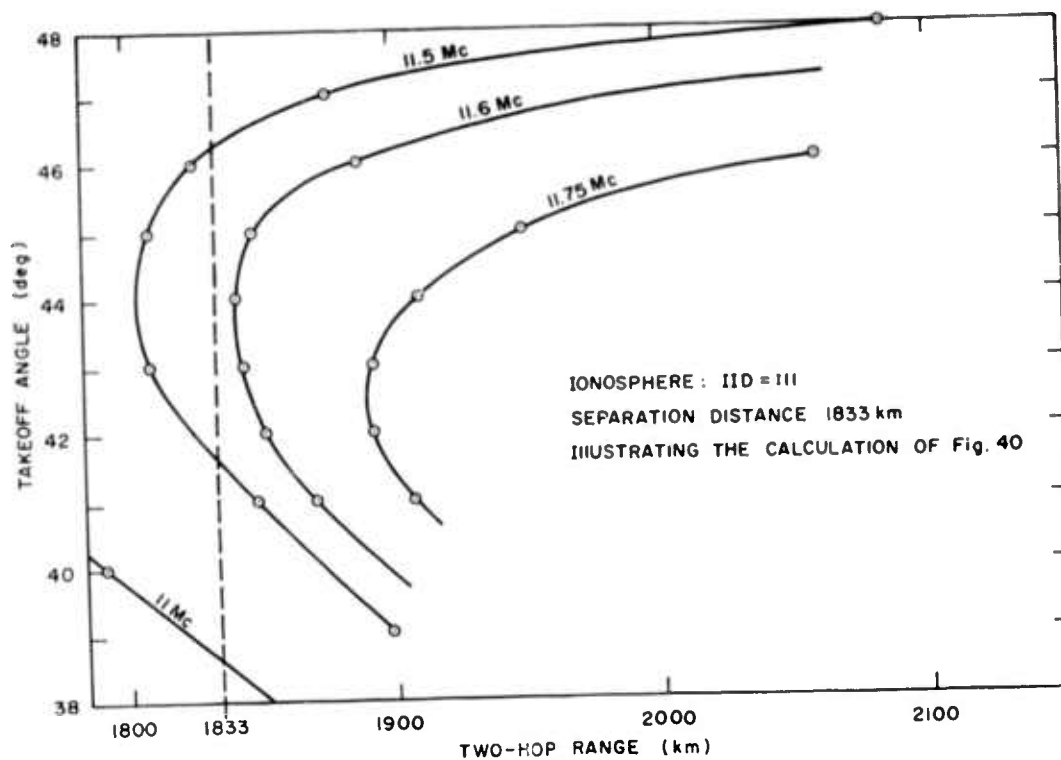


FIG. 54. GRAPH ILLUSTRATING SYNTHESIS OF IID 111 IONOGRAM.

The search process during the generation of Fig. 40 involved the following: first, an 11-Mc raytracing was run, which revealed the existence of a propagation path at a takeoff angle near 39 deg. From this point and the other points that had so far been found on the ionogram, it could be determined that a nose of the two-hop curve should be nearby. Consequently, raytracing was carried out at 11.50 and 11.75 Mc. As seen in Fig. 40, the 11.50-Mc raytracing yielded two points differing in group time delay by a little over $3/4$ msec while the 11.75-Mc raytracing indicated that the two-hop skip distance was near 1900 km. Then, from a sketch similar to Fig. 54, it was determined that the nose of the curve should be very near 11.6 Mc. The raytracing was done as shown and, although no propagation path existed to 1833 km, the results were sufficiently close to enable completion of the nose of the ionogram with a high degree of confidence in the resulting shape.

B. DETAILS OF THE E-LAYER EFFECT IN IID 012

This section will demonstrate in some depth the method of making the synthetic ionograms, and it should aid in understanding the reason for some of the details on an oblique ionogram when E layers are present. To be particularly lucid, a small group of frequencies and takeoff angles was selected and much more raytracing was done with this group than was actually necessary to produce the synthetic records presented here. This exercise also serves to show that the output of the computer is self-consistent.

Examination of the ionograms shows that there is a great deal of structure on the 012 ionosphere records in the vicinity of 15 Mc. Consequently, raytracing was done every half megacycle between 14 and 17 Mc. Each ray was computed to three hops, resulting in 357 raysets distributed among the seven frequencies, and cost a total of \$3.19. The 51 raysets at 16.5 Mc are printed out in Fig. 55 to illustrate the nature of these data. (Costs would have been nearer \$20 if the ionosphere had been tilted.)

The 357 punched cards containing raysets were then processed by another computer program, which carried out the interpolation required to

IID	FREQ	HOP	BETA	PSI	GROUP	TIME	PHASE	RANGE	HT	INUMB
	KC		DEG	DEG	MS	MS	MS	KM	KM	
5	012	16500.	1	-0.	0.00000	8.3091459	8.2803628	2460.8286	100.67194	0
5	012	16500.	1	0.50000	0.50000	7.9761093	7.9464349	2360.7081	100.89111	0
5	012	16500.	1	1.00000	1.00000	7.7020122	7.6700891	2277.8420	101.27844	0
5	012	16500.	1	1.50000	1.50000	7.5744097	7.5360850	2237.6220	102.27307	0
5	012	16500.	1	2.00000	2.00000	11.9650155	11.7774438	3499.7526	154.83795	0
5	012	16500.	1	2.50000	2.50000	10.8634642	10.7012025	3176.8231	155.26105	0
5	012	16500.	1	3.00000	3.00000	10.2184529	10.0668895	2986.3963	155.99445	0
5	012	16500.	1	3.50000	3.50000	9.6987062	9.5540372	2832.3865	156.61340	0
5	012	16500.	1	4.00000	4.00000	9.2539648	9.1142068	2700.1885	157.38287	0
5	012	16500.	1	4.50000	4.50000	8.8617662	8.7254902	2583.2815	158.26825	0
5	012	16500.	1	5.00000	5.00000	8.5104737	8.3766471	2478.2839	159.24292	0
5	012	16500.	1	5.50000	5.50000	8.1910506	8.0627251	2383.7148	160.30334	0
5	012	16500.	1	6.00000	6.00000	7.9075174	7.7760791	2297.2784	161.45306	0
5	012	16500.	1	6.50000	6.50000	7.6429422	7.5118673	2217.5209	162.68372	0
5	012	16500.	1	7.00000	7.00000	7.4013109	7.2700695	2144.4388	164.01904	0
5	012	16500.	1	7.50000	7.50000	7.1767746	7.0449752	2076.3470	165.20233	0
5	012	16500.	1	8.00000	8.00000	6.9748954	6.8418192	2014.7944	166.61475	0
5	012	16500.	2	-0.	0.00000	16.6182919	16.5607257	4921.6572	100.67194	0
5	012	16500.	2	0.50000	0.50000	15.9522185	15.8928697	4721.4162	100.89111	0
5	012	16500.	2	1.00000	1.00000	15.4040744	15.3401781	4555.6840	101.27844	0
5	012	16500.	2	1.50000	1.50000	15.1481193	15.0721700	4475.2441	102.27307	0
5	012	16500.	2	2.00000	2.00000	23.9300311	23.5548875	6999.4652	154.83795	0
5	012	16500.	2	2.50000	2.50000	21.7269285	21.4024050	6353.6461	155.26105	0
5	012	16500.	2	3.00000	3.00000	20.4369059	20.1337790	5972.7926	155.99445	0
5	012	16500.	2	3.50000	3.50000	19.3974123	19.1081743	5664.7731	156.61340	0
5	012	16500.	2	4.00000	4.00000	18.5079296	18.2284136	5400.3770	157.38287	0
5	012	16500.	2	4.50000	4.50000	17.7235324	17.4509804	5166.5630	158.26825	0
5	012	16500.	2	5.00000	5.00000	17.0209475	16.7532942	4956.5677	159.24292	0
5	012	16500.	2	5.50000	5.50000	16.3901012	16.1254501	4767.4296	160.30334	0
5	012	16500.	2	6.00000	6.00000	15.8150948	15.5521582	4594.5568	161.45306	0
5	012	16500.	2	6.50000	6.50000	15.2858845	15.0237346	4435.0417	162.68372	0
5	012	16500.	2	7.00000	7.00000	14.8026217	14.5401391	4288.8776	164.01904	0
5	012	16500.	2	7.50000	7.50000	14.3535491	14.0899503	4152.6940	165.20233	0
5	012	16500.	2	8.00000	8.00000	13.9497907	13.6836383	4029.5888	166.61475	0
5	012	16500.	3	-0.	0.00000	24.9274378	24.8410885	7382.4857	100.67194	0
5	012	16500.	3	0.50000	0.50000	23.9283278	23.8393044	7082.1243	100.89111	0
5	012	16500.	3	1.00000	1.00000	23.1060364	23.0102670	6833.5260	101.27844	0
5	012	16500.	3	1.50000	1.50000	22.7232289	22.6082549	6712.8661	102.27307	0
5	012	16500.	3	2.00000	2.00000	35.8950462	35.3323312	10499.1978	154.83795	0
5	012	16500.	3	2.50000	2.50000	32.5903926	32.1036072	9530.4691	155.26105	0
5	012	16500.	3	3.00000	3.00000	30.6553588	30.2006686	8959.1888	155.99445	0
5	012	16500.	3	3.50000	3.50000	29.0961185	28.6622615	8497.1595	156.61340	0
5	012	16500.	3	4.00000	4.00000	27.7618942	27.3476204	8100.5655	157.38287	0
5	012	16500.	3	4.50000	4.50000	26.5852985	26.1764705	7749.8145	158.26825	0
5	012	16500.	3	5.00000	5.00000	25.5314212	25.1299412	7434.8516	159.24292	0
5	012	16500.	3	5.50000	5.50000	24.5851517	24.1861752	7151.1443	160.30334	0
5	012	16500.	3	6.00000	6.00000	23.7226422	23.3282373	6891.8351	161.45306	0
5	012	16500.	3	6.50000	6.50000	22.9288266	22.5356019	6652.5626	162.68372	0
5	012	16500.	3	7.00000	7.00000	22.2039325	21.8102086	6433.3163	164.01904	0
5	012	16500.	3	7.50000	7.50000	21.5301235	21.1349254	6229.0410	165.20233	0
5	012	16500.	3	8.00000	8.00000	20.9216860	20.5254574	6044.3832	166.61475	0

FIG. 55. PRINTED RAYSETS AT 16.5 Mc FOR IID 012.

give all the oblique-ionogram data for ranges of 1000, 2000, 3000, 4000, 5000, 6000, 7000, and 8000 km. An example of the output of this particular program is shown on Fig. 56. Each line in that printout represents a propagation-path delay that should be entered on one of the synthetic ionograms. For example, the first line shows that, at frequency 16.5 Mc on IID 012, there is a one-hop upper-ray mode that reaches a range of 3000 km, has a takeoff angle of 1.802 deg, and has an excess group time delay of 0.227 msec. This "excess group time delay" (symbolized TE) is simply the accumulated group time delay along the 3000-km path from which the computer has subtracted the time required for a light ray to traverse 3000 km. It turns out to be quite convenient to work with excess delay rather than total delay, because the excess delay is not a strong function of ground range. The last column gives a relative measure of the signal strength as 15.98 db along this particular raypath. This information was not used on ionograms given here.

The 16.5-Mc data are particularly interesting because of the ray that takes off at 2 deg. This ray reaches a two-hop range of 6999.4652 km. The rays both above and below this particular ray reach a shorter ground range. Consequently, the computer gives no answer for 7000 km, although a human examiner can make the logical judgment that, for practical purposes, the 2-deg ray actually did reach 7000 km and thus should be entered on the oblique ionogram. This is a good example of one of the many reasons for having some form of human intervention in long, involved sequences of computer calculations.

Seven pages of calculations such as those shown on Fig. 56 were carried out by an IBM 7090 at a total cost of \$1.25 (rental is \$250/hr).

Figure 57 shows, in somewhat idealized form, the ranges of the various raypaths that were computed as a function of their takeoff angle at each of the seven frequencies. Dotted lines are shown where the exact shape of the crossover curve is not known. The reader can compare Fig. 55 with the 16.5-Mc curve on Fig. 57 to see how the latter was generated. On Fig. 55 it can be seen that the jump in range between 1.5- and 2-deg takeoff angles is, indeed, abrupt. Figure 57 is particularly interesting because it can be interpreted to show the basic reason for most of the structures on the IID 012 oblique ionograms at frequencies between 14

IID	FREQ	TE	MODE	RANGE	BETA	DB
12	16500.0					
		.227	1U	3000.0	1.802	15.98
		.265	1L	3000.0	2.964	24.19
		.520	2L	4000.0	8.126	26.29
		.308	2U	5000.0	1.604	12.97
		.500	2L	5000.0	4.897	23.77
		.453	2U	6000.0	1.802	12.97
		.529	2L	6000.0	2.964	21.18
		.779	3L	6000.0	8.126	24.53
		.323	3L	7000.0	.665	23.03
		.389	3U	7000.0	1.538	11.21
		.749	3L	7000.0	5.791	22.85
		.534	3U	8000.0	1.670	11.21
		.758	3L	8000.0	4.143	21.54

FIG. 56. COMPUTED IONOGRAM POINTS TAKEN FROM DATA OF FIG. 55.

and 17 Mc. For example, if the 6000-km ionogram is to be generated, draw a vertical line through 3000 km; the intersections of the various curves with this vertical line would indicate the existence of two-hop propagation modes. (This works only for nontilted ionospheres.) Similarly, one could draw a vertical line through 2000 km, and intersections with this line would represent propagation modes via three hops to a ground range of 6000 km. Thus, if one draws these two lines, each intersection will represent an entry of data on the ionogram. This process is illustrated in Fig. 58, where the 6000-km ionogram is shown with these intersections plotted. Notice that the curves are smooth except for the break at 16 Mc, which is introduced by the change in the horizontal-scale compression ratio on Granger equipment.

In essence, the dots on Fig. 58 represent the amount of information that a digital computer can easily produce without human intervention. If price were no object, one can easily see that the entire process could be made totally automatic.

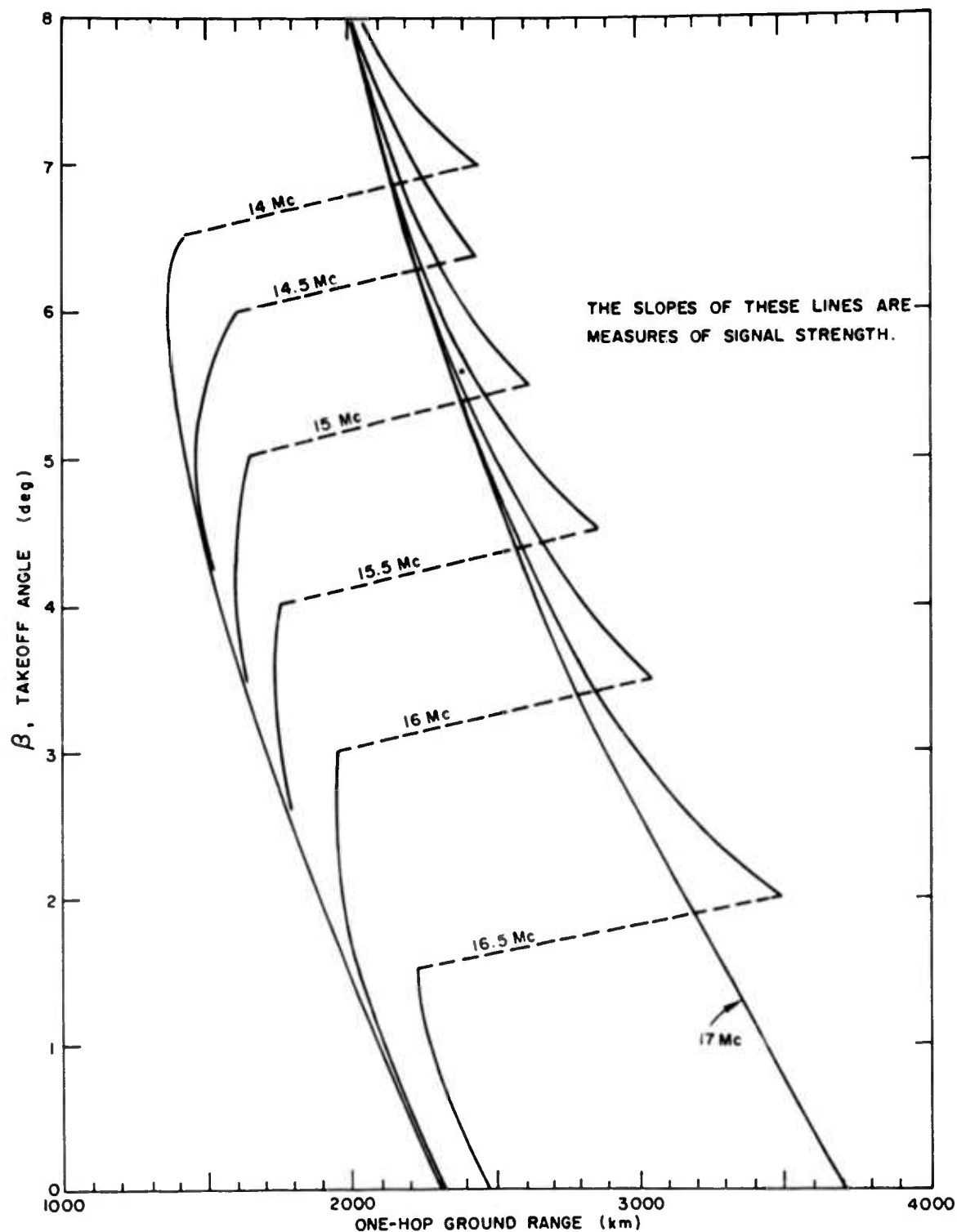


FIG. 57. GRAPH OF RAYPATH RANGE VS TAKEOFF ANGLE FOR IID 012.

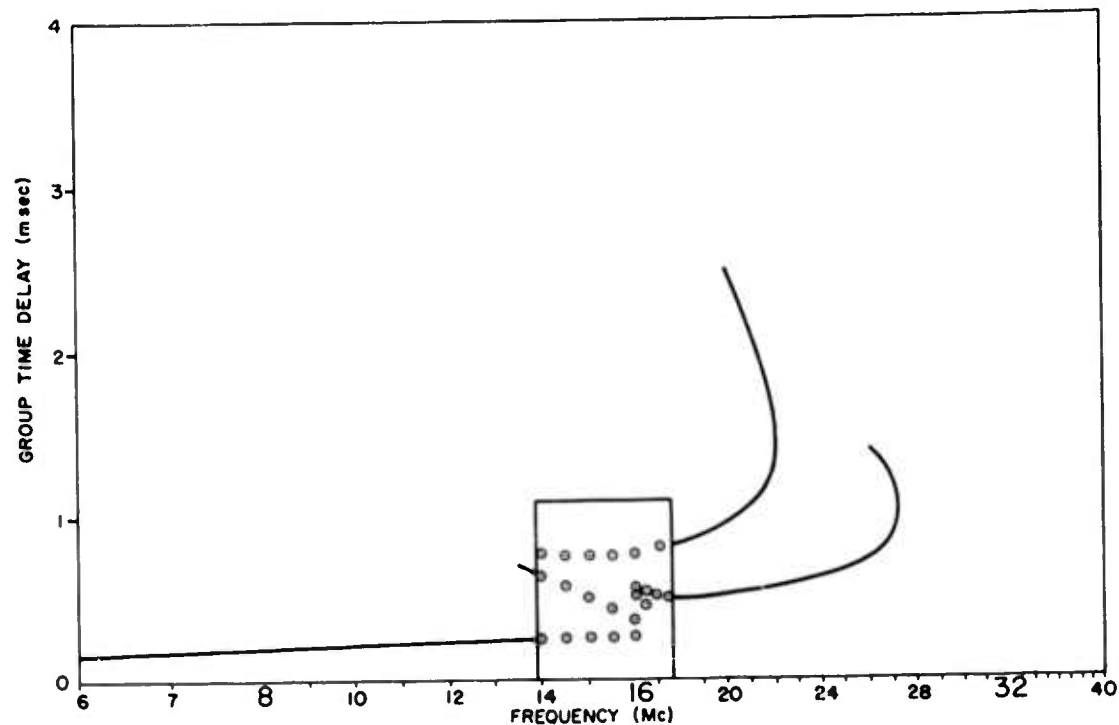


FIG. 58. PARTIALLY SYNTHESIZED IONOGRAM SHOWING POINTS PLOTTED DIRECTLY FROM THE COMPUTER OUTPUT.

C. ORIGIN OF A ONE-HOP TRACE IN A 5000-km IONOGRAM

A commonly encountered "rule of thumb" says that one-hop rays travel only about 4000 km. Consequently, it is rather surprising to find a one-hop trace on a 5000-km ionogram such as is shown for IID 011 on Fig. 8. This phenomenon can be visualized more clearly using Fig. 59, which shows the takeoff angle of various rays plotted against the ground range that the rays achieved in one hop. Notice that the energy density at the ground will be proportional to the quantity $d\mathcal{E}/dR$, which is the slope of the various curved lines on the figure. (However, energy density does not become infinite when the curves are vertical; see for example, Ref. 2.)

A respectably high energy density propagates to ranges well in excess of 5000 km. In fact, it can be seen that strong 31-Mc signal levels exist between 5460 and 5500 km via lower rays. The cause of the one-hop trace on Fig. 8 can be understood by examination of the intersections of the curved lines with the vertical line through 5000 km. It can be seen that the echo has significant strength only in the frequency interval of approximately 30.8 to 30.9 Mc, and these signals propagate at extremely low takeoff angles, which are normally heavily attenuated in the terminal equipment.

Also, it should be pointed out that this electron-density distribution has a far smoother N-h profile than is normally encountered in nature, and the resulting families of mathematically smooth curves such as on Fig. 59 probably do not exist in the natural situation. Experimental oblique soundings showing one-hop propagation at a range of 5600 km are shown and analyzed in Ref. 3.

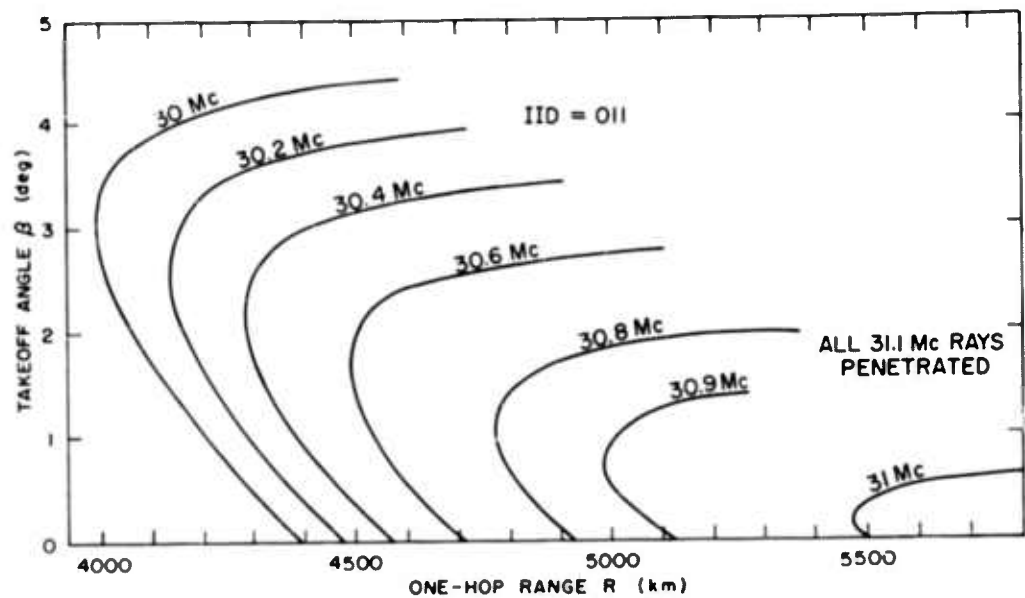


FIG. 59. LONG-RANGE, ONE-HOP PROPAGATION IN A CHAPMAN LAYER FOR IID 011.

VII. SELECTED EXPERIMENTAL IONOGRAMS SHOWING AGREEMENT WITH THEORY

A few experimental oblique ionograms are presented here to show that the structures that have been synthesized are actually found in nature. All of the records given here were selected from Refs. 4, 5, and 6, and are reproduced with the kind permission of the authors. A more thorough literature search would undoubtedly turn up many more records exhibiting appropriate structures.

On Fig. 60 are a number of examples illustrating the situation when the electron-density profile is a single smooth curve, such as a Chapman layer (IID 011, 053, 054, 055, 056) or a parabolic layer (IID 111 or 124). In the original presentations the vertical axes were labeled in kilometers, but two different conversion constants were used: 300 km per msec, and 150 km per msec. Unfortunately both of these conventions can be supported by a line of reasoning. In order to avoid confusion, all vertical axes here are labeled in msec, which is unambiguous. Also, the figures from Ref. 4 have a logarithmic frequency scale whereas the figures from Refs. 5 and 6 have a linear frequency scale.

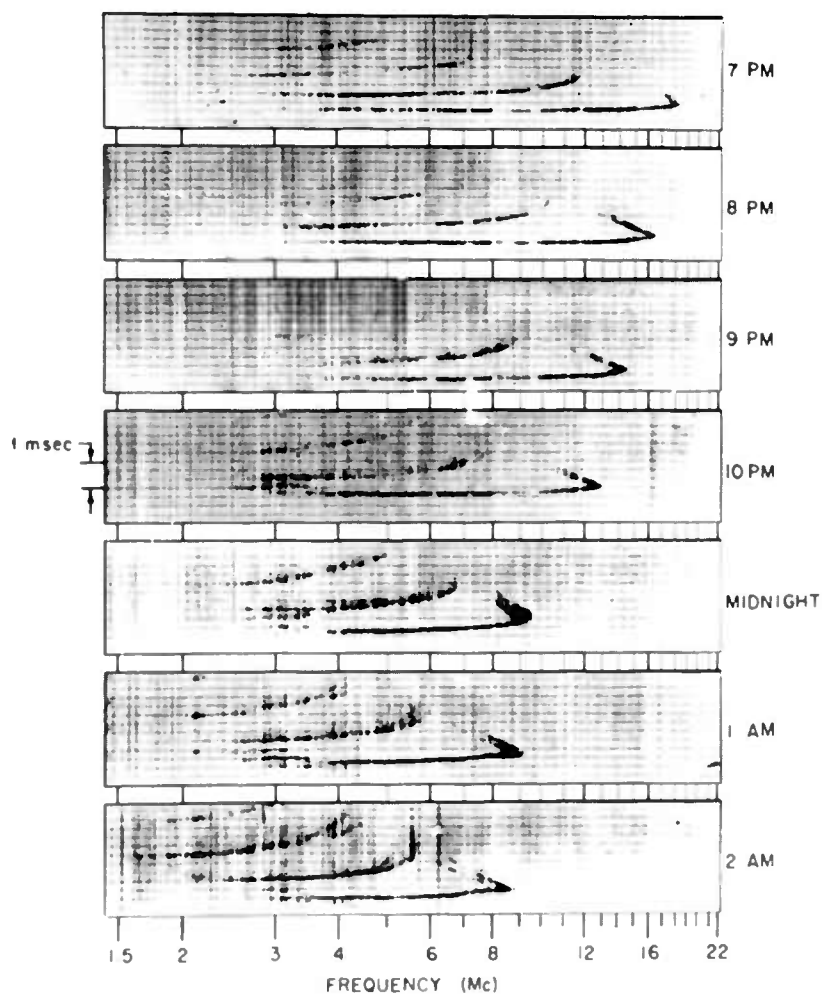
Notice the striking similarities between these ionograms and those that were presented, for example, in the first set of ionograms of IID 011. The multiple-hop echo structures are quite similar in detail to the theoretical ones. Two differences can be noticed: the ordinary and extraordinary traces can be distinguished on the experimental ionograms, and the noses of the one-hop echoes appear to be sharper than the noses of the synthetic ionograms. These differences would indicate that the actual electron-density profiles were not as blunt-nosed in the vicinity of the electron-density peak as were the mathematical models of ionospheres used for synthesis.

Figure 61 shows experimental evidence of the presence of E layers such as were simulated by IID 012 and 089. A wide variety of effects is seen; the relative strengths of the E and F_2 layers can be seen to vary from one record to the next. Figure 61b shows clearly the so-called "line of impenetrability," which is Möller's term for the locus of the left-hand ends of the F-layer traces in the presence of an E layer. This line can clearly be followed on the various synthetic ionograms, where the channel between the E and F traces seems to follow a smooth locus from hop to hop.

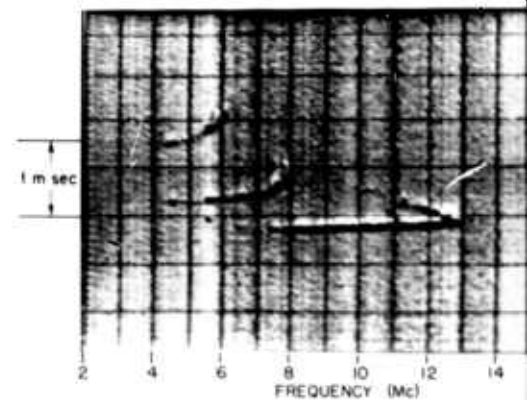
Figure 61e shows striking changes in the relative proportion of E and F echoes at Boulder during a twilight period.

Figure 62 shows five records that are similar in nature to synthetic ionograms calculated for IID 133. The curious shape of the F_2 trace, which comes down at a steep angle, turns around, and goes back up in the direction from which it came, can be understood by reference to the 133 synthetic ionograms. These patterns apparently reflect an ionospheric structure that is closely related to 012 and, in fact, the transition between the types is evident in the sequence given on Fig. 61e.

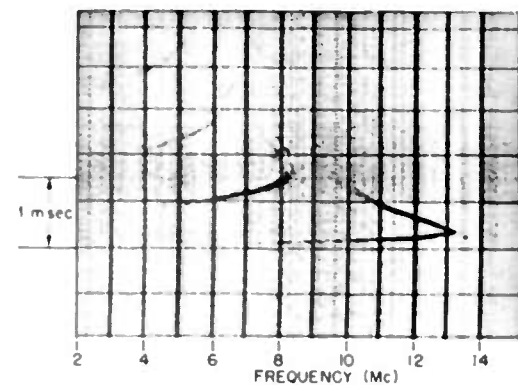
**Best
Available
Copy**



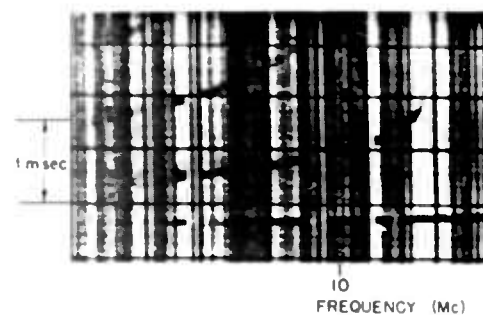
a. From Möller [Ref. 4], Fig. C1.3a on page 103.



b. From Agy and Davies [Ref. 5], page 157.

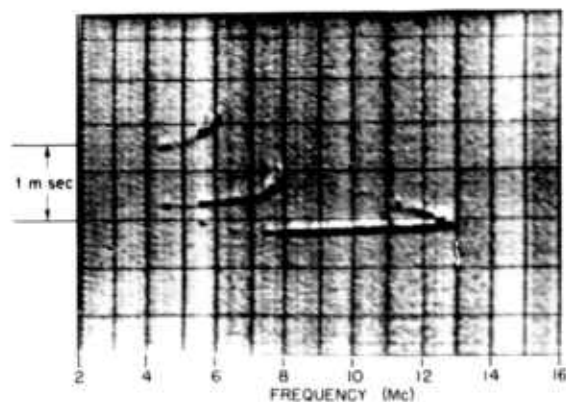
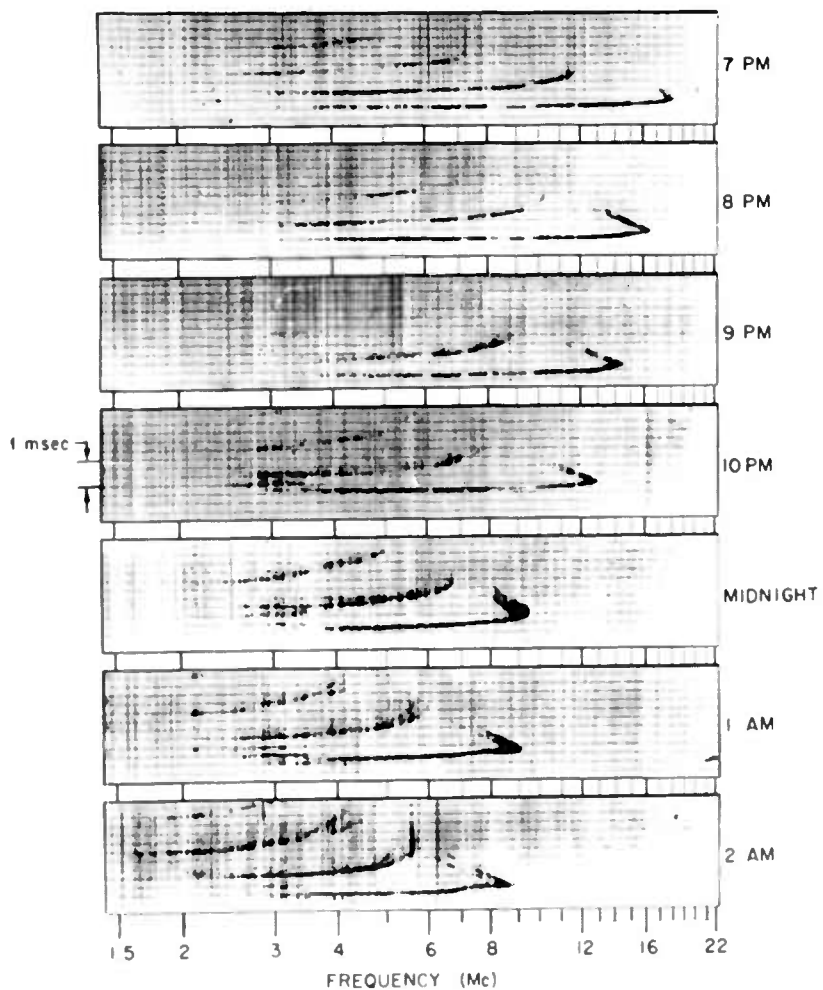


c. From Agy and Davies [Ref. 5], on page 167.

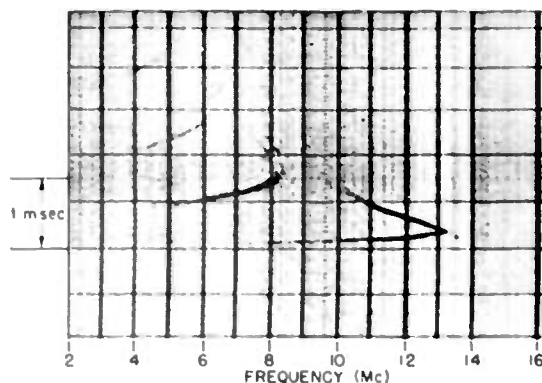


d. From Agy, Davies, and Salaman record, April 30, 1957, Section

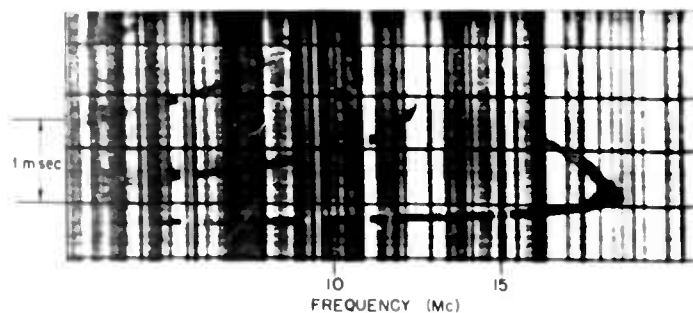
FIG. 60. EXPERIMENTAL IONOGRAMS TO THOSE OF IID 011.



b. From Agy and Davies [Ref. 5], 1815 record on page 157.

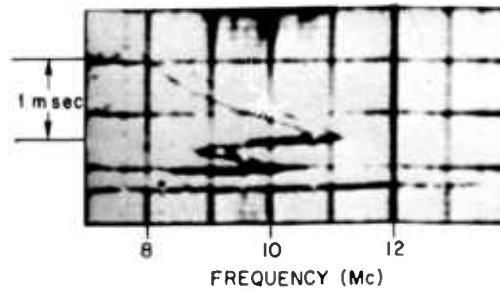


c. From Agy and Davies [Ref. 5], 2112 record on page 167.

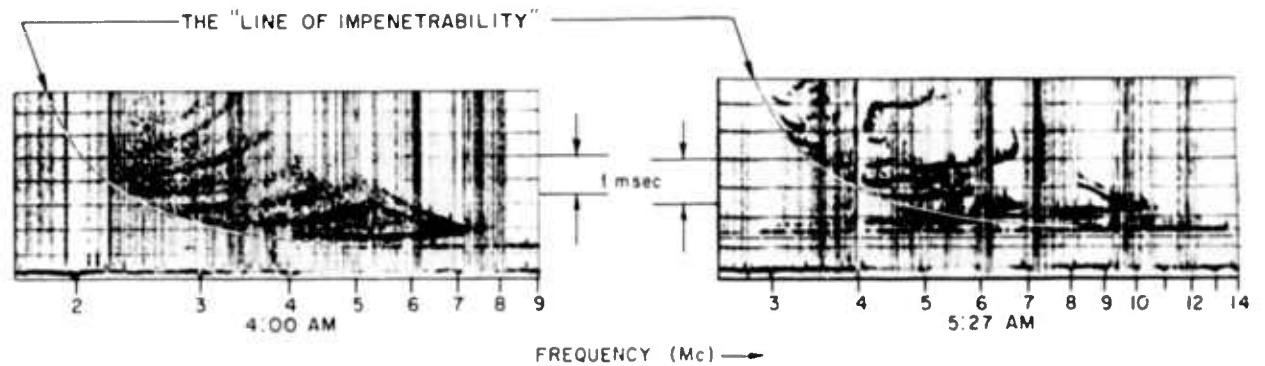


d. From Agy, Davies, and Salaman [Ref. 6], 2101 record, April 30, 1957, Section III-4.

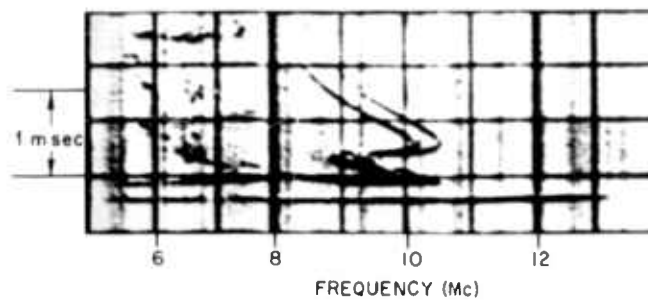
FIG. 60. EXPERIMENTAL IONOGRAMS SIMILAR TO THOSE OF IID 011.



a. From Agy, Davies, and Salaman [Ref. 6], 0952 record, Sept. 12, 1952, Section I-4.

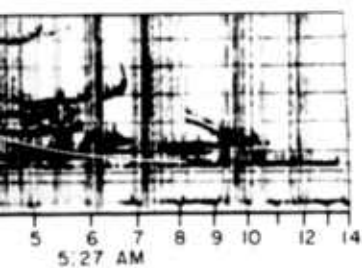


b. From Möller [Ref. 4], Fig. B2.4 on page. 41.



c. From Agy, Davies, and Salaman [Ref. 6], 1127 record, April 2, 1952, Section I-1.

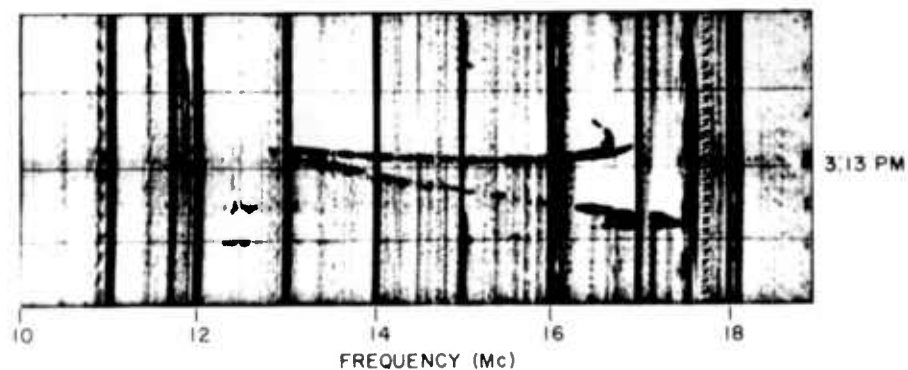
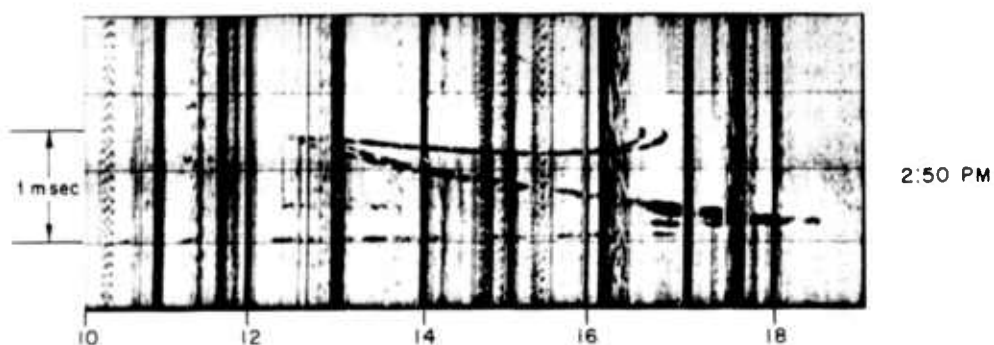
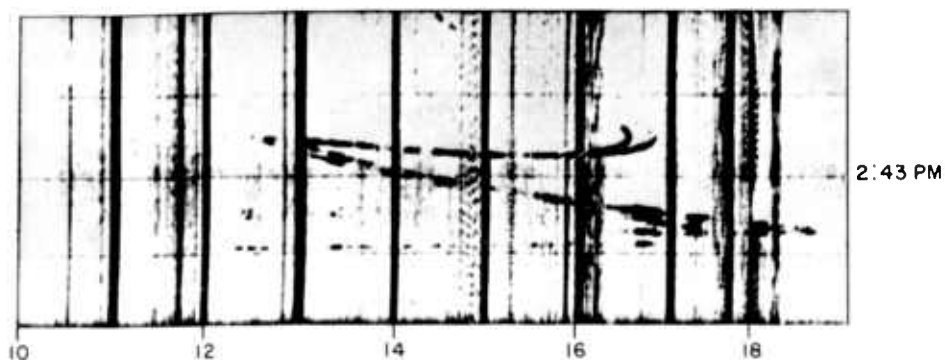
0952



. 41.

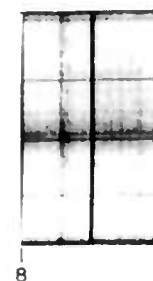
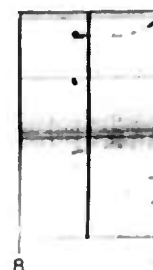
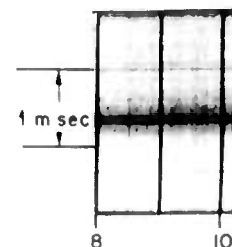
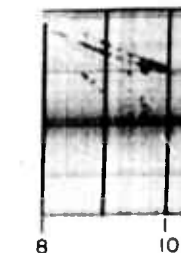


1127



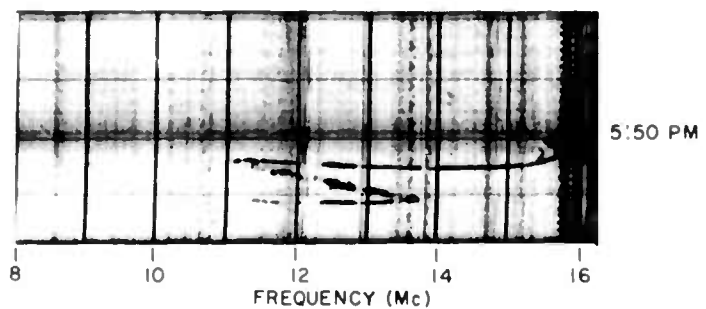
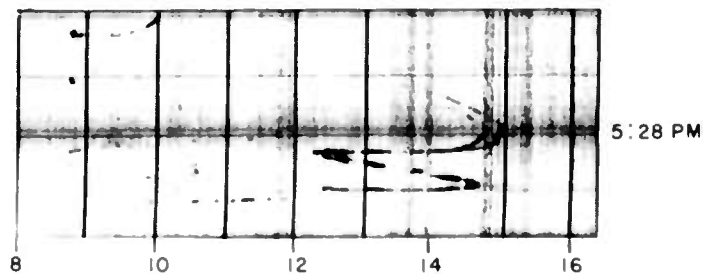
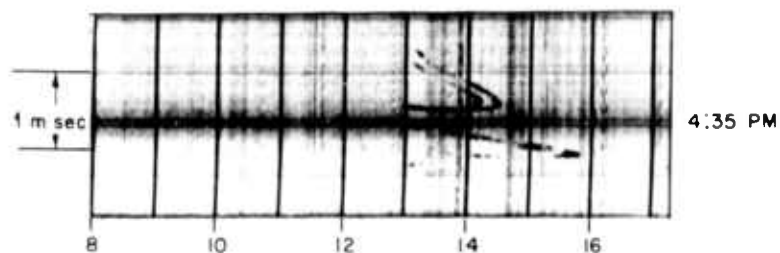
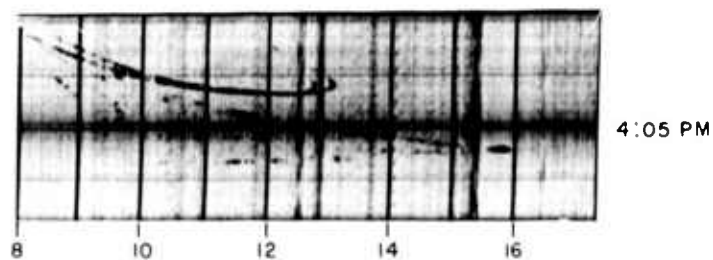
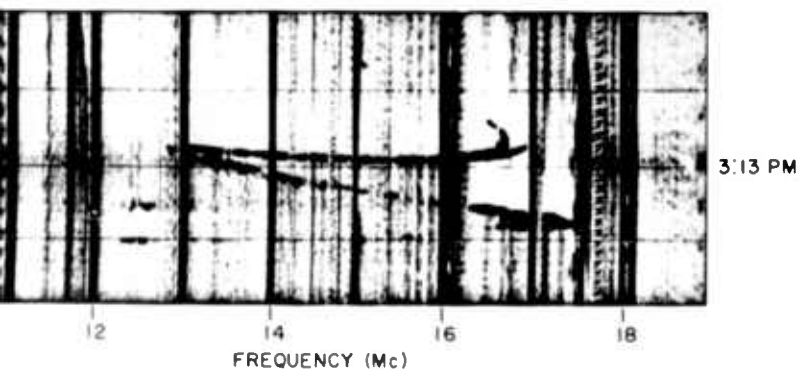
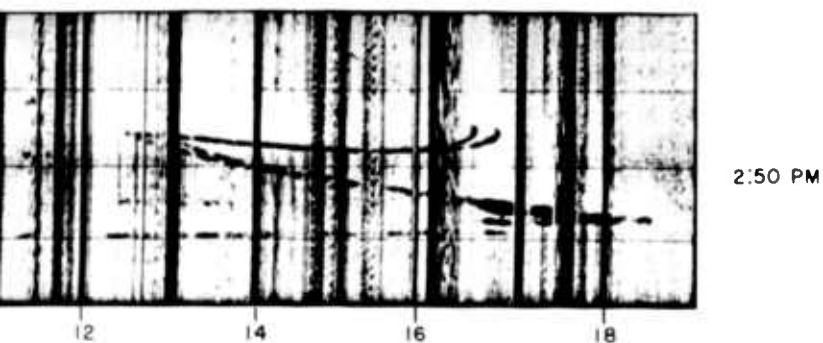
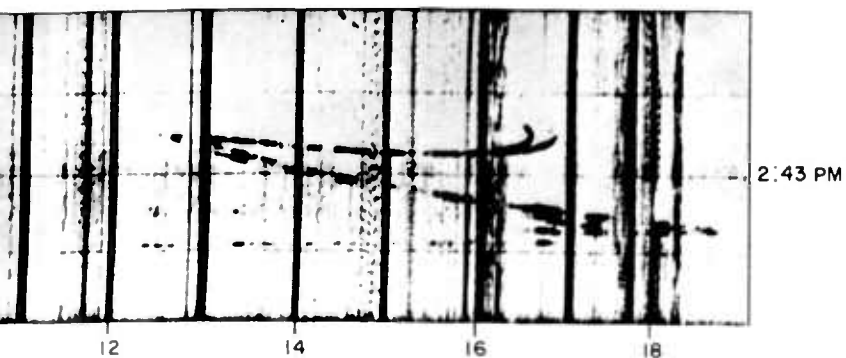
d. From Agy, Davies, and Salaman [Ref. 6], May 5, 1958 records, Section III-6.

2



e. From Ag June 9,

FIG. 61.
TO THO
- 85 -

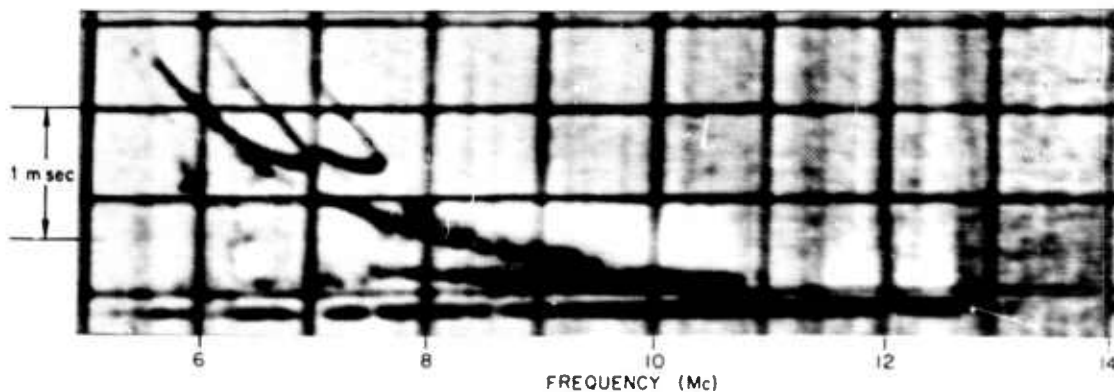


From Agy, Davies, and Salaman [Ref. 6], May 5, 1958 records, Section III-6.

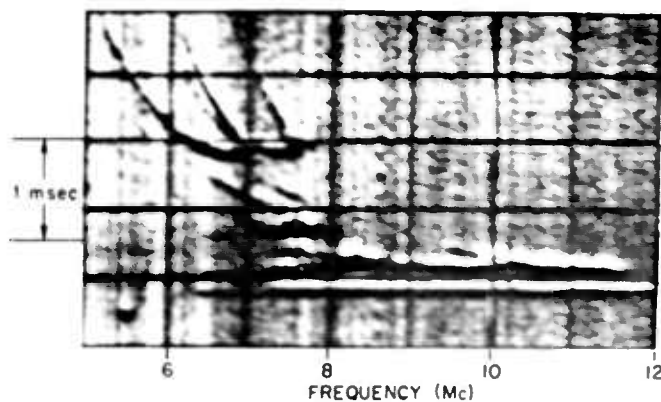
c. From Agy, Davies, and Salaman [Ref. 6], June 9, 1958 records, Section III-2.

3

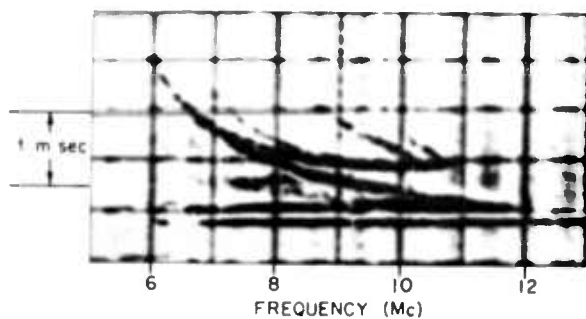
FIG. 61. EXPERIMENTAL IONOGRAMS SIMILAR TO THOSE OF IID 012.



a. From Agy, Davies, and Salaman [Ref. 6], 1132 record, Sept. 26, 1952, Section I-4.

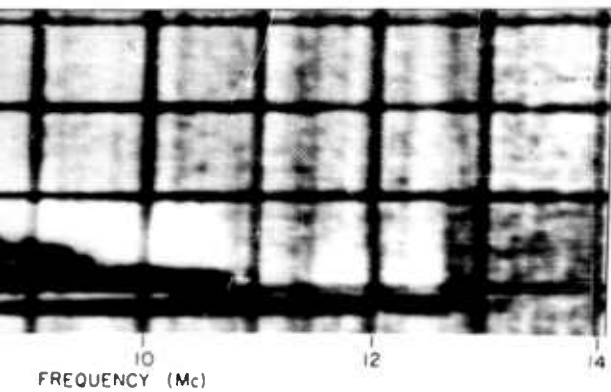


b. From Agy, Davies, and Salaman [Ref. 6], 1508 record, May 28, 1952, Section I-1.

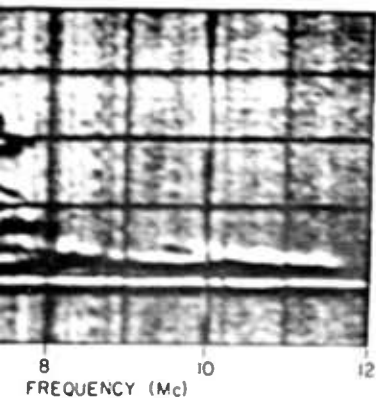


c. From Agy, Davies, and Salaman [Ref. 6], 1220 record, June 25, 1952, Section I-1.

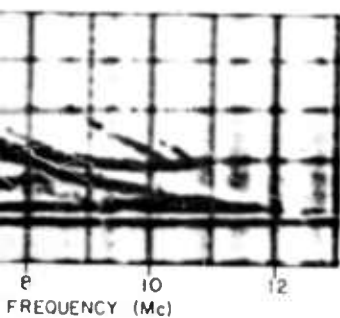
FIG. 62. EXP



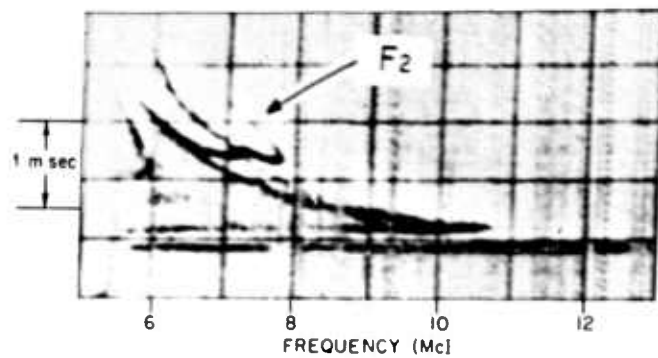
es, and Salaman [Ref. 6],
ept. 26, 1952, Section I-I.



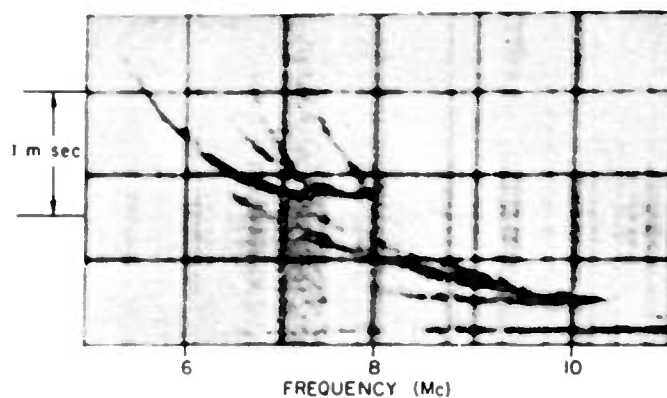
es, and Salaman [Ref. 6], 1508
5, 1952, Section I-I.



es, and Salaman [Ref. 6], 1220
5, 1952, Section I-I.



d. From Agy and Davies [Ref. 5], 1120 record
on page 171.



e. From Agy and Davies [Ref. 5], 1146 record
on page 165.

FIG. 62. EXPERIMENTAL IONOGRAMS SIMILAR TO THOSE OF IHD 133.

2

SEL-64-106

VIII. SUMMARY

A method has been described that permits the synthesis of artificial oblique ionograms by means of a modern high-speed digital computer at a reasonable cost. Other organizations may wish to carry out this procedure, either to check theories concerning the origin of certain oblique-ionogram details, or to build up a more comprehensive "library" of well-understood ionogram structures. Actual computer programs are not included here because the potential user will doubtless prefer to receive such programs in the form of punched cards.

Thirty-nine oblique ionograms are synthesized by the method described in order to illustrate the nature of the ionograms that would be obtained experimentally in the presence of ionospheres similar to those assumed. Simple models illustrating the most gross ionospheric features were used for this first effort. However, it should be understood that the method is useful for any electron-density distribution that can be described to the computer. This includes horizontal gradients of a wide variety of descriptions, and also traveling, localized, ionospheric irregularities.

POSTSCRIPT (December 1964)

Prior to the final printing of this report, the author received a private communication describing similar work by J. W. Finney of NBS and H. G. Möller who was temporarily at NBS. They made only one ionogram, but in it they showed the effect of magnetoionic splitting for a particular path. Readers will find interesting comparisons between our techniques. Used together, they would complement each other quite well, since the programs given here are fast and inexpensive and therefore suitable for extensive investigations or preliminary attempts. The more precise (but more expensive) method of Finney and Möller could be used for study of the ionogram perturbations which are caused by the geomagnetic field.

REFERENCES

1. T. A. Croft and L. Gregory, "A Fast, Versatile Ray-Tracing Program for IBM 7090 Digital Computers," Rept. SEL-63-107 (TR 82, Contract Nonr 225(64)), Stanford Electronics Laboratories, Stanford, Calif., Oct 1963.
2. K. G. Budden, "Radio Waves in the Ionosphere," Cambridge Press, 1961 (see particularly, paragraphs 11.7 and 15.25).
3. D. B. Muldrew and R. G. Maliphant, "Long-Distance One-Hop Ionospheric Radio-Wave Propagation," J. Geophys. Res., 67, No. 5, p. 1805, May 1962.
4. H. G. Möller, "Variable-Frequency Pulse Transmission Tests at Oblique Incidence over Distances between 1,000 and 2,000 km," Westdeutscher Verlag, Cologne, Germany, 1963.
5. Vaughn Agy and Kenneth Davies, "Ionospheric Investigations Using the Sweep-Frequency Pulse Technique at Oblique Incidence," J. Res., Nat. Bur. Stds. - D. Radio Propagation, 63D, 2, pp. 151-174, Sep-Oct 1959.
6. Vaughn Agy, Kenneth Davies, Roger Salaman, "An Atlas of Oblique-Incidence Ionograms," National Bureau of Standards, Tech. Note 31, Boulder Laboratories, Nov 1959.

ONR-ARPA DISTRIBUTION LIST

(Revised by ONR July 1964)

No. of
Copies

No. of
Copies

NAVY

Chief of Naval Research
Department of the Navy
Washington, D. C. 20360
1 Attn: Code 402C
2 Attn: Code 418

Director
Naval Research Laboratory
Washington 25, D.C.
1 Attn: Code 5320 (Mr. J. M. Headrick)
1 Attn: Code 2027

Chief of Naval Operations
Department of the Navy
Washington 25, D.C.
1 Attn: OP-723E
1 Attn: OP-071E

Director, Special Projects Office
Department of the Navy
Washington 25, D.C.
1 Attn: Code SP-204

Commander
Pacific Missile Range
Point Mugu, California
1 Attn: Code 3215

Commander
Naval Missile Center
Point Mugu, California
1 Attn: Code N03022

Commanding Officer and Director
U. S. Navy Electronics Laboratory
San Diego, California 92152
1 Attn: Mr. H. J. Wirth
1 Attn: Library

Commanding Officer
U. S. Naval Ordnance Laboratory
Corona, California 91720
1 Attn: Mr. V. E. Hildebrand
(Code 453)

AIR FORCE

Headquarters
Air Force Systems Command
Foreign Technology Division
Wright-Patterson AFB, Ohio
1 Attn: TDC (Mr. Zabatakas)
1 Attn: TDEED (Mr. W. L. Picklesimer)
1 Attn: TDATA (Mr. G. A. Long, Jr.)
1 Attn: TDCE (Mr. M. S. J. Graebner)

Headquarters, RTD
Bolling AFB
Washington, D.C. 20332
1 Attn: RTHC (Col. Richard Cosel)

Rome Air Development Center
Research and Technology Division
Griffiss Air Force Base, New York
1 Attn: EMASR (Mr. Vicent J. Coyne)
1 Attn: RAVEL-3 (Mr. G. R. Weatherup)
1 Attn: RALCS (Mr. Salvador DiGennaro)

Commander
USAF Security Systems
San Antonio, Texas
1 Attn: ODCR (Mr. Walter L. Anderson)

Headquarters, USAF
Office of Assistant Chief of Staff, Intelligence
Washington, D.C. 20330
1 Attn: AFNICA (Lt. Col. Brubaker)

ONR-ARPA DISTRIBUTION LIST

<u>No. of Copies</u>		<u>No. of Copies</u>	
	<u>AIR FORCE</u>		U. S. Army, SLAG
	Headquarters		P. O. Box 7157
	North American Air Defense Command		Apex Station
	Ent AFB		Washington, D.C. 20004
	Colorado Springs 12, Colorado	1	Attn: Mr. N. R. Garofalo
1	Attn: NPSD-A (Col. M. R. Cripe)		
1	Attn: NELC-AP		<u>DOD</u>
	Headquarters, AFCRL		Director
	L. G. Hanscom Field		Advanced Research Projects
	Bedford, Massachusetts		Agency
1	Attn: CRUP (Dr. G. J. Gassman)	1	Washington 25, D. C.
1	Attn: CRUI (Mr. W. F. Ring)		Attn: Mr. Alvin Van Every
	Headquarters, USAF		Director
	Office of Assistant Chief of Staff		Weapons Systems Evaluation
	for Intelligence		Group
	Policy and Programs Group, AFNINC		Office of the Director of
	Washington 25, D.C.		Defense Research and
	Headquarters, SAC		Engineering
	Offutt AFB		Washington 25, D.C.
	Omaha, Nebraska		Office of Assistant Chief of
1	Attn: Mr. Eugene Jackson		Staff for Intelligence
	<u>ARMY</u>		Department of the Army
	Chief, Army Security Agency	1	Room 2B457, The Pentagon
	Arlington Hall Station		Washington 25, D.C.
	Arlington, Virginia		Attn: Mr. Joseph Grady
1	Attn: Col. James E. Helgestad		Office of the Assistant
	Commanding Officer		Director
	U. S. Army Material Command		Intelligence and Reconnaissance
	Washington 25, D. C.		Office of the Director of
1	Attn: AMCRD-D		Defense Research and
	Commanding Officer		Engineering
	U. S. Army Munitions Command	1	Room 3E119, The Pentagon
	Picatinny Arsenal		Washington 25, D. C.
	Dover, New Jersey		Attn: Mr. Howard A. Staderman
1	Attn: SMUPA-VA6		Defense Intelligence Agency
	Commanding Officer		Pentagon Annex #3, Room 303
	U. S. Army Electronics Research Unit		Washington 25, D. C.
	P. O. Box 205	1	Attn: AQ-2A (Captain James
	Mountain View, California		Stewart)
1	Attn: Mr. Joseph Bert		

ONR-ARPA DISTRIBUTION LIST

<u>No. of Copies</u>		<u>No. of Copies</u>	
	<u>DOD</u>		Aero Geo Astro Corporation
	Deputy Director		13624 Magnolia Avenue
	Research and Technology		Corona, California
	Office of the Director of Defense	1	Attn: Mr. A. W. Walters
	Research and Engineering		Astrophysics Research
	Room 3E1030, The Pentagon		Corporation
	Washington 25, D.C.		2444 Wilshire Blvd., Room 512
1	Attn: Dr. Chalmers W. Sherwin	1	Santa Monica, California
	Office of the Assistant Director		Attn: Dr. Alfred Reifman
	(Defense Systems)		HRB Singer, Inc.
	Defense Research and Engineering		Science Park
	Room 3D138, The Pentagon		State College, Pennsylvania
	Washington 25, D.C.	1	Attn: Library
1	Attn: Mr. Daniel Fink		Institute for Defense Analyses
	Director		1666 Connecticut Avenue
	National Security Agency		Washington 9, D.C.
	Fort George G. Meade, Maryland	1	Attn: Dr. Paul von Handel
1	Attn: K-344 (Mr. Charles Gandy)		Institute of Science and
1	Attn: C3/TDL		Technology
	Director		The University of Michigan
	Defense Intelligence Agency		P.O. Box 618
	Room 1C917, The Pentagon		Ann Arbor, Michigan
	Washington 25, D.C.	1	Attn: BAMIRAC Library
1	Attn: DIAST-B (Mr. Thomas Brooke)		Massachusetts Institute of
	Director		Technology
	Defense Intelligence Agency		Center for Space Research
	Room 3B259, The Pentagon		Building 33-109
	Washington 25, D.C.	1	Cambridge, Massachusetts
1	Attn: DIAIS-I (Col. John G. Johnson)	1	Attn: Dr. J. V. Harrington
	Defense Documentation Center		Massachusetts Institute of
	Cameron Station		Technology
	Alexandria, Virginia 22314		Lincoln Laboratory
	20 Copies	1	Lexington 73, Massachusetts
	<u>OTHER</u>		Attn: Dr. J. H. Chisholm
	ACF-E Industries		MITRE Corporation-E Bldg.
	3355-52nd Avenue		Room 353
	Hyattsville, Maryland		Bedford, Massachusetts
1	Attn: Mr. William T. Whelan	1	Attn: Mr. William A.
			Whitcraft, Jr.

ONR-ARPA DISTRIBUTION LIST

No. of
Copies

No. of
Copies

OTHER

1	<p>National Bureau of Standards Boulder Laboratories Boulder, Colorado Attn: 85.20 (Mr. L. H. Tveten)</p>	1	<p>University of California Mathematics Department Berkeley 4, California Attn: Dr. Edmond J. Pinney</p>
1	<p>Pickard and Burns, Inc. Research Department 103 Fourth Avenue Waltham 54, Massachusetts Attn: Dr. John C. Williams</p>		
1	<p>Princeton University James Forrestal Research Center Sayre Hall Princeton, New Jersey Attn: Dr. Edward Frieman</p>		
1	<p>RAND CORPORATION 1700 Main Street Santa Monica, California Attn: Dr. Ivan Selin</p>		
1	<p>Attn: Dr. Cullen Crain</p>		
1	<p>Attn: Library</p>		
1	<p>Raytheon Company Communication and Data Processing Operations 1415 Boston-Providence Turnpike Norwood, Massachusetts Attn: Mr. L. C. Edwards</p>		
1	<p>Stanford Research Institute Menlo Park, California Attn: Dr. David Johnson</p>		
	<p>Mr. Thurston B. Soisson Box 3164 SW Station Washington, D. C.</p>		
1	<p>Sylvania Electronics Systems Electronic Defense Laboratories P. O. Box 205 Mountain View, California Attn: Mr. John Don Carlos</p>		

UNCLASSIFIED

UNCLASSIFIED